Photophysics and Photochemistry of Blue Phosphorescent Iridium Complexes

January 2010

Kazuyoshi Tsuchiya

Graduate School of Engineering

CHIBA UNIVERSITY

（千葉大学学位申請論文）

Photophysics and Photochemistry of Blue Phosphorescent Iridium Complexes

2010 年 1 月

千葉大学大学院工学研究科

共生応用化学専攻共生応用化学コース

土屋　和芳

Contents

Chapter 1

General Introduction

1-1. OLED

Organic Light Emitting Diode (OLED) is electronic light emitting device composed of multiple organic thin layers. In 1987, C. W. Tang, et al. reported the first OLED.[1] The scheme of a typical OLED device is shown in Fig. 1-1. OLED devices are usually composed of several organic thin layers. Those work as electron injecting, electron transporting, light emitting, hole transporting, and hole injecting units. To obtain high performance OLED, all of these materials must be developed. Particularly light emitting material is important because its luminescent ability reflects directly to the electroluminescent efficiency of OLED. In OLED, an emissive material is electrically excited. The mechanism is depicted in Fig. 1-2.[2] As Fig. 1-2, the ratio of generation of singlet excited state and triplet excited state molecules is 25:75 because of spin multiplicities of a hole and an electron. If emissive material is fluorescent material, only 25 % of electrical energy is converted to the light energy in maximum, while if emissive material is phosphorescent material, 100 % of electrical energy is converted to light in maximum (including intersystem crossing from singlet excited state to triplet). Ir complexes have a potential as highly phosphorescent material and therefore 100 % internal luminescent quantum efficiency become possible theoretically. Other factors to improve OLED performance are the electron-hole recombination efficiency, excited state energy confinement ability, low driving voltage, and external quantum efficiency. These factors are achieved by developments of charge transporting materials and optically optimized device structure.

High performance OLED needs several functionalized materials as mentioned above and phosphorescent quantum yield of emissive material directly reflects the luminescent efficiency of OLED. Obtaining highly luminescent material is very important, among such attempts phosphorescent material is an ideal material for achieving high luminescent efficiency.

Next I describe the nature of triscyclomethalated Ir complexes.

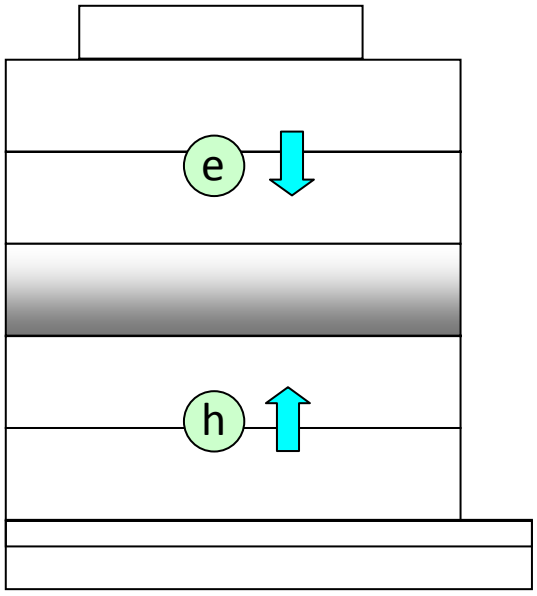

Aluminum Electrode (Cathode)

Electron Injecting Layer

Electron Transporting Layer

Emissive Layer (Host + Guest)

Hole Transporting Layer

Hole Injecting Layer

ITO-coated (Anode)
Glass Substrate

LiF (electron injection material)

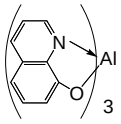

Alq_3 (electron transporting material)

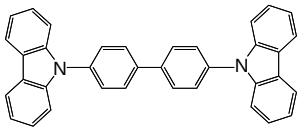

CBP (host material)

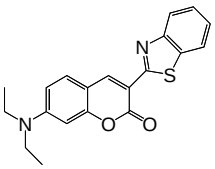

coumarin 6 (fluorescent material)

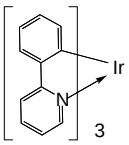

$Ir(ppy)_3$ (phosphorescent material)

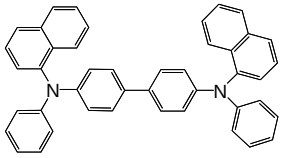

NPD (hole transporting material)

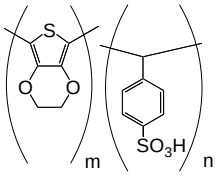

PEDOT:PSS (hole injection material)

Figure 1-1. Scheme of typical OLED device composed of functional multi-thin layers and structures of typical materials for OLED. Guest means small amount of fluorescent or phosphorescent dopant material used in host materials.

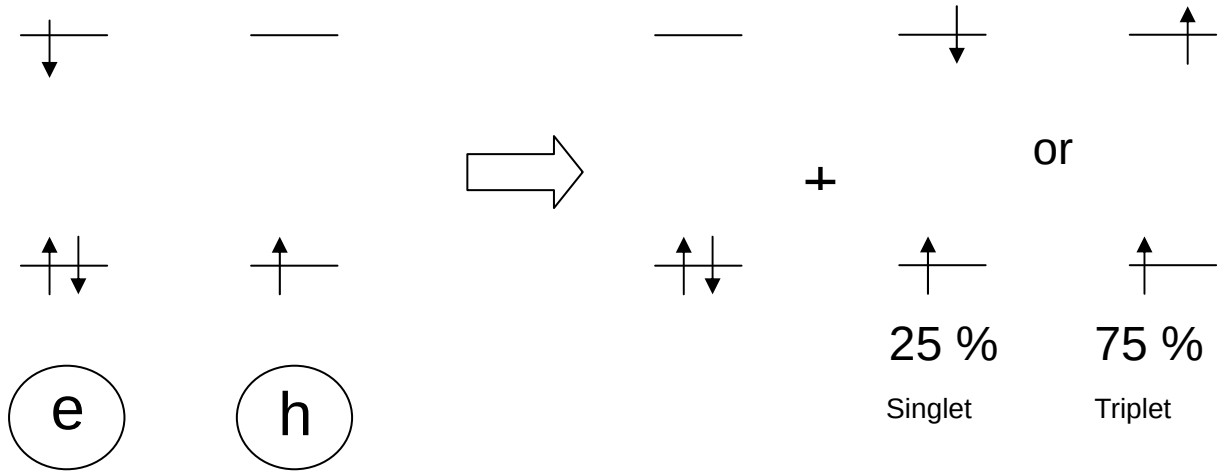

Figure 1-2. Excited state generation by hole-electron recombination.

1-2. Phosphorescent Iridium Complexes

1-2-1. Triscyclometalated Ir complexes; their structures, phosphorescent properties, and molecular orbitals.

Phosphorescent organic complexes have a biaryl ligand such as phenylpyridine. In 1985, R. J. Watts and co-workers have reported the photophysical properties of *fac*-tris(phenylpyridinato) Ir complex,[3] and in 2003 A. B. Tamayo et al. have reported the properties and structures determined by a single crystal X-ray crystallography of several triscyclometalated Ir complexes including *fac*-Ir(ppy)$_3$ (Fig. 1-3, Fig 1-4).[4] Complex *fac*-Ir(ppy)$_3$ showed strong green phosphorescence at room temperature. This is due to strong spin-orbit coupling of Ir atom. In common organic compound, phosphorescence quantum yield is almost zero because radiative deactivation from triplet excited state to singlet ground state is spin-forbidden and radiative rate constant is very small compared to nonradiative rate constant. In Ir complexes, strong spin orbit coupling enhances the intersystem crossing to triplet excited state from singlet excited state and also increases the radiaive rate constant from triplet excited state to singlet ground state. The increased radiative rate constant is compatible to the nonradiative rate constant. Generally, Ir complexes have absorption band derived from the electronic transition from Ir d orbital to ligand π^* orbital. This is called MLCT transition

(Fig 1-5).[5,6] This shows strong phosphorescence in visible area at room temperature. The color of phosphorescence is easily tunable by changing ligand structure. In the field of photochemistry, Ir complex have been useful to multitude of photonic applications including singlet oxygen sensitizer,[7] oxygen sensor,[8] Hg ion sensor,[9] biological labeling reagent,[10] and phosphorescent material for OLED.[11] The study of Ir complex as a phosphorescent material for OLED have been attracted significant attention recently.

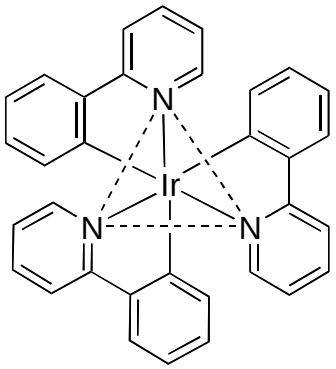

Figure 1-3. The structure of *fac*-Ir(ppy)$_3$

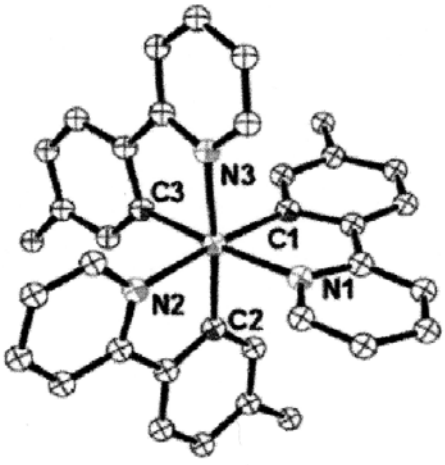

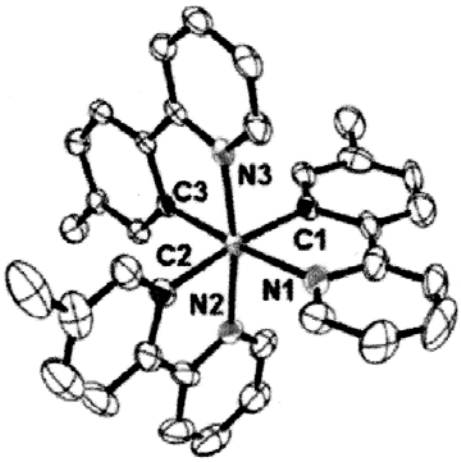

***fac*-Ir(*tpy*)$_3$** ***mer*-Ir(*tpy*)$_3$**

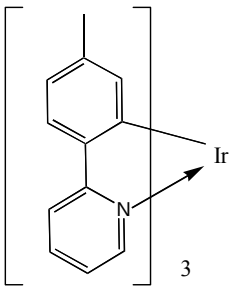

Ir(tpy)$_3$

Figure 1-4. The ORTEP diagrams of *fac*- and *mer*-Ir(tpy)$_3$ obtained by a single crystal X-ray crystallography (adopted from *J. Am. Chem. Soc.* **2003**, *125*, 7377) The detailed explanation of *fac* and *mer* isomers is described in section 1-4-1.

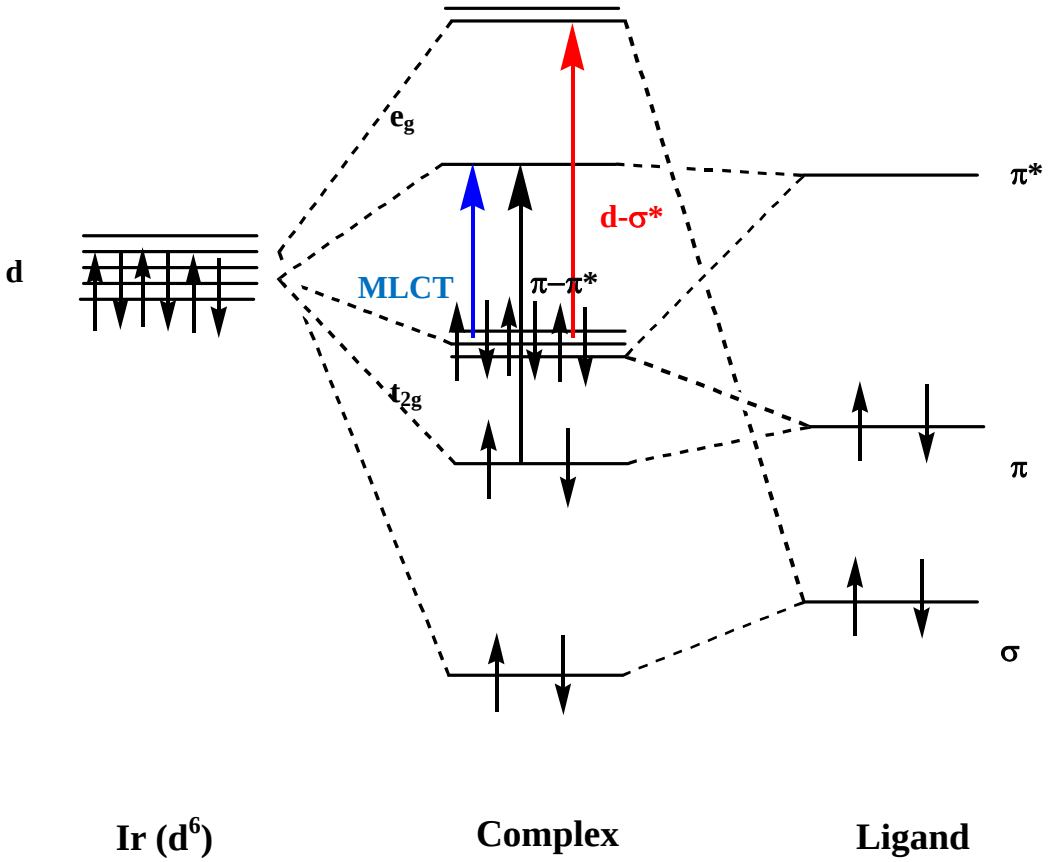

Figure 1-5. The energy diagram of a octahedral Ir complex.

1-2-2. Emission color dependence on ligand structure

The photophysical property of Ir (III) triscyclometharated complexes strongly depends on the ligand structure. The molecular orbital of the octahedral complexes is composed of Ir-d orbitals and ligand π and σ orbitals as mentioned above.

The photophysical properties such as emission wavelength, quantum yield, and emission lifetime are largely depend on the properties of ligand π and π* orbitals (and they also depend on the nature of ligand σ orbital. This will be explained in the next section and also in chapter 2 and 3). If the ligand π-π* energy band gap is large, the emission energy of the Ir complex having this ligand is also large, vice versa, if the ligand π-π* energy band gap is small, the emission energy of the Ir complex is also small. The examples are shown in Figure 1-6. The emission color is tuned by changing a LUMO energy level or a HOMO

energy level. In $Ir(piq)_3$,[11b] isoquinoline is used instead of pyridine of $Ir(ppy)_3$, and this results in large decreasing of LUMO energy and therefore leading red color emission. In $Ir(thpy)_3$,[11b] thiophene is used instead of phenyl of $Ir(ppy)_3$, and this results in increasing of HOMO energy and orange color emission is obtained. In $Ir(dfppy)_3$,[4] substitution of fluorine atom at phenyl moiety results in decreasing HOMO energy and greenish-blue color emission is obtained. In $Ir(ppz)_3$,[4] The pyrazole is used instead of pyridine of $Ir(ppy)_3$. Pyrazole has large π^* orbital energy and this results in high LUMO energy level. Blue color emission is obtained at 77 K glassy matrix or in solid state but negligible emission is obtained at an ambient temperature in solution.

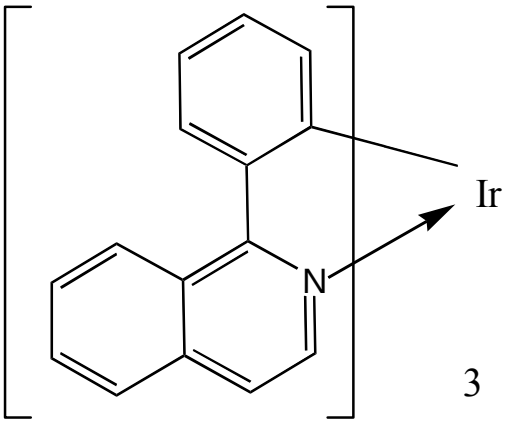

$Ir(piq)_3$ (red phosphorescence)

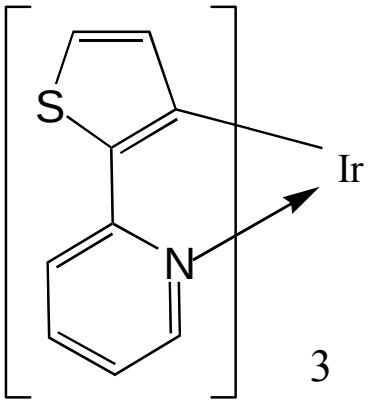

$Ir(thpy)_3$ (orange phosphorescence)

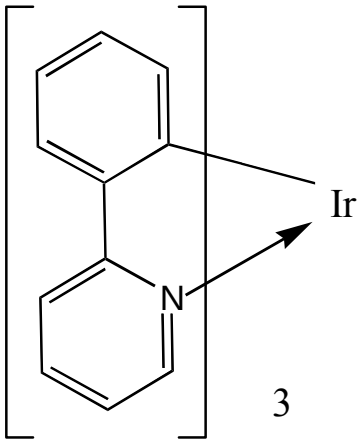

$Ir(ppy)_3$ (green phosphorescence)

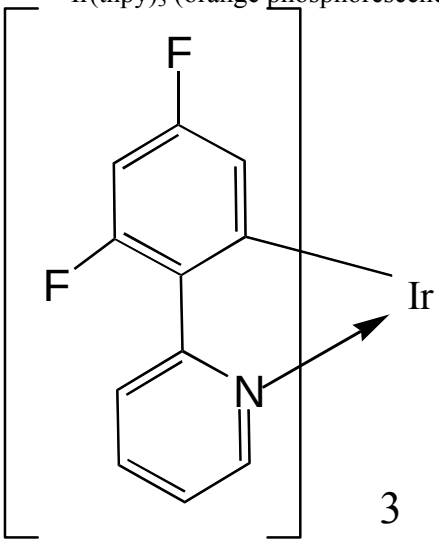

$Ir(dfppy)_3$ (greenish-blue phosphorescence)

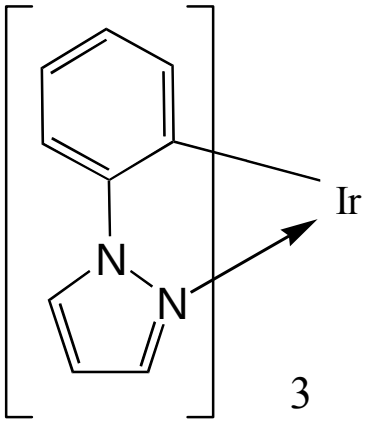

$Ir(ppz)_3$ (blue phosphorescence at 77K, but not emissive at an ambient temperature in solution)

Figure 1-6. Ir complexes emit red, green and blue phosphorescence.

.

1-2-3. DFT calculation study

Density functional theory (DFT) calculation is efficient tool for understanding how the emission color depends on the ligand structure or the functional group.[4, 12] DFT calculations provide the location of a molecular orbital density including HOMO and LUMO (Figure 1-7). HOMO is mainly delocalized over Ir and phenyl moiety in both *mer* and *fac* isomer and the LUMO is mainly delocalized over pyrazole moiety in $Ir(ppz)_3$. It is thought that the substitution on a phenyl moiety affects the HOMO, and replacement of heterocycle affects the HOMO. These explanations are derived by the experimental results of the emission colors and redox potential measurements.[4] The DFT calculation is also effective to know from which ligand the light is emitted in the heteroleptic Ir complexes.[13]

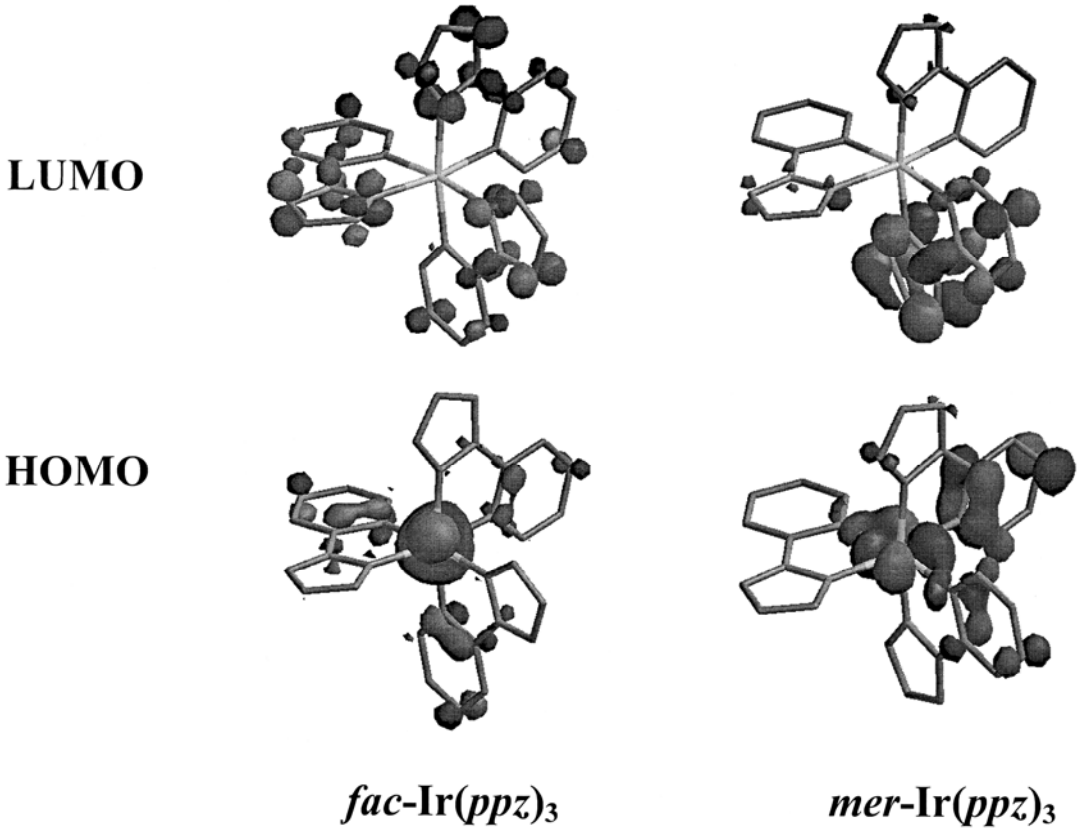

Figure 1-7. HOMO and LUMO of *fac*- and *mer*-$Ir(ppz)_3$ (adopted from *J. Am. Chem. Soc.* **2003**, *125*, 7377).

1-3. Difference in phosphorescence property between *fac* and *mer* isomers.

1-3-1. Characteristics of the *fac* and *mer* isomer

Homoleptic triscyclometalated Ir complex have two geometrical isomers. They are called *fac* and *mer* isomers. In *fac* isomer, the coordinating three pairs of carbon atom on phenyl ring and nitrogen atom on heterocycle are in trans position. In *mer* isomer, two nitrogen atoms on heterocycle are in trans position and two carbon atoms on phenyl ring are also trans position, only one pair of nitrogen atom and carbon atom is in trans position. (See Figure 1-4).

1-3-2. Separation and identification of *fac* and *mer* isomers

The *fac* isomer has a higher symmetry than the corresponding *mer* isomer has therefore ^{1} H NMR signals of the *fac* isomer are simpler than those of the *mer* isomer. The position of corresponding proton signals of three ligand of *fac* isomer is identical in ^{1} H NMR while the position of proton signals of three ligand of *mer* isomer appeared at different positions. In TLC analysis, the R_f value of *mer* isomer is higher than that of *fac* isomer in a proper solvent (the resolution is particularly large with hexane and ethyl acetate mixture as a developing solvent. For example, the R_f value of *mer*-Ir(ppz)$_3$, is 0.43 and that of *fac*-Ir(ppz)$_3$ is 0.31 when developed by the mixture of 70 % of hexane and 30 % of ethyl acetate.). The solubility in organic solvents is also different. Generally, the solubility of *fac* isomer is lower than *mer* isomer, and separation of small amount of *mer* isomer from *fac* isomer rich mixture is relatively easy by recrystallization or column chromatography. For such a reason, the separation and identification of *fac* and *mer* isomers are possible (although the separation become difficult when the solubility of both *fac* and *mer* isomers are very low).

1-3-3. Difference in photophysical property between *fac* and *mer* isomers

The luminescent property of both *fac* and *mer* isomers of some complexes have been reported

(Figure 1-8, Figure 1-9, Table 1-2).[4,14,15] The photophysical properties, such as, the shapes of UV-Vis absorption spectra, the emission wavelength, and the emission quantum yield (and emission lifetime) are different between *fac* and *mer* isomers (photophysical property is defined as the property appeared by the light absorption-deactivation process without chemical reaction). The shape of absorption spectrum of *fac* isomer has a peak-like shape at the ^{1}MLCT absorption band (λ = 320 ~ 420 nm) while the shape of absorption spectrum of *mer* isomer has a smooth slope-like shape at the same area.

The emission maximum of *fac* isomer is slightly shorter than that of *mer* isomer. The reason is explained as following. The *mer* isomer has same atom in trans position (N-Ir-N and C-Ir-C) and the length of one or both pairs of these bonds become to be longer in the excited state than that of C-Ir-N bond of excited *fac* isomer, results in the larger stokes shift of *mer* isomer than that of *fac* isomer.[4]

The emission quantum yield of *fac* isomer is larger than that of *mer* isomer. The emission lifetime measurement revealed that the nonradiative rate constant of *mer* isomer is much larger than that of *mer* isomer. The reason why *mer* isomer has such a large nonradiative rate constant is not clear and to understand this reason is one of the subjects in my study.

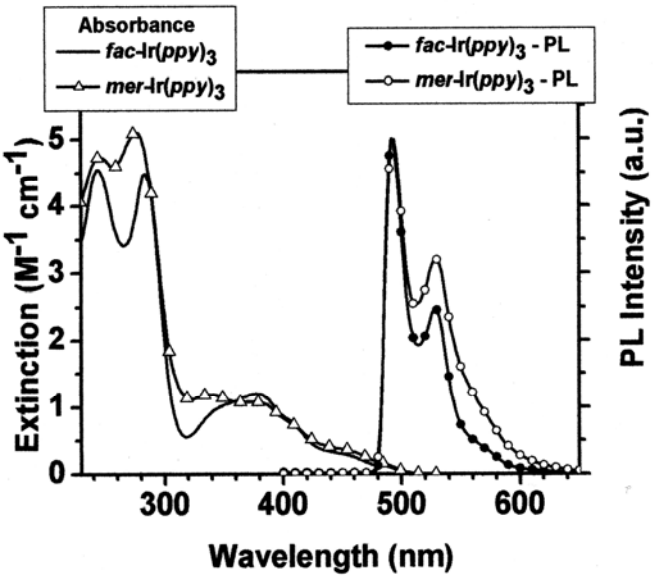

Figure 1-8. Absorption and PL spectra of *fac*-Ir(ppy)$_3$ and *mer*-Ir(ppy)$_3$ (adopted from *J. Am. Chem. Soc.* **2003**, *125*, 7377-7387).

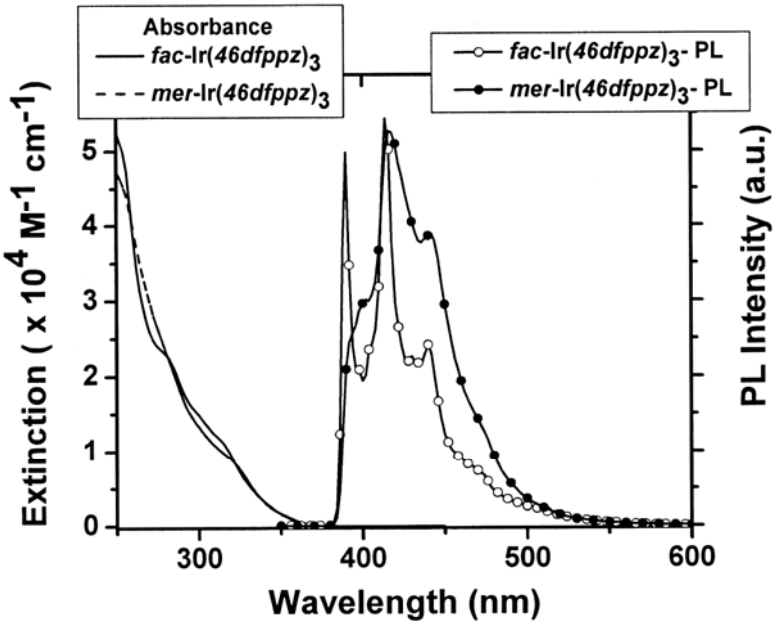

Figure 1-9. Absorption and PL spectra of *fac*-Ir(dfppy)$_3$ and *mer*-(dfppy)$_3$ (adopted from *J. Am. Chem. Soc.* **2003**, *125*, 7377-7387).

Table 1-2. Luminescent quantum efficiencies, lifetimes, and the radiative/nonradiative decay rates for Ir(C^N)$_3$ complexes at room temperature (adopted from *J. Am. Chem. Soc.* **2003**, *125*, 7377-7387).

Complex	Φ_{PL}	τ / μs	k_r / 10^5 s^{-1}	k_{nr} / 10^5 s^{-1}
***fac*-Ir(tpy)$_3$**	0.40	1.9	2.1	3.2
***mer*-Ir(tpy)$_3$**	0.036	0.15	2.4	64
***fac*-Ir(dfppy)$_3$**	0.43	1.6	2.7	3.6
***mer*-Ir(dfppy)$_3$**	0.053	0.21	2.5	45

1-4. Photochemical *mer* to *fac* one-way isomerization

mer-Ir(ppy)$_3$[4] and *mer*-Ir(dfppy)$_3$[14] are photochemically isomerized to the corresponding *fac* isomers. It was proposed that photochemical isomerization occurs through the state requiring thermal activation (Figure 1-10).[14]

The first generated excited state is ^{1}MLCT state, then, this intersystem crosses to ^{3}MLCT state. From ^{3}MLCT state, phosphorescence and vibrational nonradiative decay occurs. Thermal activation in the equilibrium from ^{3}MLCT state to ^{3}LF state (i.e. d-σ* state) leads to photochemical isomerization. The transition from ^{3}LF state to the ground state is forbidden and therefore is not emissive.

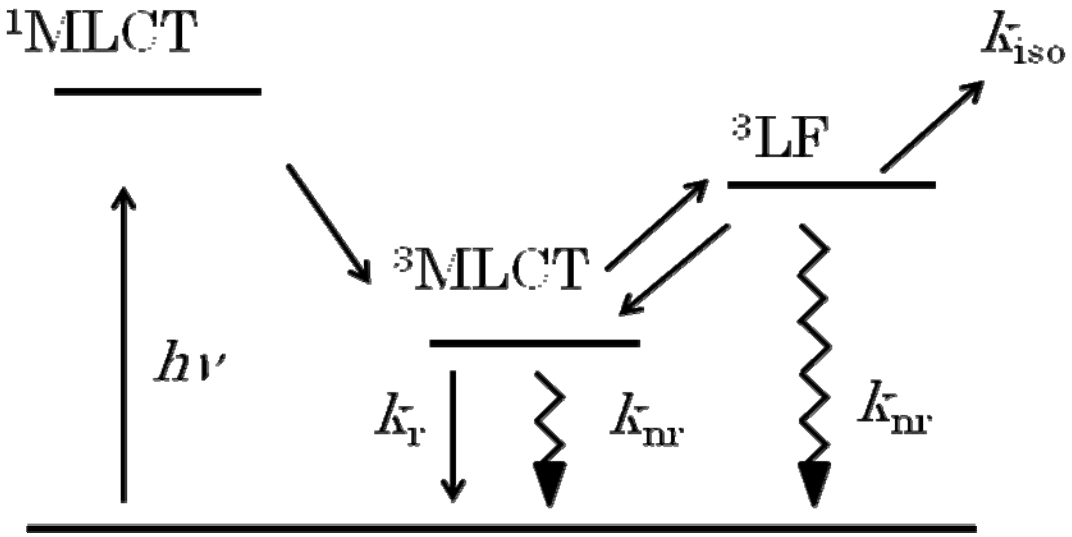

Figure 1-10. A scheme showing the excited states, and responsible state for photochemical isomerization (adopted from *Chem. Lett*. **2003**, *32*, 886-887).

The luminescent property and the isomerization quantum yields of Ir complexes having two kinds of ligand have been investigated (Figure 1-11, Table 1-3).[15] *mer*-Ir(tpy)$_3$ showed inefficient photochemical isomerization (Φ_{ISO} = 1.8 $\times$ 10^{-4}). It has been reported that the isomerization occurs from ^{3}LF excited state which is produced by thermal activation for *mer*-Ir(tpy)$_3$. *mer*-Ir(ppz)$_3$ also showed the efficient photochemical isomerization (Φ_{ISO} = 0.072). It is also thought that the thermal activation to ^{3}LF state is very high in *mer*-Ir(ppz)$_3$ and the phosphorescent quantum yield becomes very small. In this study, it was proposed that the axial bond property was responsible in photochemical isomerizaton ratio. Therefore, the photochemical isomerization was occurred by axial Ir-N bond rapture. In the case of Ir(tpy)$_3$, *mer* isomer, which also show photochemical isomerzation, has lower phosphorescent quantum yield than the *fac*-isomer, and the Φ_{ISO} of *mer*-Ir(ppz)$_3$, which emits negligible phosphorescence, is much larger than *mer*-Ir(tpy)$_3$. Ir complexes having high Φ_{ISO} value tend to low phosphorescent quantum yield and seems that isomerization process relates to nonradiative deactivation process. Understanding of the photochemical isomerization mechanism may be useful to improve phosphorescent quantum yield.

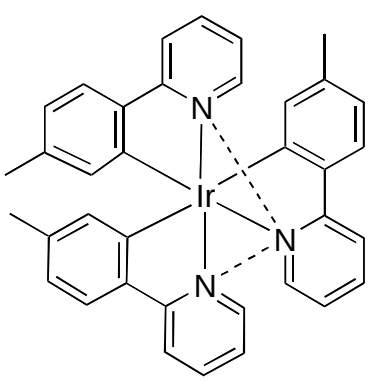

mer-Ir(tpy)$_3$

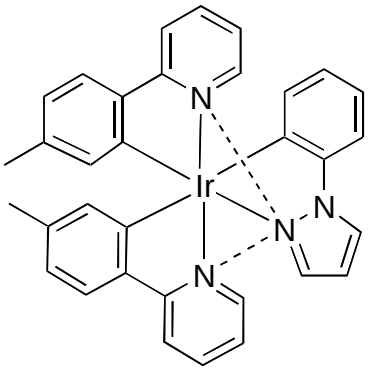

mer-Ir(tpy)$_2$(ppz)

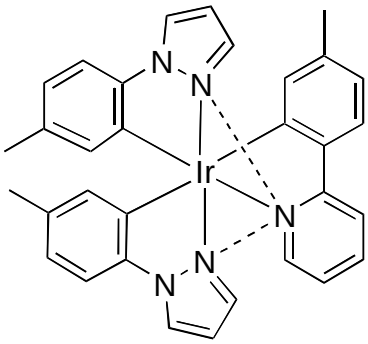

mer-Ir(tpy)(ppz)$_2$

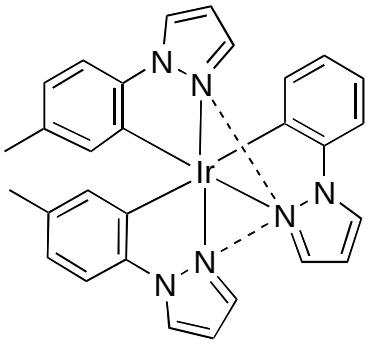

mer-Ir(ppz)$_3$

Figure 1-11. Structures of *mer*-Ir(tpy)$_3$, *mer* Ir(tpy)$_2$(ppz), *mer*-Ir(tpy)(ppz)$_2$, and *mer*-Ir(ppz)$_3$.

Table 1-3. Phosphorescence and isomerization properties in THF at 298 K (adopted from *Chem. Phys. Lett.* **2006,** *424*, 353).

Complex	Ir(tpy)$_3$	Ir(tpy)$_2$(ppz)	Ir(tpy)(ppz)$_2$	Ir (ppz)$_3$
Meridional				
τ / μs	0.24	0.064	0.40	No
Φ_P	0.062	0.012	0.068	Emission
Φ_{iso}	1.8×10^{-4}	2.8×10^{-4}	0.012	0.072
Facial				
τ / μs	1.7	1.5	1.8	No
Φ_P	0.39	0.35	0.37	Emission

1-5. Difficulty of obtaining a blue phosphorescent material

For full color display, red, green, and blue colors are required. Although *fac*-Ir(ppy)$_3$ emits strong green phosphorescence and *fac*-Ir(piq)$_3$ emits red phosphorescence, *fac*-Ir(dfppy)$_3$ emits greenish blue color phosphorescence. Pure blue color phosphorescence color is difficult to obtain. One of the strong candidate is Ir(ppz)$_3$, however, it does not emit efficiently at an ambient temperature (see Figure 1-6). To clarify why Ir(ppz)$_3$ is not emissive at room temperature, and a finding of alternative highly blue phosphorescent material for fabricating a high performance full color OLED display are aim of this research. In 2005, relatively highly blue phosphorescent Ir complexes having imidazole based carbene ligand have been reported by T. Sajoto, *et. al*. (Φ_{PL} of *fac*-Ir(pmb)$_3$ and *mer*-Ir(pmb)$_3$ is 0.04 and 0.002 in solution respectively)[6] and reported phosphorescent quantum yield of *fac*-Ir(pmb)$_3$ have been revised in 2009 (Φ_{PL} of *fac*-Ir(pmb)$_3$.is 0.37 in solution).[17] Investigation and improvement this type of Ir complexes is also one of my subject (chapter 3).

1-6. Major purpose of this study

Ir complexes are attractive materials for fabrication OLED device as mentioned above. Their photophysical and photochemical property is still obscure. To obtain highly blue color phosphorescent Ir complexes is also still not achieved. The understanding of the excited state of Ir complexes is very important to obtain Ir complexes with highly phosphorescent performance.

I was interested in why *mer* isomers tend to show low phosphorescent quantum efficiency than *fac* isomer. I thought that understanding the photochemical geometrical isomerization mechanism is efficient to obtain answer and accounting for photochemical enantioselective isomerization with geometrical isomerization may clarify the photochemical isomerization mechanism. The usual Ir complexes synthesized by thermal or photochemical reaction are racemic compound and no chirality is observed at the measurement of photochemical geometrical isomerization. To distinguish chilality of Ir complexes, I adopted the chiral HPLC analysis. I synthesized racemic *fac* and *mer*-Ir(ppz)$_3$ by literature method and carried out the enantiomeric separation by using chiral HPLC from racemic Ir complexes. The isolated

enantiomer is then photochemically or thermally isomerized and the chilality of the resulting isomers is carefully analysed. The experimental procedure, results and discussion are descried in chapter 2.

Next I tried to obtain highly blue phosphorescent Ir complexes. I interested in the Ir carbene type complexes (see 1-5). To improve phosphorescent property and understanding ther photophysical and photochemical property, Ir carbene complexes having several funcutional groups were studied The experimental procedure, results and discussion are descried in chapter 3

1-7. References

[1] C. W. Tang, S. A. VanSlyke, *Appl. Phys. Lett.* **1987,** 51(12), 913.

[2] J. Kido, *All of Organic electroluminescence,* Nippn Jitsugyo Publishing, 2003

[3] K. A. King, P. J. Spellane, R. J. Watts, *J. Am. Chem. Soc.* **1985**, 107, 1431-1432.

[4] A. Tamayo, B. D. Alleyne, P. I. Djurovich, S. Lamansky, I. Tsyba, N. N. Ho, R. Bau, M. E. Thompson, *J. Am. Chem. Soc.* **2003**, *125*, 7377–7387.

[5] Y. Sasaki (Ed.), *Photochemistry of metal complexes.* Sankyo Publishing year.

[6] F. Alary, J.-L. Heully, L. Bijeire, P. Vicendo, *Inorg. Chem*. **2007**, *46*, 3154-3165.

[7] a) Demas, J. N.; Harris, E. W.; McBride, R. P. *J. Am. Chem. Soc.* **1977**,*99*, 3547, b) Demas, J. N.; Harris, E. W.; Flynn, C. M.; Diemente, D. *J.Am. Chem. Soc.* **1975**, *97*, 3838, c) Gao, R.; Ho, D. G.; Hernandez, B.;Selke, M.; Murphy, D.; Djurovich, P. I.; Thompson, M. E. *J. Am. Chem.Soc.* **2002**, *124*, 14828.

[8] a) M. C. DeRosa, P. J. Mosher, G. P. A. Yap, K.-S. Focsaneanu, R. J. Crutchley, C. E. B. Evans, *Inorg. Chem*. **2003**, *42*, 4864-4872, b) M. C. DeRosa, D. J. Hodgson, G. D. Enright, B. Dawson, C. E. B. Evans, R. J. Crutchley, *J. Am. Chem. Soc*. **2004**, *126*, 7619-7626, c) L. Huynh, Z. Wang, J. Yang, V. Stoeva, A. Lough, I. Manners, M. A. Winnik, *Chem. Mater.* **2005**, *17*, 4765-4773, d) S. M. Boriso, I. Klimant, *Anal. Chem.* **2007**, *79*, 7501-7509.

[9] Q. Zhao, T. Cao, F. Li, X. Li, H. Jing, T. Yi, C. Huang, *Organometallics*, **2007**, *26*, 2077-2081.

[10] a) K. K.-W. Lo, D. C.-M. Ng, C.-K. Chung, *Organometallics*, **2001**, *20*, 4999-5001, b) L.-L.

Wu, C.-H. Yang, I-W. Sun, S.-Y. Chu, P.-C. Kao, H.-H. Huang, *Organometallics,* **2007**, *26*, 2017-2023.

[11] a) S. Lamansky, P. Djurovich, D. Murphy, F. A.-Razzaq, H.-E. Lee, C. Adachi, P. E. Burrows, S. R. Forrest, M. E. Thompson, *J. Am. Chem. Soc.* **2001**, *123*, 4304-4312, b) A. Tsuboyama, H. Iwawaki, M. Furugori, T. Mukaide, J. Kamatani, S. Igawa, T. Moriyama, S. Miura, T. Takiguchi, S. Okada, M. Hoshino, K. Ueno, *J. Am. Chem. Soc.* **2003**, *125*, 12971-12979.

[12] P. Jeffrey Hay, *J. Phys. Chem. A* **2002**, *106,* 1634-1641.

[13] Y. You, S. Y. Park, *J. Am. Chem. Soc*. **2005**, *127,* 12438-12439.

[14] T. Karatsu, T. Nakamura, S. Yagai, A. Kitamura, M. Matsushima, Y. Hori, T. Hagiwara, *Chem. Lett.* **2003**, *32*, 886–887.

[15] T. Karatsu, E. Itoh, S. Yagai, A. Kitamura, *Chem. Phys. Lett.* **2006**, *424*, 353–357.

[16] a) T. Sajoto, P. I. Djurovich, A. B. Tamayo, M. Yousufuddin, R. Bau, M. E. Thompson, R. J. Holmes, S. R. Forrest, *Inorg. Chem.* **2005**, *44*, 7992–8003. b) b) T. Sajoto, P. I. Djurovich, A. B. Tamayo, J. Oxgaard, A. A. Goddard III, M. E. Thompson, *J. Am. Chem. Soc*, **2009**, *131*, 9813–9822.

Chapter 2

Chirality in the Photochemical *mer*→*fac* Geometrical Isomerization of Tris(1-phenylpyrazolato,*N*,$C^{2'}$)iridium(III)

2-1. Abstract

Irradiation of the optically resolved *mer*-Δ- isomer of tris(1-phenylpyrazolato,*N*,$C^{2'}$)iridium(III) with 366-nm light in CH_3CN purged with argon at 25 °C gave 59% *fac*-Δ and 41% *fac*-Λ (18%*ee*) at the end of geometrical isomerization. Formation of the intermediate *mer*-Λ species was not observed, this is quite characteristic when compared with the corresponding thermal isomerization reaction. This enantiomeric photoisomerization is rationally explained by a mechanism based on Ir–N bond dissociation at the top or bottom axial ligand. This reaction mechanism is explained by the potential energy surface of the triplet excited state.

2-2. Introduction

Iridium triscyclometalated complexes have recently attracted significant attention because of their supreme phosphorescence performance for OLEDs (organic light-emitting diodes).[1–5] For those materials, understanding of the behavior of the excited states including radiative and nonradiative processes are very important to prepare complexes with high emission efficiency and stability. Triscyclometalated complexes such as tris(2-phenylpyridinato,*N*,$C^{2'}$)iridium(III) [$Ir(ppy)_3$] have meridional (*mer*) and facial (*fac*) geometrical isomers. The *fac* isomer is the thermodynamically controlled product in their synthesis and is generally strongly phosphorescent, whereas the corresponding *mer* isomer is the kinetically controlled product and weakly phosphorescent in solution at ambient temperature. Although several reports on the preparation of *mer* isomers have recently appeared for iridium complexes, their photochemical properties remains unclear.[6,7] Among them, tris(1-phenylpyrazolato,*N*,$C^{2'}$)- iridium(III) [$Ir(ppz)_3$, Scheme 1] is

interesting material to study, as both the *mer* and *fac* isomers give no phosphorescence in solution at ambient temperature.[6,7] The main reason for this was reported to be the location of the thermally equilibrated nonradiative excited state just above the emissive state,[8,9] and the absence of phosphorescence from the *mer* isomer is partly due to the *mer*→*fac* geometrical isomerization.[6,7] $Ir(ppz)_3$ is reasonably phosphorescent in the solid phase, and therefore, a blue-emitting OLED device has been fabricated.[10] In addition, $Ir(ppz)_3$ is not only used as a part of a dopant to give white emission,[11] but it is also used as a material for electron blocking layer.[12]

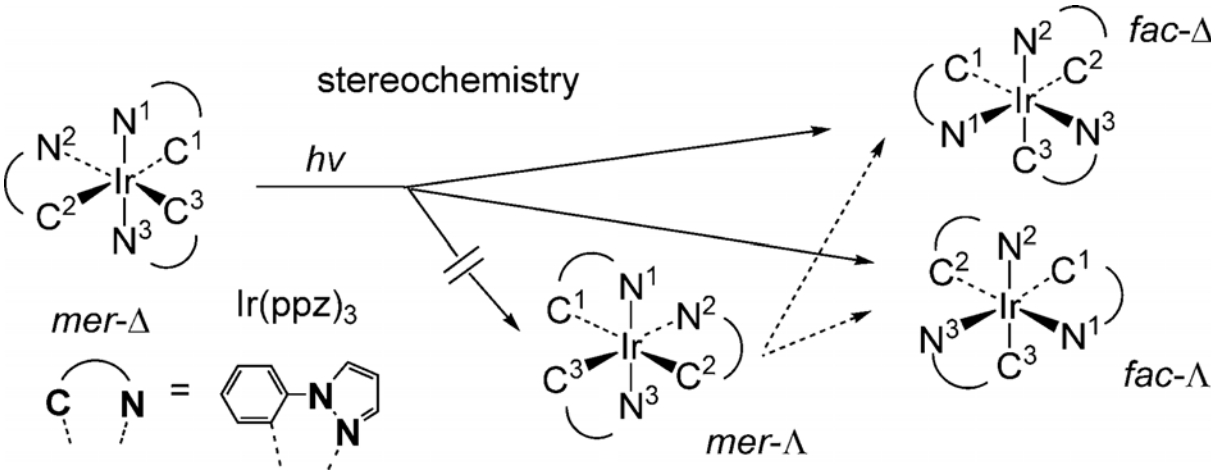

Scheme 1. Enantiomers and geometrical isomers in the photochemical isomerization of $Ir(ppz)_3$.

In this work, how the chirality of the *mer* isomer is transferred to the *fac* isomer in the photochemical *mer*→*fac* geometrical isomerization of $Ir(ppz)_3$ was investigated. Interestingly, it was found that the intermediate *mer*-Λ is not generated upon irradiation of *mer*-Δ. This cannot be explained by faster *mer*→*fac* isomerization than *mer*-Δ→*mer*-Λ isomerization, that is, the two processes are not parallel. The isomerization seems to proceed through a ligand dissociation association mechanism, and as a result, the geometrical isomerization must accompany the optical isomerization. Once *mer*-Λ is produced by the irradiation of *mer*-Δ, both isomers behave similarly. Thus, selective disappearance of only *mer*-Λ does not occur. In this chapter, plausible mechanism based on DFT calculations is proposed.

2-3. Result and discussion

2-3-1. Synthesis, enantiomaeric separation, and CD spectra measurement

$Ir(ppz)_3$ was synthesized according to the method reported previously (Scheme 2-1).[8]

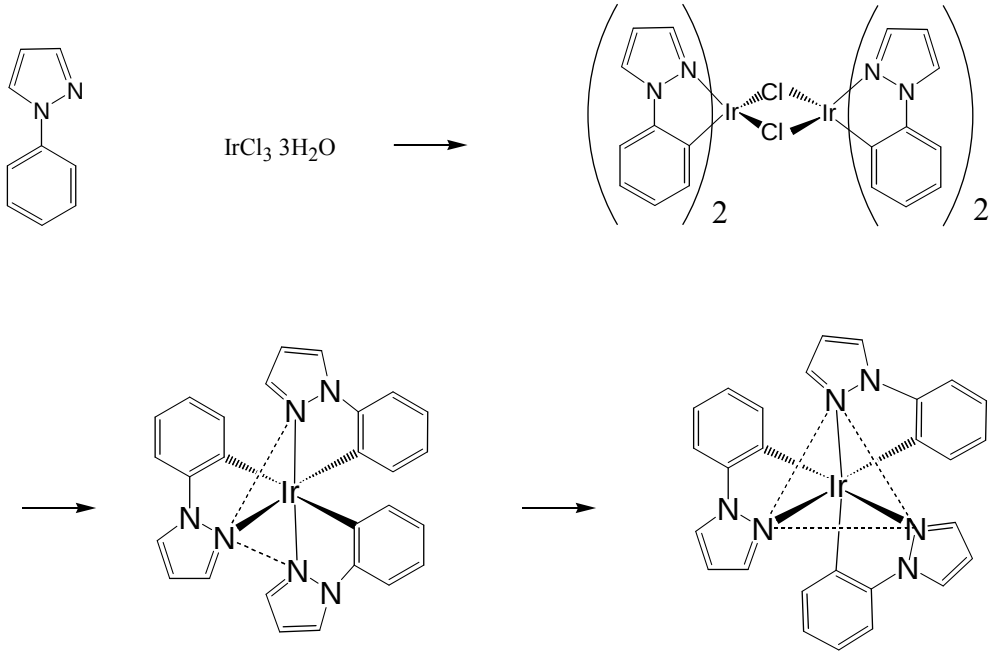

Scheme 2-1. Syntheses of racemic *mer*-$Ir(ppz)_3$ and racemic *fac*-$Ir(ppz)_3$.

The *mer* and the *fac* isomers were separated by using conventional column chromatography, and both isomers were optically resolved to their Λ and Λ isomers (isomeric purity >98%) by using semi-preparative chiral HPLC. Here, optical isomers having shorter and longer retention times in the HPLC can be determined as the Δ and Λ isomers, respectively, by comparing their circular dichroism (CD) spectra with those reported for the optically resolved diastereomeric $Ir(ppy)_3$ derivatives (abbreviated to $Ir(pppy)_3$), chiralities of which were determined by X-ray crystallography.[13–16] (The comparision was also done to the enantiomers of *fac*-$Ir(ppy)_3$ I separated and the first peak compound on HPLC was assigned to the Δ isomer and the second peak compound was assigned to the Λ isomer. Δ isomer of $Ir(pppy)_3$ has a negative CD signal at the wavelength region from 370 nm to 500 which dichloism is seemed to be derived from the ^{1}MLCT absorption and Λ isomer of $Ir(pppy)_3$has a positive CD signal at the same region. The first peak compound of *fac*-$Ir(ppz)_3$, *mer*-$Ir(ppz)_3$, and *fac*-$Ir(ppy)_3$ on HPLC also have a negative CD signal at the

[1]MLCT absorption region and assigned to Δ isomer. The CD spectra of the *mer*-Δ, *mer*-Λ, *fac*-Δ, and *fac*-Λ isomers of Ir $(ppz)_3$ in CH_3CN are shown in Figure 2-1. The CD spectra of the enantiomers showed good mirror images of each other for both the *mer* and *fac* isomers. In Figure 2-2 and Figure 2-3, the CD spectra of *mer*-Ir$(ppy)_3$ and the CD spectra of *fac*-Ir$(pppy)_3$ are also depicted.

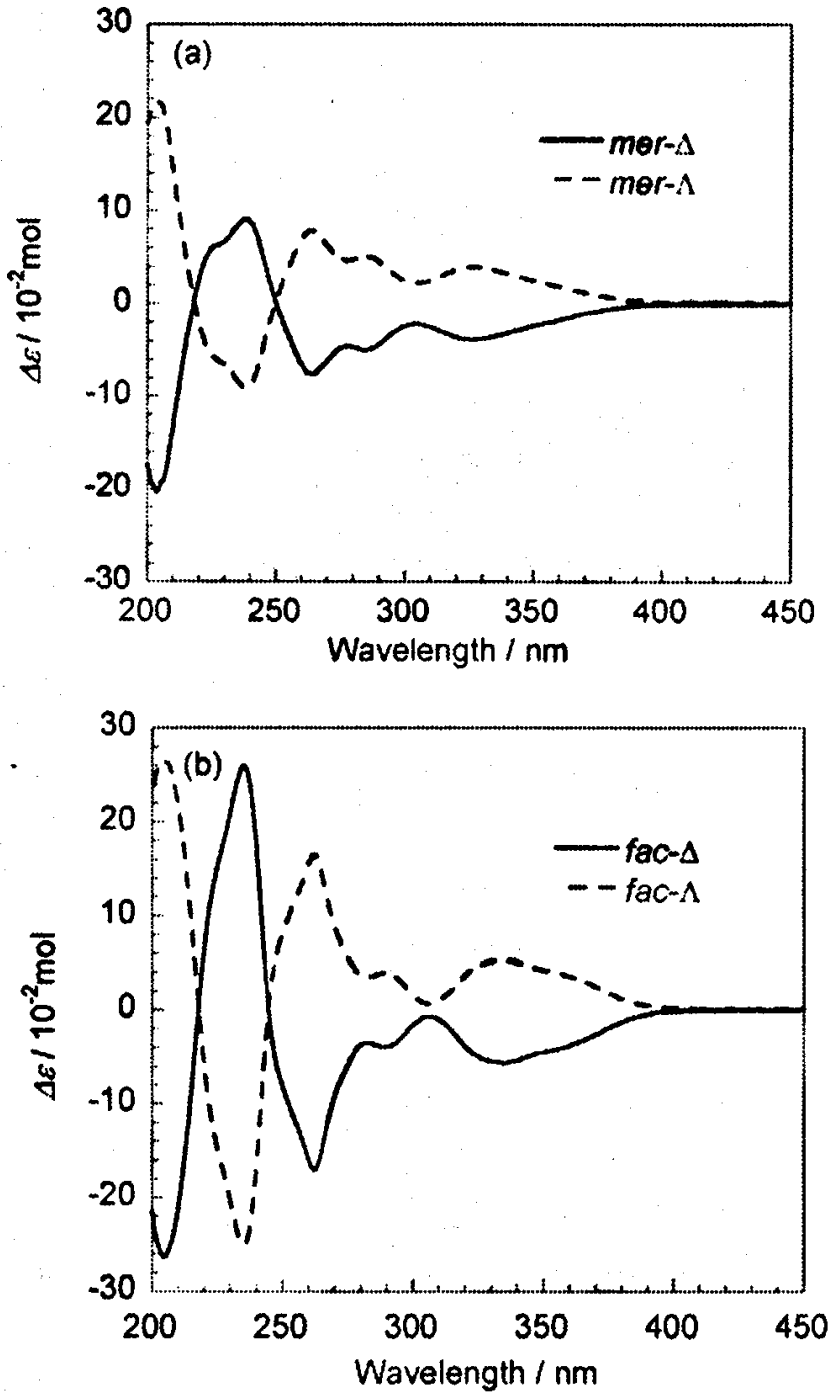

Figure 2-1. CD spectra of enantiomers of (a) *mer*-Ir$(ppz)_3$ and (b) *fac*-Ir$(ppz)_3$ in CH_3CN.

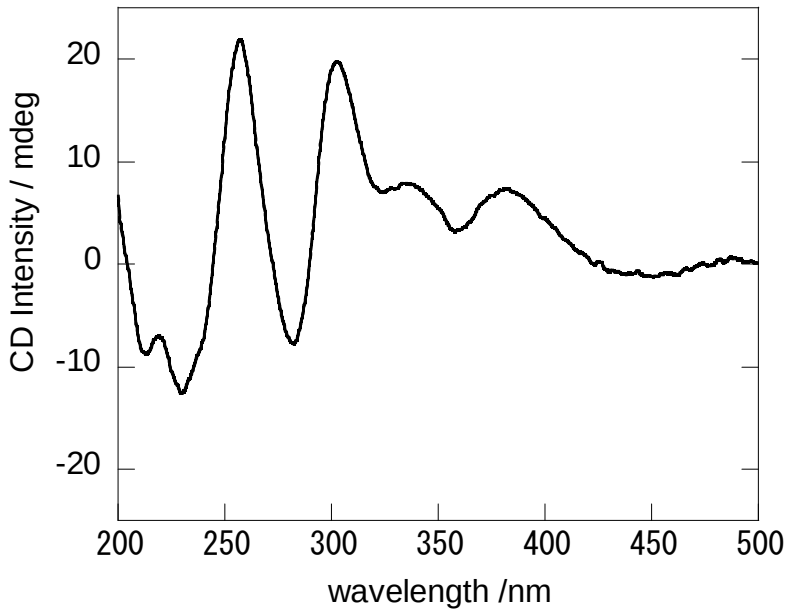

Figure 2-2. CD spectrum of Δ-*mer*-Ir(ppy)$_3$

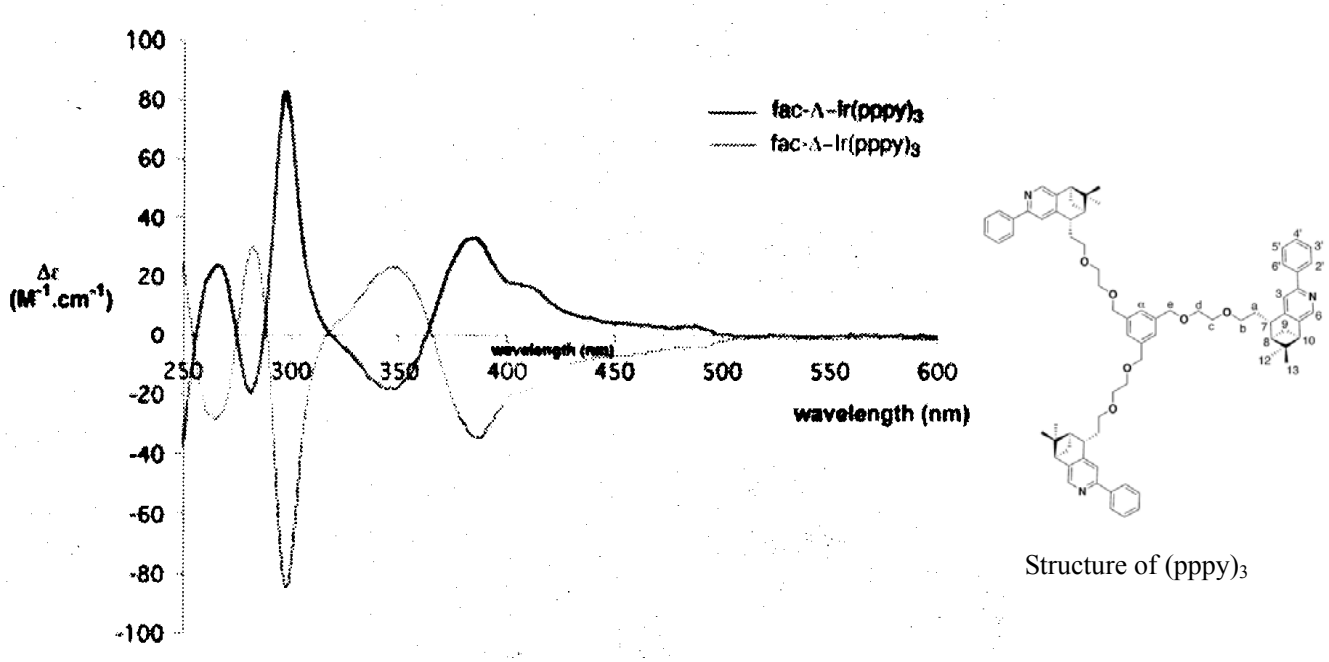

Figure 2-3. CD spectra of *fac*-Δ-Ir(pppy)$_3$ and *fac*-Λ-Ir(pppy)$_3$ (298 K, in CH_2Cl_2). (*J. Am. Chem. Soc.* **2004**, *126*, 9339.)

2-3-2. Phothchemical isomerization of each enantiomers

Each isomer (*mer*-Δ, *mer*-Λ, *fac*-Δ, and *fac*-Λ) was irradiated in CH_3CN purged by argon by using a 1 cm ×1 cm quartz cuvette by a 366-nm mercury lamp. The isomerization can be followed by HPLC (Figure 2-4, 2-5, 2-6), CD spectroscopy (Figure 2-7-a,b) or UV/Vis absorption (Figure 2-8),

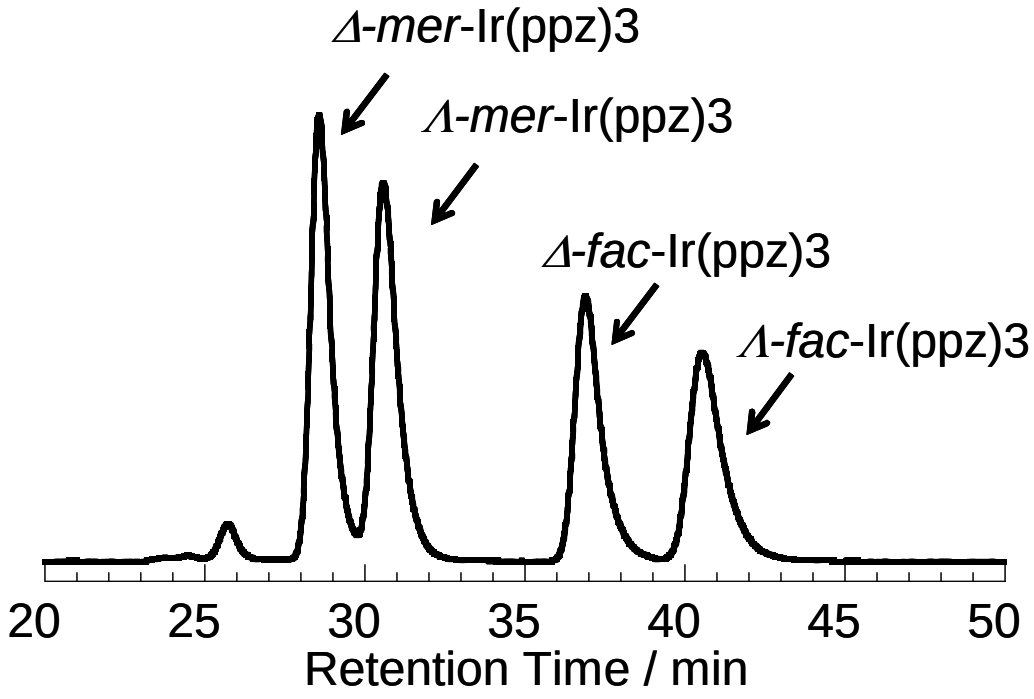

Figure 2-4. HPLC chart of enantiomers of *mer*- and *fac*-$Ir(ppz)_3$ obtained using the normal silica gel column (ϕ = 1.0 cm) and *chiral pak AD-H* (ϕ = 1.0 cm) linked in this order. The eluent was a mixture of hexane and ethanol (98:2).

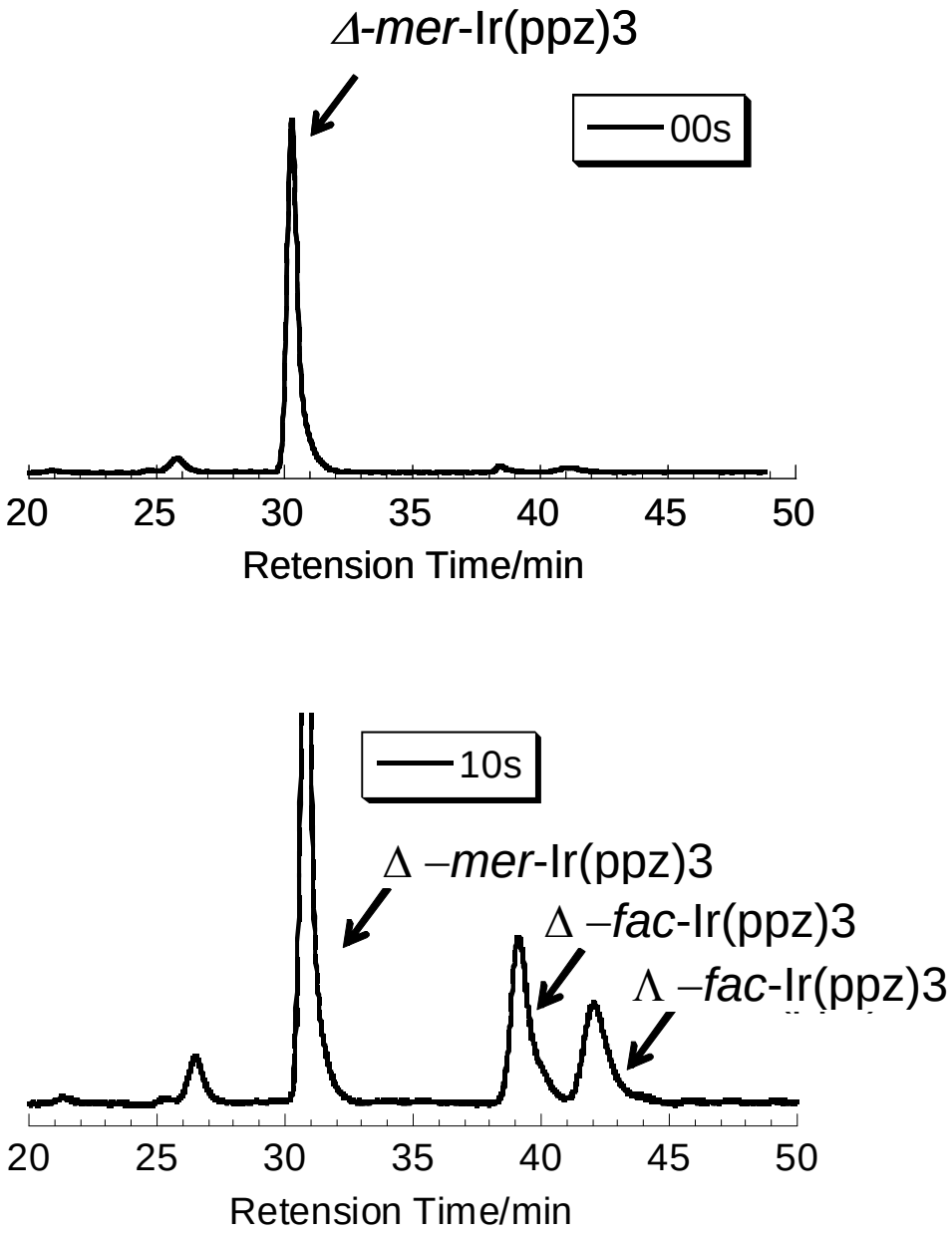

Figure 2-5. Photochemical isomerization of *mer*-Δ-Ir(ppz)$_3$ analysed by HPLC. The normal silica gel column (ϕ = 1.0 cm) and *chiral pak AD-H* (ϕ = 1.0 cm) were linked in this order. The eluent was a mixture of hexane and ethanol (98:2).

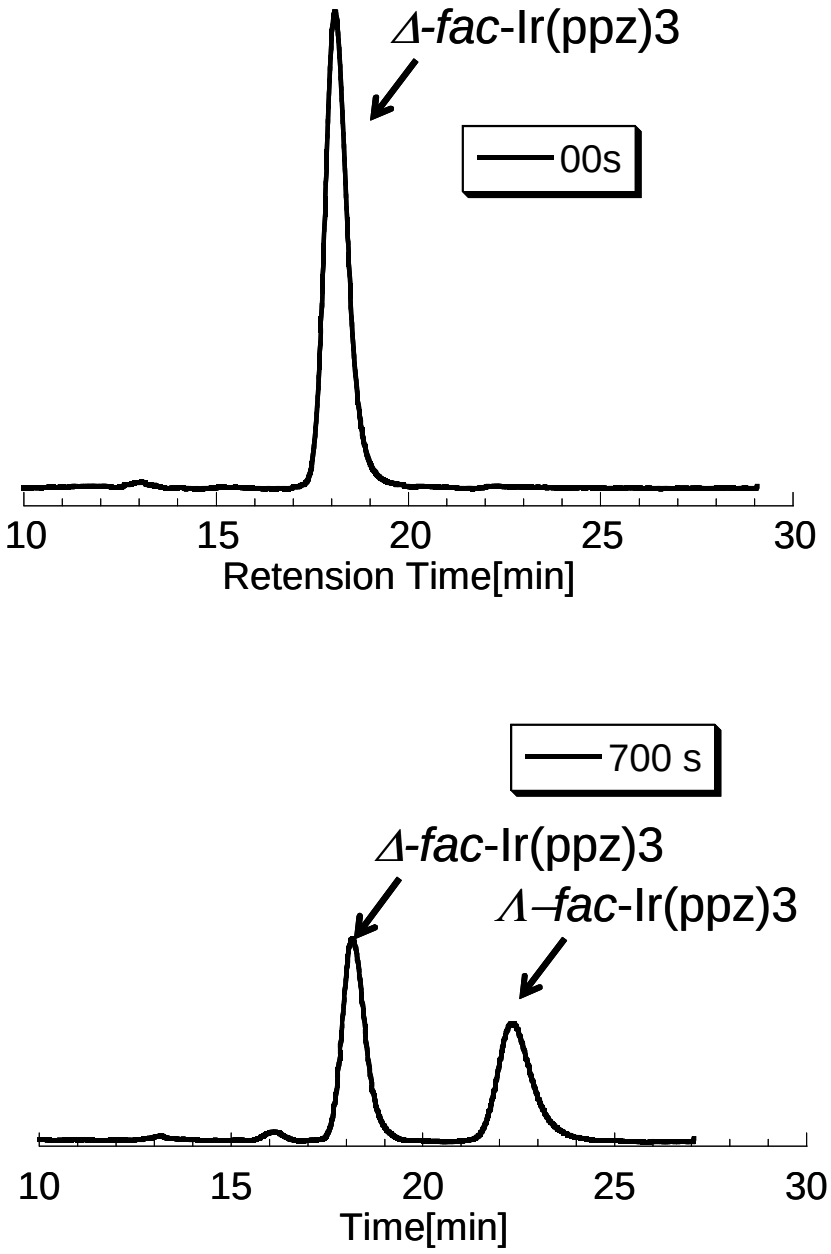

Figure 2-6. Photochemical isomerization of *mer*-Δ-Ir(ppz)$_3$ analyzed by HPLC. The normal silica gel column (ϕ = 1.0 cm) and *chiral pak AD-H* (ϕ = 1.0 cm) were linked in this order. The eluent was a mixture of hexane and ethanol (98:2).

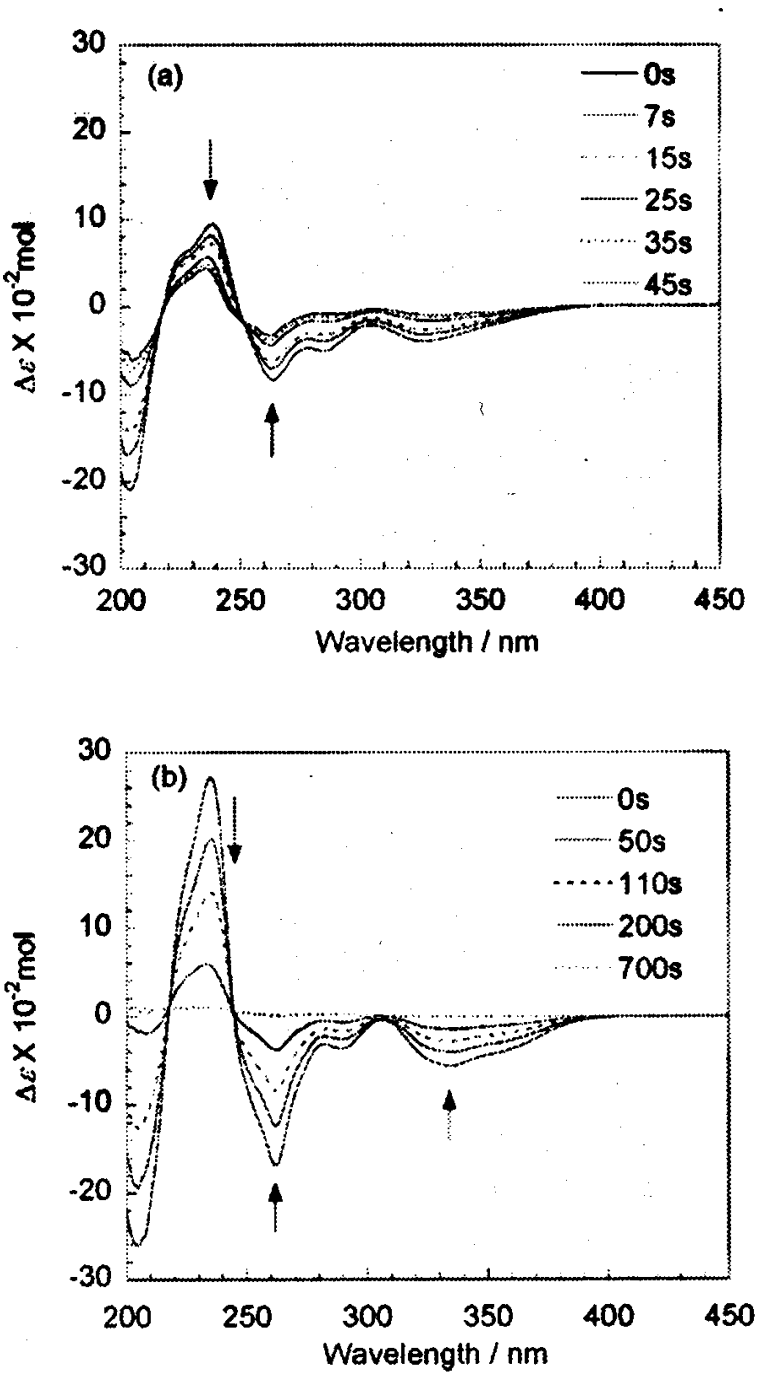

Figure 2-7. (a) CD spectral changes of the enantiomers of *mer*-Δ and (b) *fac*-Δ during photoirradiation by 366nm light.

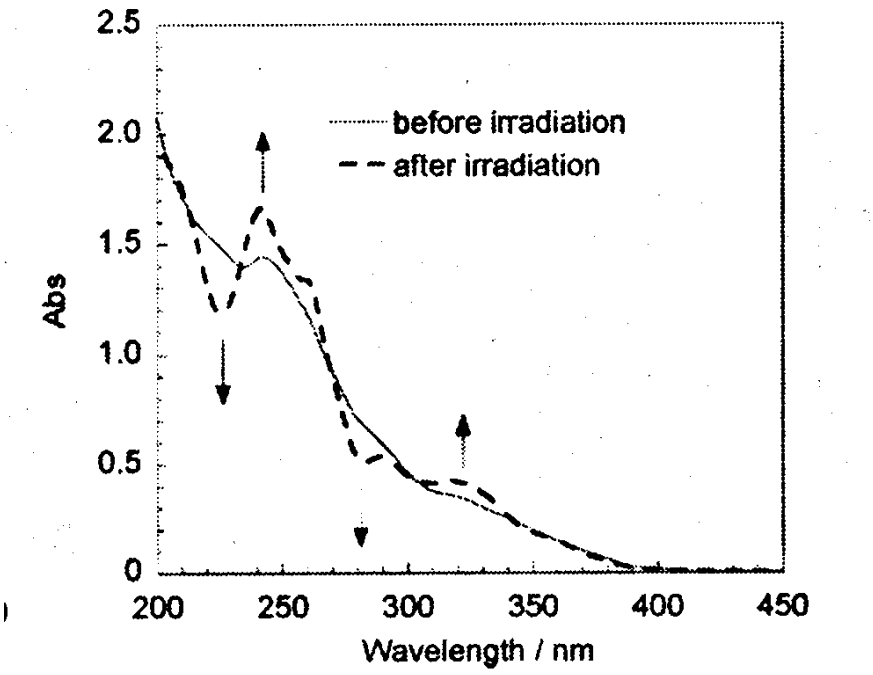

Figure 2-8. UV absorption spectral change before and after irradiation of *mer*-Δ

The enantiomer excess (*ee*) values were determined by both chiral HPLC and CD spectroscopy, and those values essentially matched within experimental errors. Surprisingly, the irradiation of the *mer*-Δ isomer gave 59% *fac*-Δ and 41% *fac*-Λ (18%*ee*) at 25 °C at the end of geometrical isomerization. When isomerization is followed by CD spectra, the CD signal decreases in its intensity as shown in Figure 2-7a, and it does not completely disappear even at the end point of the geometrical isomerization achieved by the 45 s irradiation. Surprisingly, no formation of the *mer*-Λ isomers was observed during the geometrical isomerization (Figure 2-5, 2-9).

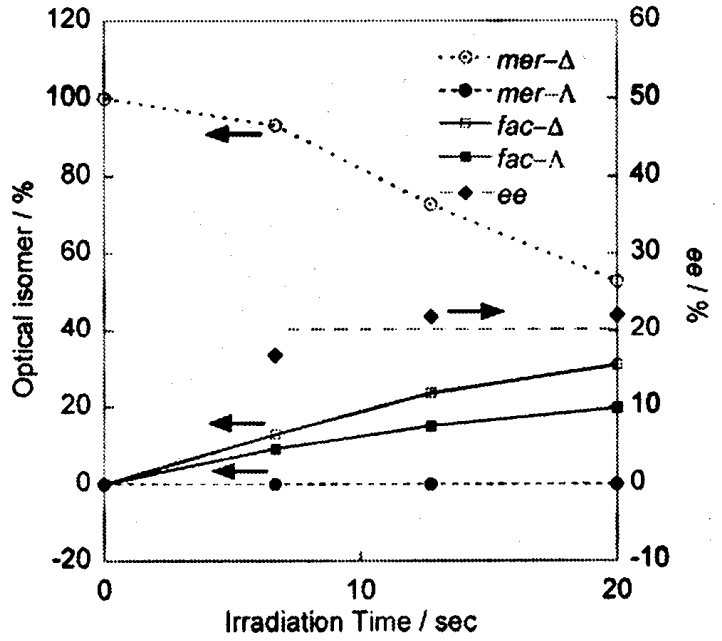

Figure 2-9. Conversion and formation of the optical isomer by irradiation and their enantiomer excess value.

To further surprise, enantioselectivity increased with temperature. Both of the *ee* and Φ*mer*→*fac* values increased as follows: 14%*ee*, Φ = 0.065 at –35 °C, 18%*ee*, Φ = 0.072 at 25 °C, and 23%*ee*, Φ = 0.073 at 70 °C. This phenomenon occurred similarly for the other enantiomers, that is, the irradiation of *mer*-Λ gave 18%*ee* of *fac*-Λ. Prolonged irradiation of the enantiomerically enriched solution of the *fac* isomers for 700 s gave complete racemization at all temperatures examined. The Δ-*fac* to Λ-*fac* racemization quantum yield in CH_3CN was 0.0041 at 25 °C, which value is much smaller than the *mer* to *fac* geometrical isomerization quantum yield and the enatioselectivity is certainly 23%ee.

2-3-3. Discussion of Photochemical isomerization mechanism

For the understanding of the photochemistry of the transition- metal complexes including triscyclometalated complexes, Adamson's empirical rule[17] and VC (Vanquickienborne–Ceulemans) theory[18] have been widely applied. The VC theory quantum chemically extends the selection rule by using the angular overlap model,[18c,18d] which includes not only σ-bond interaction but also π-bond interaction between the central Ir metal and the ligands. Photochemical substitution reactions of octahedral complexes obey two rules.

(i) The leaving ligand is located on the axis characterized by the weakest ligand field (LF).

(ii) The leaving ligand on the labialized axis is the one exhibiting the strongest LF.

In the case of *mer*-Ir(ppz)$_3$, there are three axes, and each axis has a pair of terminal coordination of (N,N), (N,C), and (C,C) to the central iridium atom. Therefore, the weakest LF combination is the N–Ir–N axis, which is photoactive. For this axis, both N–Ir bonds are the same, and thereby, the second rule is negligible. Recently the properties of a series of iridium triscyclometalated complexes composed of 4-toluylpyridine (tpy) and 1-phenylpyrazole (ppz) ligands were reported.[7b] The values of $\Phi_{mer\rightarrow fac}$ depend on the kind of axial ligands. Complexes possessing two ppz ligands such as Ir(ppz)$_3$ and Ir(ppz)$_2$ (tpy) have higher $\Phi_{mer\rightarrow fac}$ (0.12 and 0.072, respectively) values than Ir(tpy)$_3$ and Ir(tpy)$_2$(ppz) complexes (1.8×10^{-4} and 2.3×10^{-4}, respectively). These results indicate that the bond dissociation occurs at the axial ligand, which matches the above rule, and the reason is not simply that the ppz ligand is much more labile than the ppy ligand. In a separate experiment, the irradiation of *fac*-Δ did not produce *mer* isomers but instead produced *fac*-Λ with a quantum yield of 0.004 as mentioned above (this is ca. 1/18 of that of the geo- metrical isomerization). This photochemical reaction induced complete racemization (equal amounts of the enantiomers). If the reaction starts from the *fac*-Δ isomer, the CD signal disappears completely after irradiation for 700 s (Figure 2-7). This reaction may proceed through the Bailer twist mechanism as proposed for Ru complexes, because the racemization quantum yields are of the same order.[19] This inefficient twisting is not the main deactivation process of excitation energy. Nonradiative deactivation via

a thermally accessible dd state might be an important route.[20] I also tried to rationalize the mechanism of the present isomerization. Route A and B in Figure 2-8 proceed by Ir–N^1 and Ir–N^3 bond dissociations of the axial ligands, respectively, and these reactions proceed through rehybridization from square pyramidal (SP) to trigonal bipyramidal (TB) intermediates.[18] On the basis of statistical treatment of this mechanism, *mer*-Δ gives 5:8 of the *mer*-Δ returning and 1:8 of each *mer*-Λ, *fac*-Δ, and *fac*-Λ isomer formation. This product distribution partly fits the experimental result of the thermal isomerization described later, but does not fit the photochemical isomerization data described above. To rationalize these experimental results, I propose a possible mechanism. The reaction proceeds through the A1 or B1 route (rectangles in Figure 2-8). An important point is that the dissociation of the two axial bonds, Ir–N^1 or Ir–N^3, results in the formation of different enantiomers of *fac*- Ir(ppz)$_3$. Route A2 is difficult because this gives the *mer*-Λ isomer, which was not experimentally observed. The difference between routes A1/B1 and A2/B2 is how the axial axis is chosen in a TB structure. TB in routes A1/B1 or A2/B2 has N–Ir–C or C–Ir–C axes, respectively. However, there are no rational reasons why A2 and B2 cannot occur. Therefore, the mechanism was modified so that the A2 and B2 routes proceed through rehybridization from the TB to SP intermediates. The C–Ir–C axis in TB is difficult to retain because of the strong *trans* effect. The TB intermediate rehybridizes to SP; recoordination of the N^1 or N^3 atom in the SP intermediate gives the *fac* isomer. The conversion from the C–Ir–C to C–Ir–N axis leads only to geometrical isomerization to form the *fac* isomer. Moreover, Ir–N^2 bond dissociation (equatorial ligand) does not lead to geometrical isomerization (Figure 2-9). Participation of solvent molecules after dissociation is expected, as proposed for the thermal isomerization.[21]

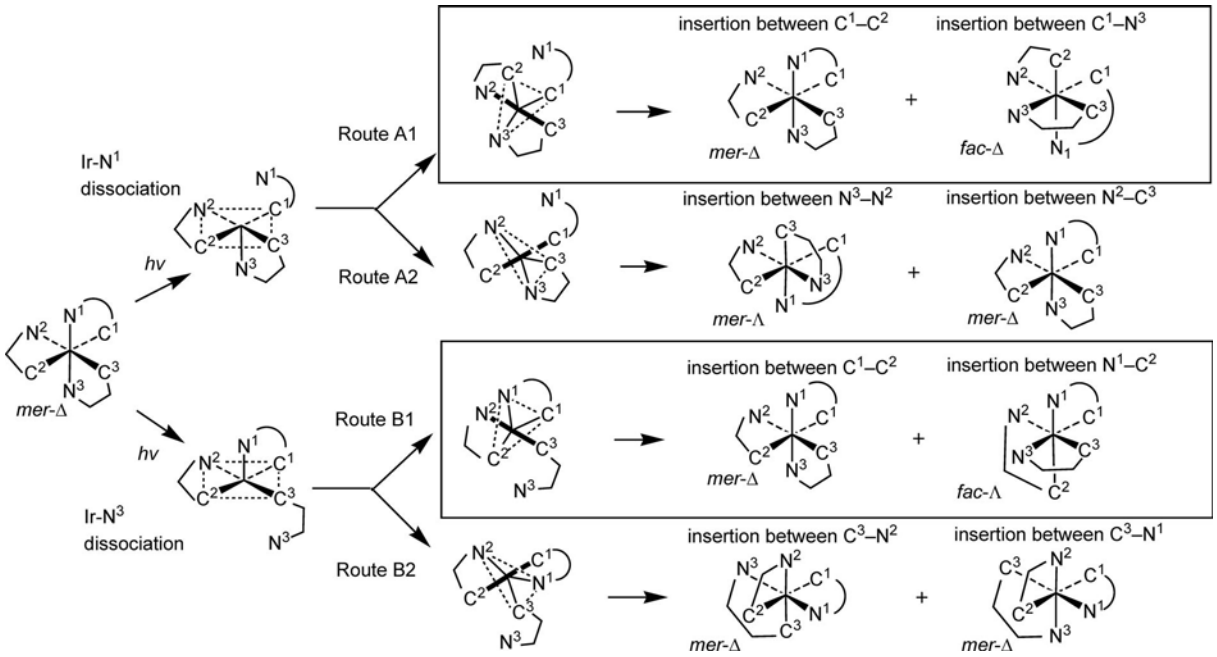

Figure 2-8. Plausible isomerization mechanism of chiral memorization in the geometrical isomerization of *mer*-Ir(ppz)$_3$ through trigonal bipyramidal intermediates. Central Ir atoms are omitted for clarity. See text for detailed explanation.

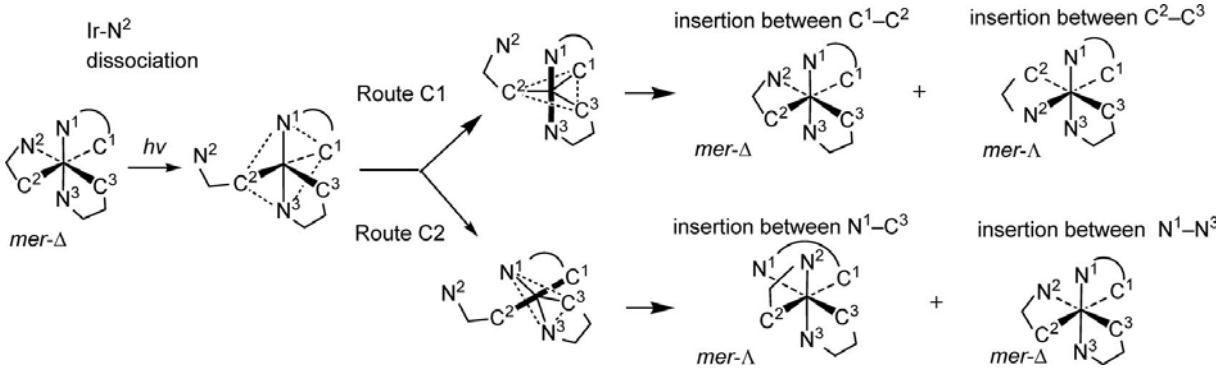

Figure 2-9. If the isomerization occurs through Ir-N^2 bond dissociation (equatorial ligand), it does not lead to geometrical isomerization.

2-3-4. Thermal isomerization

Examination of solvent effects is underway. This isomerization was examined under thermochemical

conditions. In refluxing dichlorobenzene at 180 °C for 8 h, chiral HPLC analyses indicated that 69% *mer*-Δ disappeared as a result of 55% ligand (ppz) dissociation from the complex; the formation of 9% *mer*-Λ, 1.6% *fac*-Δ, and 2.4% *fac*-Λ was also observed. Side products were formed; however, their quantitative analyses were difficult because of their low solubility. In any case, optical isomerization of the *mer* isomer occurred under thermal conditions, and this is in contrast to the results by photochemical isomerization.

2-3-5. The Potential surface of *mer*-Ir(ppz)$_3$ which axial Ir-N bond length is increased.

This plausible isomerization mechanism is rationalized by quantum chemical calculations (Figure 2-9). A UB3LYP/LANL2DZ calculation indicates that HSOMO (highest singly occupied MO) α-spin-122 and vacant MOs α-123, 124 energies are close. Bond elongation of one of the axial Ir–N bonds from the optimized structure leads to potential energy surface crossing to dissociative dd states. These HSOMO must have antibonding interactions between the Ir and axial N atoms, which is similar to the recent study of a decay process involving the tridentate ligand of an Ir complex.[20] The α-122 HSOMO orbital has metal-to-ligand charge-transfer character for the fully optimized structure as shown in Figure 2-9 (left-hand side), and the structure has Ir–N^1 and Ir–N^3 bond lengths of 2.05 and 2.04 Å, respectively, which match the values obtained by X-ray single crystal analysis (Ir–N^1 2.205 and Ir–N^3 2.013 Å).[6] In this structure, the lowest MO having an antibonding Ir–N bond is observed at α-132, and this is far above the HSOMO. However, optimized structures having elongated Ir–N^1 or Ir–N^3 bond lengths fixed at 2.80 Å have antibonding α-122 HSOMOs. In these structures, the Ir–N^2 and Ir–N^3 bond lengths were 2.14 and 2.27 Å for the former and the Ir–N^1 and Ir–N^2 bond lengths were 2.46 and 2.15 Å for the latter structure, respectively. Energy surface crossing as shown in Figure 2-9 leads to bond dissociation of the Ir–N^1 or Ir–N^3 bond, and this produces Λ-*fac* and Δ-*fac* isomers, respectively, as shown in Figure 2-9. The shape of the potential energy surface controls the direction of bond elongation (Ir–N^1 or Ir–N^3) and finally the *ee* values. Calculated potential energies for bond-elongated structures were 2.8 kcalmol–1 higher (Ir–N^1 2.80 Å) and 0.5 kcalmol–1 lower (Ir–N^3 2.80 Å) than the energy of the fully optimized structure. These single-point energy calculation results do not fit the results of the *ee* values, because it is preferable to proceed to the B route to give the *fac*-Δ isomer. More calculations for the whole potential energy surface

are necessary to obtain, for example, activation energies in the reaction coordinate. Those detailed calculations, including TD-DFT calculations, will be continued in our laboratory.

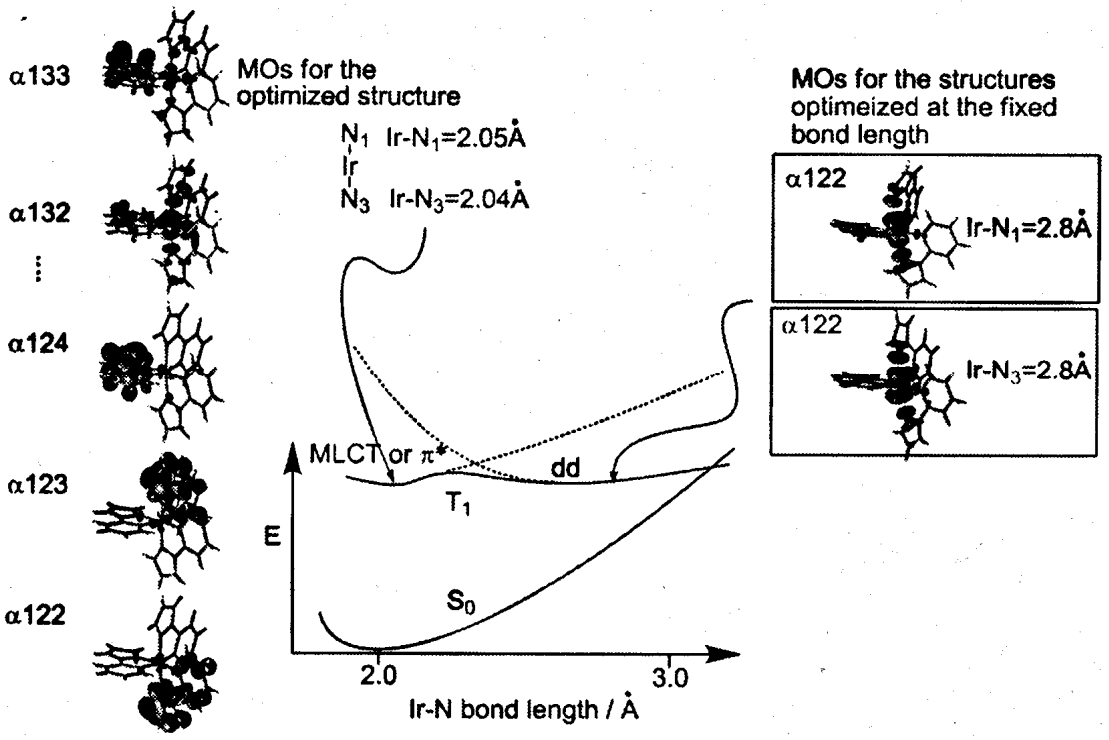

Figure 2-9. MOs and energy levels of *mer*-Ir(ppz)$_3$ calculated by UB3LYP/LANL2DZ. Positions of individual atoms in the structures match those shown in the structure on the left-most side of Figure 2-7.

2-4. Conclusions

In conclusion, Δ–Λ optical isomerization accompanied in photochemical *mer–fac* geometrical isomerization was investigated for optically resolved $Ir(ppz)_3$ in solution. Irradiation of the optically resolved *mer*-Δ isomer with 366-nm light in CH_3CN purged with argon at 25 °C gave 59:41 *fac*-Δ/*fac*-Λ (18%*ee*) at the end of geometrical isomerization. The lack of formation of the intermediate *mer*-Λ speciesis quits characteristic in comparison to the corresponding thermal isomerization process. This photoisomerization is rationally explained by a mechanism based on axial $Ir–N^1$ or $Ir–N^3$ bond dissociation–rehybridization–recoordination. Some DFT/UB3LYP calculation results of the triplet excited state rationally explain the selectivity of this isomerization. To obtain further understanding, the measurements of photochemical enantioselective isomerization of *mer*-$Ir(ppy)_3$, *mer*-$Ir(ppy)_2(ppz)$, and *mer*-$Ir(ppy)(ppz)_2$ is now underway.

2-5. Experimental Section

2-5-1. General Information and Material

All Chemicals used for synthesis were purchased from Aldrich, Kanto chemical, TCI, Wako Pure Chemical Industries, and Fluya metal and used without further purification. *mer*-$Ir(ppz)_3$ was prepared via the di-nuclear complex.[13] *fac*-Ir(ppz)3 was prepared from *mer*-Ir(ppz)3 by photochemical isomerization. ^1H NMR and ^{13}C NMR spectra were recorded on JEOL JNM-LA 400 and Bruker AVANCE 300. Mass spectra (FAB) were recorded on a JEOL JMS-AX500 double focusing mass spectrometer. In HPLC, the enantiomeric separations were performed on *chiral pak AD-H* (Daisel Chemical Industries). The peak was detected by photodiode array multi channel detector (JASCO MD-2015 Plus).

2-5-2. Synthesis

Tetrakis(2-phenylpyrazol-C^2,N')(μ-dichloro)diiridium : $[(ppz)_2Ir(\mu\text{-}Cl)]_2$

A mixture of $IrCl_3$ $3H_2O$ (1.0 g, 2.84 mmol), 2-phenylpyrazole (0.86 g, 5.94 mmol) 70 ml 2-ethoxyethanol and 23 ml of water was placed in a 200 ml flask, then degassed at the ambient temperature followed by injection nitrogen gas. The mixture was heated at 110 C for 20 h. The mixture was cooled to the ambient temperature and 30 ml of water was added, then the precipitate was filtrated and washed with water and methanol, then dried under reduced pressure gave 1.34 g of yellow solid. ^{1}H NMR (400 MHz, DMSO): δ = 8.93 (d, J = 2.4 Hz, 2 H), 8.79 (d, J = 2.4 Hz, 2 H), 8.44 (d, J = 1.7 Hz, 2 H), 8.09 (d, J = 2.2 Hz, 2 H), 7.59 (d, J = 7.0 Hz, 2 H), 7.54 (d, J = 7.0 Hz, 2 H), 6.95-6.81 (m, 8 H), 6.68-6.65 (m, 4 H), 6.17 (d, J = 7.5 Hz, 2 H), 5.79 (d, J = 7.2 Hz, 2 H) ppm.

***mer*-Ir(ppz)$_3$**

A mixture of $[(ppz)_2Ir(\mu\text{-}Cl)]_2$, 2-phenylpyrazole (0.40 g, 2.8 mmol), Na_2CO_3 (0.69 g, 6.5 mmol) and 80 ml of ethylene glycol was placed in a 200 ml flask, then degassed at the ambient temperature followed by injection nitrogen gas. The mixture was heated at 140 C for 20 h. The mixture was cooled to the ambient temperature and 80 ml of water was added, then the precipitate was filtrated and washed with water and methanol. The solid was dissolved by CH_2Cl_2 and short column chromatography using CH_2Cl_2, reprecipitation from CH_2Cl_2-methanol gave 0.47 g of pale yellow solid in 29 % yield. ^{1}H NMR (400 MHz, CDCl3): δ = 8.00 (dd, J = 2.4, 0.5 Hz, 1 H), 7.95 (dd, J = 2.9, 0.7 Hz, 1 H), 7.91 (dd, J = 2.6, 0.7 Hz, 1 H), 7.281 (dd, J = 7.7, 0.8 Hz, 1 H), 7.24 (dd, J = 10.0, 0.8 Hz, 1 H), 7.19 (dd, J = 13.7,0.8 Hz, 1 H), 7.15 (d, J = 1.2 Hz, 1 H), 7.05 (dd, J = 7.1, 1.5 Hz, 1 H), 6.99–6.85 (m, 6 H) 6.81–6.75 (m, 3 H), 6.49 (dd, J = 7.5, 1.4 Hz, 1 H), 6.35–6.34 (m, 2 H), 6.30 (dd, J = 2.8, 2.2 Hz, 1 H) ppm. ^{13}C NMR (100 MHz, CDCl3): δ = 152.3, 151.4, 145.9, 144.6, 142.9, 140.1, 139.9, 139.3, 139.0, 135.8, 135.2, 132.6, 126.3, 126.3, 126.0, 125.9, 124.8, 122.4, 121.9, 120.0, 111.5, 110.9, 110.9, 107.3, 107.3, 107.0 ppm. MS (FAB): m/z = 621.89.

***fac*-Ir(ppz)$_3$**

0.13 g of *mer*-Ir(ppz)$_3$ and 130 ml of CH_3CN was placed in a 200 ml of Pyrex glass flask and Ar gas was bubbled for 1 h. The solution was irradiated by the light of 400 W Xe short ark lamp for 20 h. The solvent was evaporated and the residual white solid was purified by short column chromatography and reprecipitation from CH_2Cl_2 – methanol gave 0.10 g of the white solid in 83% yield. ^{1}H NMR (400 MHz,

CDCl3): δ = 7.97 (d, J = 2.7 Hz, 3 H), 7.19 (dd, J = 7.8, 1.1 Hz, 3 H), 6.978 (d, J = 2.1 Hz, 3 H), 6.914 (ddd, J = 7.8, 7.1, 1.6 Hz, 3 H), 6.843 (dd, J = 7.5, 1.5 Hz, 3 H), 6.776 (ddd, J = 7.4, 7.2, 1.2 Hz, 3 H), 6.376 (dd, J = 2.4, 2.4 Hz, 3 H) ppm. ^{13}C NMR (99.45 MHz, $CDCl_3$): δ = 144.2, 139.8, 137.5, 136.7, 125.8, 124.9, 120.4, 110.8, 106.7 ppm. MS (FAB): m/z = 622.00.

2-5-3. Enantiomeric Separation

Enantiomerical separations were performed using HPLC equipped with Chiralpak AD-H column (Daisel Chemical, ϕ = 1.0 cm which is chiral compound coated silica type.). In this column, hexane, 2-propanol and ethanol were usable as eluent. First the mixture of hexane and 2-propanol (80 : 20) was used and the separation in HPLC was very good for both *mer*- and *fac*-Ir(ppz)$_3$, Although the ability of 2-propanol for separation these enantiomers are enough high, the almost of separated enantiomers decomposed when the solvent was evaporated. Next, the mixtures of hexane - ethanol (90:10) and hexane - ethanol (95:5) were chosen for the separation of *fac*-Ir(ppz)$_3$ and *mer*-Ir(ppz)$_3$ respectivery. The separated enantiomers were not decomposed when the solvent was evaporated. In the cases of both *mer*- and *fac*-Ir(ppz)$_3$,10 mg of the complex was dissolved in 700 μl of dicholoroethane and 20 μl of the solution was injected at intervals of 15 min. In the case of *mer*-Ir(ppz)$_3$, the one separation was not satisfactory and twice of separation was acquired. Finally the enantiomeric separations were successfully performed by such a method. More than 98 % enantiomerical pure Δ-*mer*-Ir(ppz)$_3$, Λ-*mer*-Ir(ppz)$_3$, Δ-*fac*-Ir(ppz)$_3$ and Λ-*fac*-Ir(ppz)$_3$ were obtained in 80 to 90 % yield. These purities were also checked by ^{1}H NMR. Although the single X-ray crystallography enables the assignment of which HPLC peak is Δ or Λ, the single crystals was not obtained. The amount of separated complexes was very small and obtaining single crystal seemed very difficult. By comparison their CD spectra to that of Ir(pppy)$_3$[13] and separated *fac*-Ir(ppy)$_3$, the first peak was assigned to Δ and second peak was assigned to Λ.

2-5-4. The analysis of photochemical diastereomeric and enantiomeric isomerization

A1 The photochemical isomerization of Δ-*mer*-Ir(ppz)$_3$ and HPLC analysis

3.5 ml of CH_3CN solution of Δ-*mer*-Ir(ppz)$_3$ (About 2 × 10^{-4} M. This solution need about 700 μg of Δ-*mer*-Ir(ppz)$_3$ was prepared. This solution was added in 1 cm ×1 cm quartz cuvette and Ar babbled for 15 min. The solution was irradiated by 365 nm light of a mercury lamp. The conversion was monitored by UV- Vis absorbance. At each period of about 15 % of Δ-*mer*-Ir(ppz)$_3$ was consumed, 500 μl of solution was took out and 400 μl of solution was moved to the small test tube and to this solution 40 μl of phenanthrene.CH_3CN solution (about 10^{-3} M) was added as a internal standard then the solvent was evaporated. To this test tube 80 μl of CH_2Cl_2 was added and 20 μl of solution was injected to HPLC and analyzed the amount of each photochemically produced enantiomers. The normal silica gel column (ϕ = 1.0 cm) and chiralpak column (ϕ = 1.0 cm) were linked in this order. The eluent was a mixture of hexane and ethanol (98:2). The flow rate was 3 ml / min. One analysis takes 50 min. For Λ-*mer*-Ir(ppz)$_3$, the same methoud was applied.

A2. The photochemical isomerization of Δ-*mer*-Ir(ppz)$_3$ and measurement of CD spectra change

3.5 ml of CH_3CN solution of Δ-*mer*-Ir(ppz)$_3$ (4.0 × 10^{-5} M) was prepared and added to the quarts glass rectangular tube and Ar babbled for 15 min. This solution was irradiated by 365 nm light of a mercury lamp and the change of the CD spectra was recorded.

A3. The solvent dependence and the temperature dependence of the photochemical isomerization of Δ-*mer*-Ir(ppz)$_3$

The solvent dependence and the temperature dependence of the photochemical isomerization were analyzed by the same method to A1. The low temperature (-35 °C) condition was archived by adding dry ice to the acetone in quarts glass Dewar vessel. The high temperature (65 °C) condition was archived by using the heater equipped temperature controller (JASCO).

B1. The photochemical isomerization of Δ-*fac*-Ir(ppz)$_3$ and HPLC analysis

0.5 ml of CH_3CN solution of Δ-*fac*-Ir(ppz)$_3$ (About 1×10^{-3} M. This solution need about 500 μg of Δ-*fac*-Ir(ppz)$_3$ was prepared. This solution was added in 1 cm ×1 cm quartz cuvette and Ar babbled for 15 min. This solution was irradiated by 365 nm light of a mercury lamp. 10 μl of solution was injected to HPLC and analyzed the amount of each photochemically produced enantiomers. The only normal silica gel column (ϕ = 1.0 cm) was used . The eluent was a mixture of hexane and ethanol (95:5). The flow rate was 3 ml / min. One analysis takes 38 min. For Λ-*fac*-Ir(ppz)$_3$, the same method was applied.

B2. The photochemical isomerization of Δ-*fac*-Ir(ppz)$_3$ and measurement of CD spectra change

3.5 ml of CH_3CN solution of Δ-*fac*-Ir(ppz)$_3$ (4.0×10^{-5} M) was prepared and added to the quarts glass rectangular tube and Ar babbled for 15 min. This solution was irradiated by 365 nm light of a mercury lamp and the change of the CD spectra was recorded.

2-5-5. The analysis of thermal diastereomeric and enantiomeric isomerization

1 ml of 1,2-dichlorobenzene solution of Δ-*mer*-Ir(ppz)$_3$ (About 1×10^{-4} M) and the solution of Δ-*fac*-Ir(ppz)$_3$ (About 1×10^{-4} M) were prepared. The solution of Δ-*mer*-Ir(ppz)$_3$ was heated at 140 °C by oil-bus. The solution of Δ-*fac*-Ir(ppz)$_3$ was heated at 180 °C by oil-bus. For one analysis, 10 μl of solution was injected to HPLC and analyzed the amount of each thermally produced enantiomers. The normal silica gel column (ϕ = 1.0 cm) and chiralpak column (ϕ = 1.0 cm) were linked in this order. The eluent was a mixture of hexane and ethanol (98:2). The flow rate was 3 ml / min. One analysis takes 50 min.

2-6. References

[1] a) M. A. Baldo, D. F. O'Brien, Y. You, A. Shoustikov, S. Sibley, M. E. Thompson, S. R. Forrest, *Nature* **1998**, *395*, 151–154; b) M. A. Baldo, S. Lamansky, P. E. Burrows, M. E. Thompson, S. R. Forrest, *Appl. Phys. Lett.* **1999**, *75*, 4–6.

[2] H. Yersin (Ed.), *Highly Efficient OLEDs with Phosphorescent Materials*, Wiley-VCH,

Weinheim, **2008** references cited therein.

[3] Y.-L. Tung, S.-W. Lee, Y. Chi, Y.-T. Tao, C.-H. Chien, Y.-M. Cheng, P.-T. Chou, S.-M. Peng, C.-S. Liu, *J. Mater. Chem.* **2005**, *15*, 460–464.

[4] A. Tsuboyama, H. Iwawaki, M. Furugori, T. Mukaide, J. Kamatani, S. Igawa, T. Moriyama, S. Miura, T. Takiguchi, S. Okada, M. Hoshino, K. Ueno, *J. Am. Chem. Soc.* **2003**, *125*, 12971–12979.

[5] S. Tokito, T. Iijima, T. Tsuzuki, F. Sato, *Appl. Phys. Lett.* **2003**, *83*, 2459–2461.

[6] A. Tamayo, B. D. Alleyne, P. I. Djurovich, S. Lamansky, I. Tsyba, N. N. Ho, R. Bau, M. E. Thompson, *J. Am. Chem. Soc.* **2003**, *125*, 7377–7387.

[7] a) T. Karatsu, T. Nakamura, S. Yagai, A. Kitamura, M. Matsushima, Y. Hori, T. Hagiwara, *Chem. Lett.* **2003**, *32*, 886–887; b) T. Karatsu, E. Itoh, S. Yagai, A. Kitamura, *Chem. Phys. Lett.* **2006**, *424*, 353–357.

[8] a) T. Sajoto, P. I. Djurovich, A. Tamayo, M. Yousufuddin, R. Bau, M. E. Thompson, R. J. Holmes, S. R. Forrest, *Inorg. Chem.* **2005**, *44*, 7992–8003; b) A. B. Tamayo, S. Garon, T. Sajoto, P. I. Djurovich, I. M. Tsyba, R. Bau, M. E. Thompson, *Inorg. Chem.* **2005**, *44*, 8723–8732.

[9] G. Choi, J. Lee, N. Park, Y. Kim, *Mol. Cryst. Liq. Cryst.* **2004**, *424*, 173–185.

[10] E. J. Nam, J. H. Kim, B.-O. Kim, S. M. Kim, N. G. Park, Y. S. Kim, Y. K. Kim, Y. Y. Ha, *Bull. Chem. Soc. Jpn.* **2004**, *77*, 751–755.

[11] a) H. Kanno, R. J. Holmes, Y. Sun, S. Kena-Cohen, S. R. Forrest, *Adv. Mater.* **2006**, *18*, 339–342; b) E. L. Williams, K. Haavisto, J. Li, G. E. Jabbour, *Adv. Mater.* **2007**, *19*, 197–202; c) Y. Sun, S. R. Forrest, *Appl. Phys. Lett.* **2007**, *91*, 263503–06.

[12] a) V. I. Adamovich, S. R. Cordero, P. I. Djurovich, A. Tamayo, M. E. Thompson, B. W. D'Andrade, S. R. Forrest, *Org. Electron.* **2003**, *4*, 77–87; b) R. J. Holmes, S. R. Forresta, T. Sajoto, A. Tamayo, P. I. Djurovich, M. E. Thompson, J. Brooks, Y.-J. Tung, B.W. D'Andrade, M. S. Weaver, R. C. Kwong, J. J. Brown, *Appl. Phys. Lett.* **2005**, *87*, 243507–09; c) B. W. D'Andrade, S. Datta, S. R. Forrest, P. Djurovich, E. Polikarpov, M. E. Thompson, *Org. Electron.* **2005**, *6*, 11–20.

[13] C. Schaffner-Hamann, A. von Zelewsky, A. Barbieri, F. Barigelletti, G. Muller, J. P. Riehl, A.

Neels, *J. Am. Chem. Soc.* **2004**, *126*, 9339–9348.

[14] F. J. Coughlin, M. S. Westrol, K. D. Oyler, N. Byrne, C. Kraml, E. Zysman-Colman, M. S. Lowry, S. Bernhard, *Inorg. Chem.* **2008**, *47*, 2039–2048.

[15] a) X. Chen, Y. Okamoto, T. Yano, J. Otsuki, *J. Sep. Sci.* **2007**, *30*, 713–716; b) J. Otsuki, T. Tokimoto, Y. Noda, T. Yano, T. Hasegawa, X. Chen, Y. Okamoto, *Chem. Eur. J.* **2007**, *13*, 2311–2319.

[16] A. Auffrant, A. Barbieri, F. Barigelletti, J. Lacour, P. Mobian, J.-P. Collin, J.-P. Sauvage, B. Ventura, *Inorg. Chem.* **2007**, *46*, 6911–6919.

[17] A. W. Adamson, *J. Phys. Chem.* **1967**, *71*, 798–808.

[18] a) L. G. Vanquickienborne, A. Ceulemans, *J. Am. Chem. Soc.* **1977**, *99*, 2208–2214; b) L. G. Vanquickienborne, A. Ceulemans, *Inorg. Chem.* **1978**, *17*, 2730–2736; c) L. G. Vanquickienborne, A. Ceulemans, *Cood. Chem. Rev.* **1983**, *48*, 157–202; d) E. Larsen, G. N. La Mar, *J. Chem. Educ*. **1974**, *51*, 633–640; e) G. L. Miessler, D. A. Tarr, *Inorganic Chemistry* 2nd ed. Prentice Hall Inc, New Jersey, **2000**.

[19] G. B. Porter, R. H. Sparks, *J. Photochem.* **1980**, *13*, 123–131.

[20] L. Yang, F. Okuda, K. Kobayashi, K. Nozaki, Y. Tanabe, Y. Ishii, M. Masa-aki Haga, *Inorg. Chem.* **2008**, *47*, 7154–7165.

[21] A. R. McDonald, M. Lutz, L. S. von Chrzanowski, G. P. M. van Klink, A. L. Spek, G. van Koten, *Inorg. Chem.* **2008**, *47*, 6681–6691.

[22] M. J. Frisch, G. W. Trucks, H. B. Schlegel, G. E. Scuseria, M. A. Robb, J. R. Cheeseman, J. A. Montgomery Jr, T. Vreven, K. N. Kudin, J. C. Burant, J. M. Millam, S. S. Iyengar, J. Tomasi,V. Barone, B. Mennucci, M. Cossi, G. Scalmani, N. Rega, G. A. Petersson, H. Nakatsuji, M. Hada, M. Ehara, K. Toyota, R. Fukuda, J. Hasegawa, M. Ishida, T. Nakajima, Y. Honda, O. Kitao, H. Nakai, M. Klene, X. Li, J. E. Knox, H. P. Hratchian, J. B. Cross, C. Adamo, J. Jaramillo, R. Gomperts, R. E.Stratmann, O. Yazyev, A. J. Austin, R. Cammi, C. Pomelli, J. W. Ochterski, P. Y. Ayala, K. Morokuma, G. A. Voth, P. Salvador, J. J. Dannenberg, V. G. Zakrzewski, S. Dapprich, A. D. Daniels, M. C. Strain, O. Farkas, D. K. Malick, A. D. Rabuck, K. Raghavachari, J. B. Foresman, J. V. Ortiz, Q. Cui, A. G. Baboul, S. Clifford, J. Cioslowski, B. B. Stefanov, G. Liu, A.

Liashenko, P. Piskorz, I. Komaromi, R. L. Martin, D. J. Fox, T.Keith, M. A. Al-Laham, C. Y. Peng, A. Nanayakkara, M.Challacombe, P. M. W. Gill, B. Johnson, W. Chen, M. W.Wong, C. Gonzalez, J. A. Pople, *Gaussian 03*, Revision B.03,Gaussian, Inc., Pittsburgh, PA, **2003**.

Chapter 3

Synthesis and Photophysical Properties of Substituted Tris(Phenylbenzimidazolinato) Ir(III) Carbene Complexes as a Blue Phosphorescent Material

3-1. Abstract

Substitution effect on the photoluminescence and electrochemical properties, and photochemical stability of tris(phenyl-benzimidazolinato)Ir(III) complexes were investigated. A series of facial and meridional isomers having a general structure of $Ir(C^C)_3$ where the (C^C) is (4-R-phenyl)-benzimidazolinato (R=H, CF_3, CN, OCH_3) were prepared. They are abbreviated to $Ir(pmb)_3$; **1**, $Ir(CF_3pmb)_3$; **2**, $Ir(CNpmb)_3$; **3**, and $Ir(Opmb)_3$; **4**, respectively. In all complexes, emission quantum yields were increased and emission lifetimes were also increased along oxidation potential energies of *fac*-$Ir(CF_3pmb)_3$, *fac*-$Ir(CNpmb)_3$, and *mer*-$Ir(CNpmb)_3$ were increased. The quantum yeild slightly increases by the substitution of electro-donating group. By irradiation of 313 nm light from 400W mercury lamp for more than 20 h, no photochemical isomerisation was observed in both *fac* (**a**) and *mer* (**b**) isomers of $Ir(pmb)_3$, $Ir(CF_3pmb)_3$, and $Ir(CNpmb)_3$. All complexes excluding *fac*-$Ir(pmb)_3$ (**1a**) showed excellent photochemical stabilities in degassed anhydrous THF solution. To explore the locations of HOMO and LUMO, and lowest excitation energy of these complexes, DFT and TD-DFT calculations were performed for *fac*- and *mer*-$Ir(Opmb)_3$ (**4a** and **4b**). It was revealed that the HOMO is mainly localized over Ir metal center and phenyl moiety and the LUMO mainly localized over benzimidazole moiety. The calculated lowest excitation energies agree with the experimental values. The X-ray single crystal structures obtained for *fac*-$Ir(CF_3pmb)_3$ (**2a**) and *mer*-$Ir(Opmb)_3$ (**4b**) by X-ray single crystallography are also discussed.

3-2. Introduction

Iridium triscyclometalated complexes have recently caught significant attention because of their supreme phosphorescent performance for OLED (Organic light emitting diode).[1–5] For the fabrication of full color display, red, green, and blue colors are required for the complexes, and their emission colors can be tuned by the ligand structures.[4–6] So far, pure and highly efficient phosphorescent green materials and relatively highly phosphorescent red materials have been achieved. Red color can be also obtained by using conjugated ancillary ligand.[7] Despite numerous attempt, it remains difficult to obtain blue color. Blue color requires high energy gap, therefore attempts to decrease HOMO energy level[6–9] or increase LUMO energy level were examied.[6,10] Tris(4,6 difluorophenylpyridinato)Ir ($Ir(F_2ppy)_3$) has lower HOMO level than tris(phenylpyridinato)Ir ($Ir(ppy)_3$) and showing greenish-blue color.[6,8] Tris(phenylpyrazolinato)Ir ($Ir(ppz)_3$) has a larger LUMO energy level and show blue color emission at solid state or at 77K in glassy matrices, but no emission is obtained in fluid solution at 298 K.[6,10] By using the ancillary ligand such as pyridylpyrazolinato, blue color emission at 298 K has been achieved but this emission quantum yield remains low.[11] There are also some reports discussing why true blue color phosphorescent material is not emissive at ambient temperature. It is theoretically suggested that the emissive state of $Ir(ppz)_3$ is enough high to be thermally activated to non-emissive d_π-$d_{\sigma*}$ state at ambient temperatures.[12] In 2005, Sajoto et al. reported phenylbenzimidazolinato and phenylimidazolinato Ir complexes having carbene ligands show near UV phosphorescence with relatively high quantum efficiency at room temperature.[13] This is due to strong ligand field effect of carbene ligand. Its keep nonradiative d_π-$d_{\sigma*}$ state largely away from emissive triplet state, and it was actually used for OLED.[14] CN substituted *fac*-Ir carbene complexes showed smaller radiative rate constant than non substituted complexes.[15] The luminescent property and theoretical study about Ir carbene complexes having ancillary ligand have also been reported,[16a] and recently complexes having phosphine ligand showed true blue phosphorescent with an high external quantum efficiency in OLED.[16b] While many efforts to obtain highly efficient blue phosphorescent material were reported, the excited state properties of Ir carbene complexes remain unclear. The phosphorescence quantum yield of non substituted *fac*-$Ir(pmb)_3$ have been originally reported to be 0.04,[13a] however, corrected to be 0.37, recently.[13b] Even though, the value is smaller than the value of *fac*-$Ir(CNpmb)_3$, 0.78.[15] In this chapter, I

investigate that substituents effect on the photophysics and photochemistry of Ir carbene complexes. In addition, I describe the simple one-step synthesis of Ir carbene complexes by reaction of $IrCl_3$ and a benzimidazolium iodide precursor. I choose the phenylbenzimidazole as a ligand which have electron-withdrawing or electron-donating group as an substituent on the phenyl moieties. Both *mer*- and *fac*-isomers were prepared (Figure 3-1) to investigate their photochemical properties and geometrical isomerisation. Single crystal X-ray structures, photoluminescent property, electrochemical property and photochemical stabilities of complexes were investigated to explore substitution effect for Ir carbene complexes. DFT and TD-DFT calculation were also performed and calculated lowest excitation energy and molecule orbitals involved were obtained.

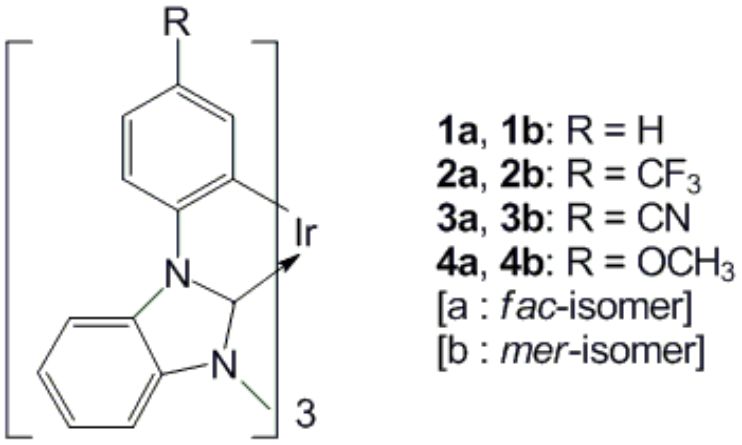

Figure 3-1. The chemical structure of complexes investigated in this chapter.

3-3. Results and Discussion

3-3-1. Synthesis

Typical syntheses of triscyclometalated Ir(III) complexes have been reported through Ir(III) μ-dichloro-bridged dimer.[6,7a] Ir carbene complexes also used such a method using iridium trichloride hydrate and 4.2 equivalent ligand iodide precursors in the presence of silver(I) oxide.[13a] Then, dimer complexes are allowed to react with ligand iodide precursors to give the final complexes (Scheme 3-1). In the case of complex **1**, yields of dimer and final complexes have been reported to be 12.7 and 98 %, respectively. Recently, one pot synthesis of Ir carbene complexes via $[Ir(\mu\text{-}Cl)(COD_2)]_2$ (COD:cycloocta-1,5-diene) has been reported.[17] $[Ir(\mu\text{-}Cl)(COD_2)]_2$ and 6 eq ligand chloride precursors were reacted in the presence of silver(I) Oxide, and yields were between 58-79% depending on solvent used.(Scheme 3-2) In this work, I succeeded one pot syntheses of Ir carbene complexes from $IrCl_3\text{-}3H_2O$ by reaction with substituted phenylbenzimidazolium iodide precursors using Ag_2CO_3 and Na_2CO_3 (Scheme 3-3). Use of these bases is one of the features of this method.

Substituted phenylbenzimidazolium iodide precursors were prepared according to the literature method.[13,18] Ir(III) triscyclometalated carbene complexes were prepared by refluxing 2-ethoxyethanol solution of $IrCl_3\text{-}3H_2O$ and ligand iodide in the presence of silver carbonate for 20 h and the mixture of *fac* isomer and *mer* isomers were obtained. These mixtures were separated by reprecipitation or column chromatography and further purified by reprecipitation from $CH_2Cl_2\text{-}CH_3OH$, to give pure complexes with yields ranging between 83 % (**2** in total, 62% and 21% for **2a** and **2b**, respectively) and 26.8 % (**3,** 5.8% and 21% for **3a** and **3b**, respectively).

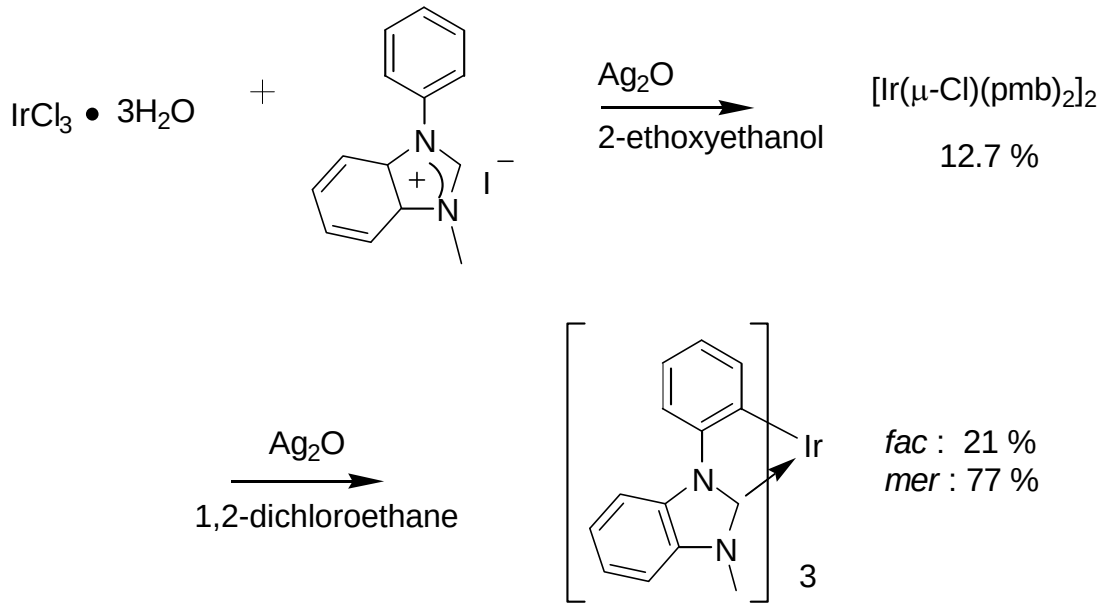

Scheme 3-1. Syntesis of Ir carbene complexes via $[Ir(\mu\text{-}Cl)(pmb)_2]_2$. All reactions were carried out under refluxing temperature in the report of *Inorg. Chem*. **2005**, *44*, 7992.

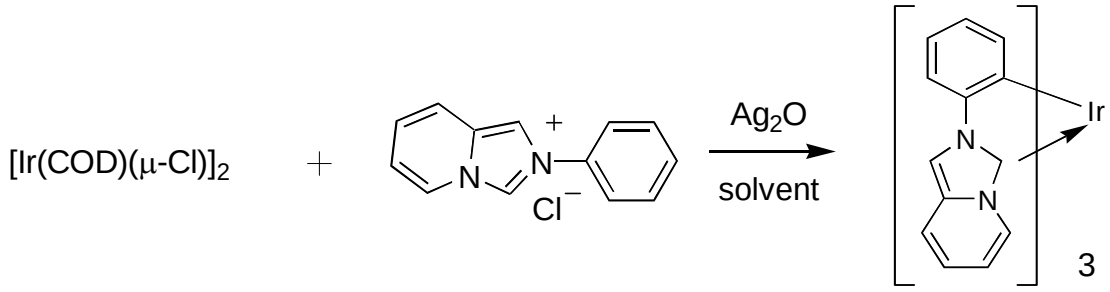

1,2-ethoxyethanol	58 % (*fac* : *mer* = 1 : 6	according to ^{1}H NMR)
1,2-dichloroethane	78 % (*fac* : *mer* = 1 : 16	according to ^{1}H NMR)
DMF	79 % (*fac* : *mer* = 1 : 3.3	according to ^{1}H NMR)

Scheme 3-2. Syntheses of Ir carbene complexes via $[Ir(\mu\text{-}Cl)(COD)_2]_2$. All reaction was carried out under refluxing temperature in the report of *Dalton. Trans*. **2008**, 916-923.

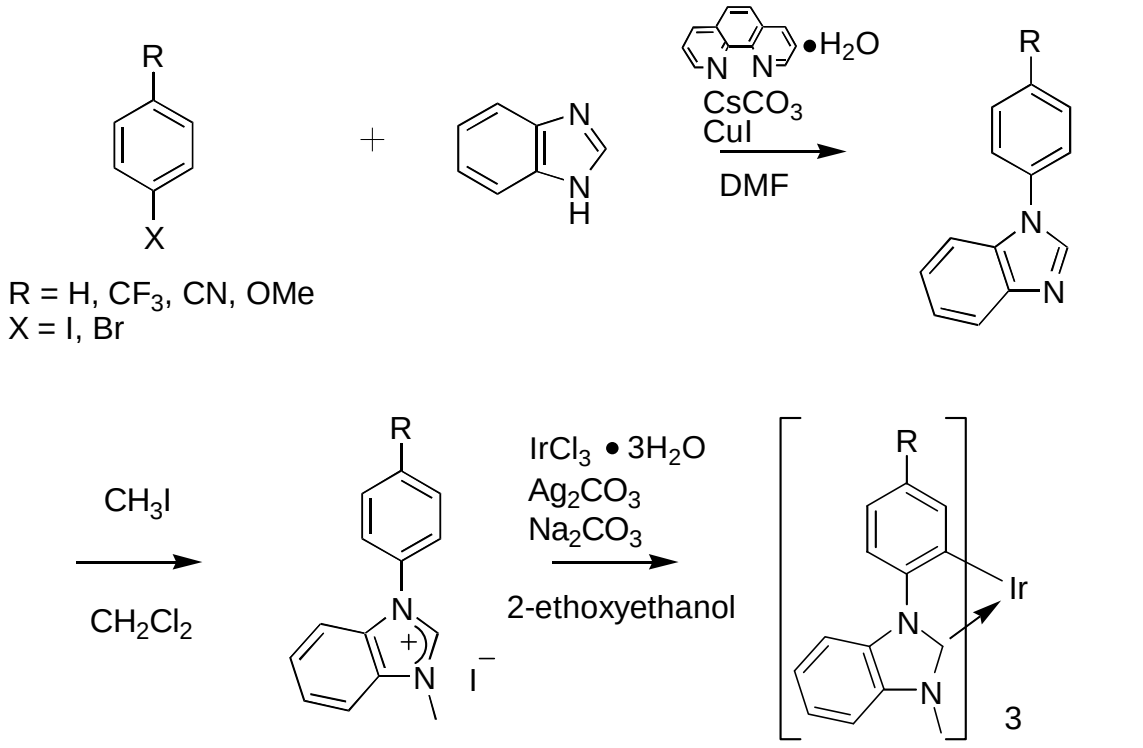

Scheme 3-3. Preparation method of Ir triscyclometalated carbene complexs used in this chapter.

.

3-3-2 Crystal structure of *fac*-Ir(CF$_3$pmb)$_3$ (2a) and *mer*-Ir(Opmb)$_3$ (4b)

The single crystal of **2a** was obtained from dichloroethane and ethanol solution by slow solvent evaporation, and the single crystal of **4b** was obtained from CH_2Cl_2 and methanol. As depicted in Figure 3-4, complex **2a** and **4b** showed a distorted octahedral geometry. Selected bond lengths of **2a** and **4b** are listed in Table 3-1. In **2a**, the average bond lengths of Ir-C_{aryl} bond (2.085(8) Å) and Ir-$C_{carbene}$ bond (2.035(9) Å) are almost identical to the average bond lengths of the mutually trans Ir-C_{aryl} bond (2.081(7) Å) and Ir-$C_{carbene}$ bond (2.026(7) Å) in **1a** reported.[13] In **4b**, the bond lengths of Ir-C_{aryl} trans to benzimidazolyl (Ir-C2, 2.076(2) Å) and Ir $C_{carbene}$ trans to phenyl (Ir-C4, 2.042(2) Å) are similar to those of **1b**, and the bond lengths of the mutually trans Ir-C_{aryl} bond (Ir-C1, Ir-C3 average = 2.105(2) Å) and Ir-$C_{carbene}$ bond (Ir-C5, Ir-C6 average = 2.020(2) Å) are almost same to that of **1b**[13] (average mutually trans Ir-C_{aryl} = 2.093(4) Å, average mutually trans Ir-$C_{carbene}$ = 2.026(4) Å). These indicate that the substituents on the phenyl moiety do not affect the core structure of complexes. The unit cell parameters of

2a and **4b** are listed in table 3-2. Both crystal systems of **2a** and **4b** are monoclinic system. In *fac*-Ir(pmb)$_3$, 1 molecule of 1,2-dichloroethame are contained in the unit cell.

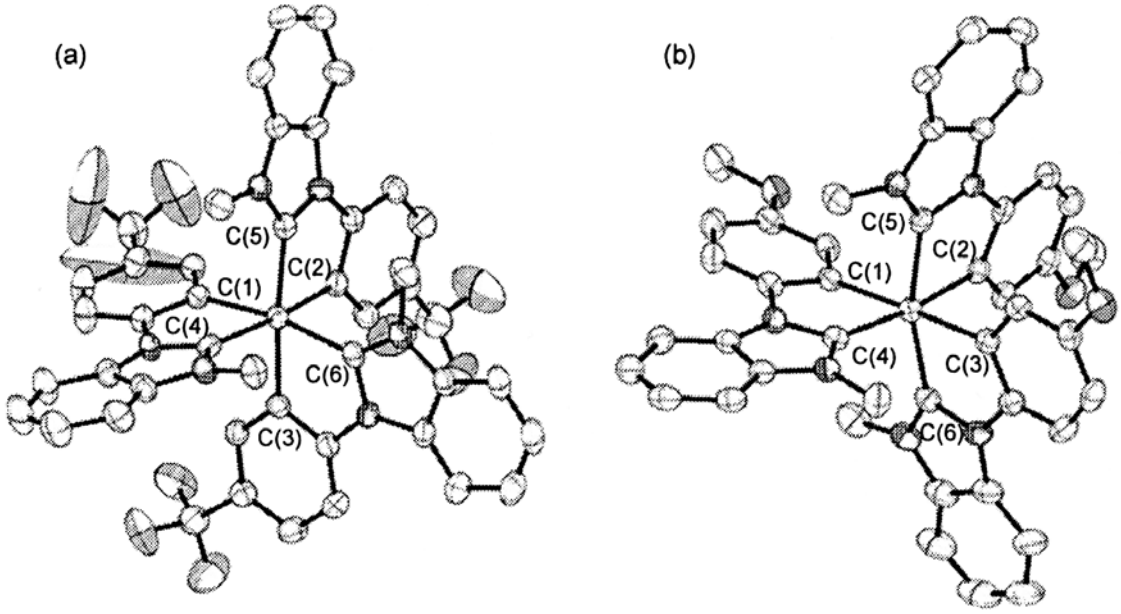

Figure 3-4. ORTEP diagram of **2a** (a) and **4b** (b). CF_3 groups of **2a** showed large thermal anisotropy due to disorder, co-crystallized with dichloroethane in(a) and H atoms are omitted in the figure.

Table 3-1. Selected Bond length in **2a** and **4b**

Bonds	**2a**	**4b**
Ir-C(1)	2.085(9)	2.117(2)
Ir-C(2)	2.085(8)	2.076(2)
Ir-C(3)	2.085(8)	2.093(2)
Ir-C(4)	2.031(9)	2.042(2)
Ir-C(5)	2.057(10)	2.009(2)
Ir-C(6)	2.0175(8)	2.030(3)

Table 3-2. Crystallographic date for **2a** and **4b.**

	fac-Ir(CF_3pmb)$_3$	*mer*-Ir(Opmb)$_3$
Empirical formula	$C_{45}H_{30}F_9IrN_6$	C45 H39 Ir N6 O3
Formula weight	1054.02	
Temperature,K	173	173
Wavelength (A)	0.71073	0.71073
Crystal system	Monoclinic	Monoclinic
Space group	P2(1)/c	P2(1)/n
Unit cell dimensions		
a (A)	15.0054(9)	12.3904(7)
b (A)	16.8387(10)	20.2761(12)
c (A)	18.7448(12)	15.3322(9)
α (deg)	90	90
β (deg)	113.1010(10)	109.7040(10)
γ (deg)	90	90
V(A^3)	4356.5(5)	3626.4(4)
Z	4	4
Density, calcd (Mg/m^3)	1.703	1.656
Absorption coefficient (mm^{-1})	3.269	3.735
F_{000}	2200	1808
θ range for data collection (deg)	1.91 to 28.53	1.73 to 28.52
Reflections collected	24179	24547
Crystal size (mm)	0.50 x 0.10 x 0.10	0.2 x 0.2 x 0.2
Refinement method	Full-matrix least-squares	Full-matrix least-squares on F^2
Data / restraints / parameters	9998 / 0 / 589	8384 / 0 / 502
Goodness-of-fit on F^2	0.965	1.035
Final R indices [I>2sigma(I)]	R1 = 0.0334, wR2 =	R1 = 0.0215, wR_2[b] = 0.0549
R indices (all data)	R1 = 0.0405, wR2 =	R1 = 0.0264, wR2 = 0.0565

3-3-3 Photophysical property

UV-Vis absorption spectra and PL spectra of **1a-4b** are shown in Figure 3-5 and 3-6. The data are summarized in Table 3-3.

Absorption band at lower energy (λ = 320 ~ 360 nm) can be ascribed to ^{1}MLCT transition for all complexes.[2] By introducing substituents, absorption and PL spectra of both *mer* and *fac* isomers were red shifted regardless of electro-withdrawing or -donating groups. The λ_{max} of the *mer*-isomer appeared at lower energy than those of *fac*-isomers as in the cases of reported triscyclometalated Ir complexes.[6,8,10] The magnitude of the red shift was in the order of CN >OCH_3 > CF_3, and red shift of PL spectra was in the same order. In the case of the *fac* isomer, the values of **1a** are Φ_{PL} = 0.44, τ = 1.3 μs, and following rate constants are calculated by using equations, $k_r = \Phi_{PL}/\tau$ and $k_{nr} = (1-\Phi_{PL})/\tau$, $k_r = 3.4 \times 10^5$ s^{-1}, $k_{nr} = 4.3 \times 10^5$ s^{-1}. The values of **2a**, **3a**, and **4a** are Φ_{PL} = 0.84, 0.71, 0.76, τ = 6.1, 14, 5.0 μs, $k_r = 1.4 \times 10^5$ s^{-1}, 0.5×10^5 s^{-1}, 1.5×10^5 s^{-1}, $k_{nr} = 0.26 \times 10^5$ s^{-1}, 0.21×10^5 s^{-1} 0.48×10^5 s^{-1}, respectively. k_r value of **3a** is almost same to the values obtained for solid state,[14] In the case of *mer* isomer, the values of **1b** are Φ_{PL} = 0.011, τ = 0.024 μs, $k_r = 4.6 \times 10^5$ s^{-1}, $k_{nr} = 412 \times 10^5$ s^{-1} and the value are **2b**, **3b**, **4b** Φ_{PL} = 0.36, 0.63, 0.054, τ = 3.0, 15, 0.26 μs, $k_r = 1.2 \times 10^5$ s^{-1}, 0.42×10^5 s^{-1}, 2.1×10^5 s^{-1}, $k_{nr} = 2{,}1 \times 10^5$ s^{-1}, 0.25×10^5 s^{-1}, 36×10^5 s^{-1} respectively. The rate constant of *mer*-Ir(pmb)$_3$ is also similar to *mer*-Ir(ppy)$_3$. Although the k_r values of all substituted complexes became smaller than that of **1**, the difference between *fac* and *mer* isomers having the same substituent is small. The k_r value is not strongly affected by the structure of geometrical isomers. The amount of decreased k_{nr} values is different between *fac* isomer and *mer* isomer for all complexes. In the case of **2a**, **2b**, **3a** and **3b**, k_{nr} values are smaller than k_r. As a result, the Φ_{PL} shows large values. In the case of **4b**, Φ_{PL} was very small as similar to the **1b**, and this is due to the large k_{nr} value and it is two orders smaller than the k_r. CF_3 and OMe groups decrease the k_r value in both *fac* and *mer* isomer and CN group largely decreased the k_r value in both *fac* and *mer* isomer. It seems that the k_r values are independent on electron density of phenyl moiety. The major non-radiative decay process of the blue phosphorescent complexes is believed to occur via the ligand field excited state (i.e. d_π-$d_{\sigma*}$ state).[13] By substitution, the energetic separation between LUMO and dd state is increased because of decrease of LUMO energy level or increase of dd state energy level, therefore k_{nr} value is decreased. CF_3 and CN groups largely decrease

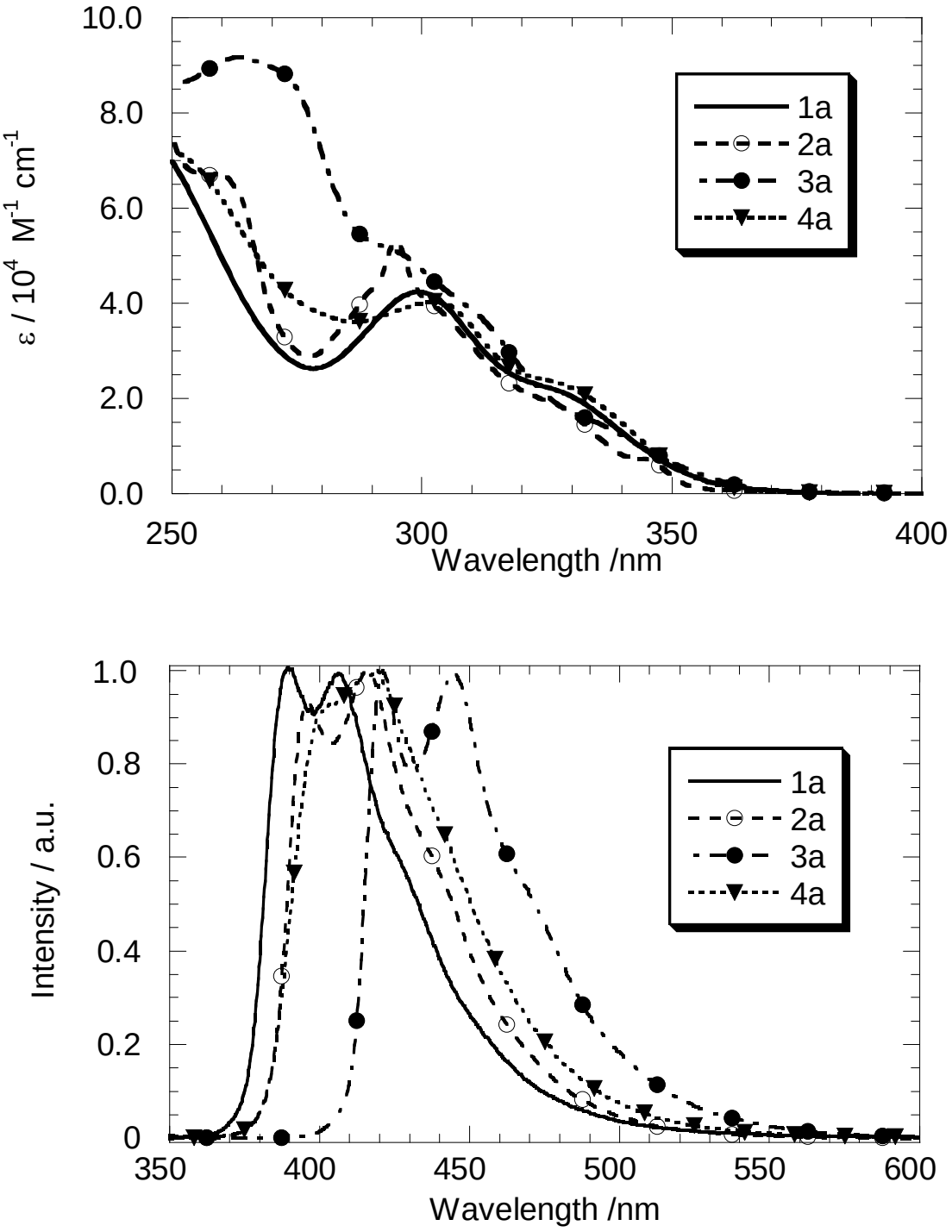

Figure 3-5. Absorption (top) and phosphorescence spectra (bottom) of *fac* isomer (**1a** – **4a**) in anhydrous THF. (Phosphorescence spectra were measured in anhydrous THF purged with argon).

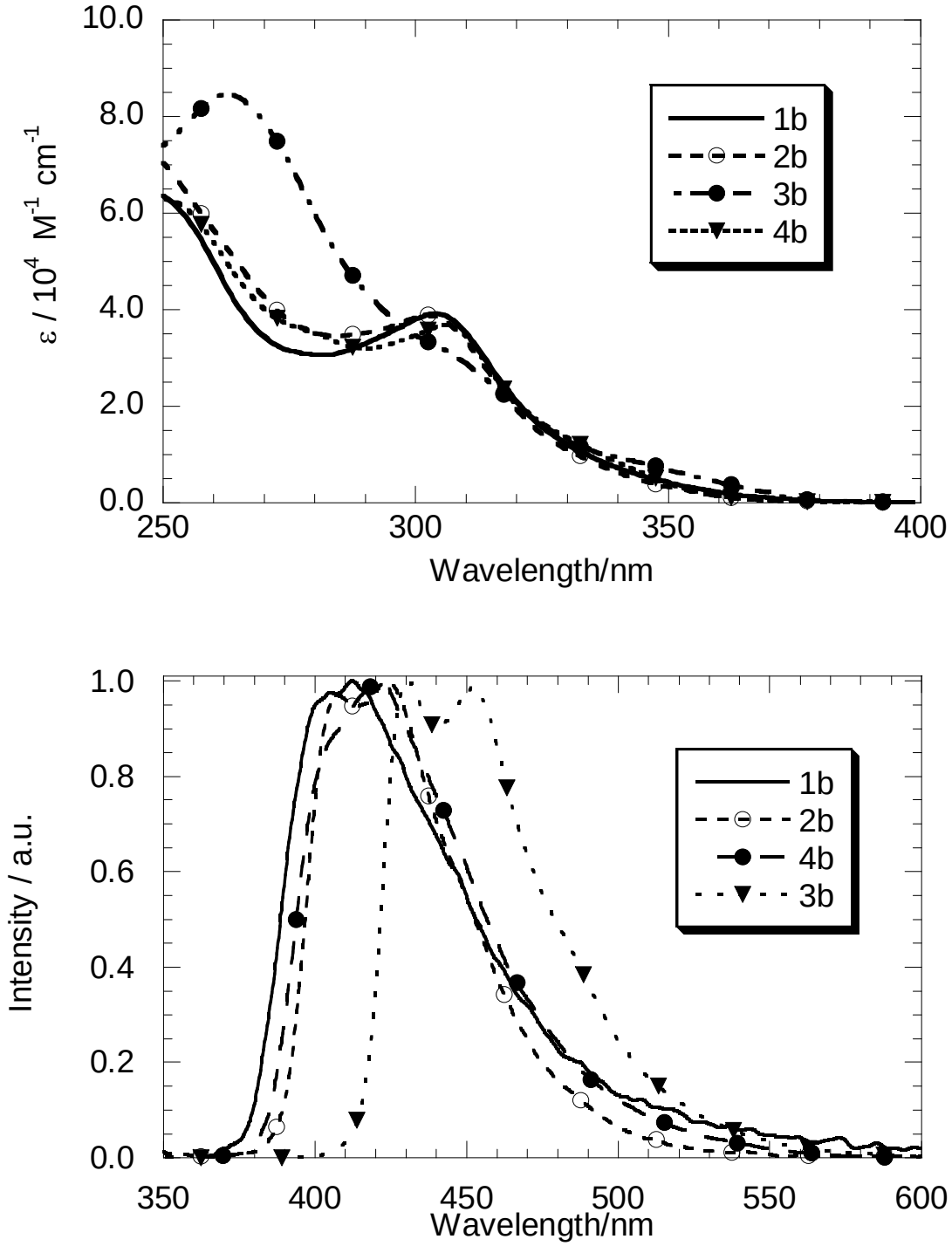

Figure 3-6. Absorption (top) and phosphorescence spectra (bottom) of *mer* isomer (**1b** – **4b**) in anhydrous THF. (Phosphorescence spectra were measured in anhydrous THF purged with argon).

Table 3-3. Photoluminescent properties of Ir complexes **1a-4b** in degassed THF.

Complex	λ_{em} / nm	Φ_{PL}[a]	τ / μs	k_r / 10^{-5} s^{-1}	k_{nr} / 10^{-5} s^{-1}
1a	390, 407	0.44	1.3	3.4	4.3
1b	405, 412	0.011	0.024	4.6	412
2a	396, 416	0.84	6.1	1.4	0.26
2b	407, 424	0.36	3.0	1.2	2.1
3a	421, 445	0.71	14	0.51	0.21
3b	430, 452	0.63	15	0.42	0.25
4a	403, 415	0.76	5	1.5	0.48
4b	407, 422	0.054	0.26	2.1	36

[a] 9,10-diphenylanthracene in cyclohexane (Φ = 0.90) is used as a reference. The formula used is $\Phi_X = \Phi_S \times (n_X / n_S)^2 \times (A_X / A_S) \times (Abs_S / Abs_X)$, where subscripts X and S indicate sample and reference, respectively. In addition, n is reflective index of solvent, A is the area of emission spectra, and Abs is absorbance at the excitation wavelength (Abs is set around 0.20).

The k_{nr} value in *mer* isomer and OMe group does not largely decrease the k_{nr} value in *mer* isomer. These results indicate that electron-withdrawing group increases energy separation between phosphorescent state and dd state, however electron-donating group just slightly increases it. **3a** and **3b** showed long lifetime (14 – 15 μs). This is most likely due to large separation between ^{1}MLCT and ^{3}LC state (the amount of energy difference was abbreviated to ΔE_{ST}. [15,19] While the ^{1}MLCT energies estimated by the absorption spectra of **3a** and **3b** were almost same to the other complexes (c.a. 350 nm), the emission energies were lower than others (c.a. 30 nm). This shows **3a** and **3b** have larger ΔE_{ST} values than those of others; this is also supported by the time-resolved PL spectrum measurement at low temperature.[14] In $Ir(ppy)_3$ based complexes, fluorine atom or methyl substitution on phenyl moiety affects to neither k_r nor k_{nr} values.[6] While Some heteroreptic Ir complexes like Ir(pic) or amide-bridged ppy and picolinato based complex

show quantum yield improvement by substitution of CF_3 group[7d, 20] . In carbene complexes, similar substitution affects both k_r and k_{nr} values; and the effect is particularly large in cyano substitution. The decrease of k_{nr} value is due to a large separation between dd state and the ^{3}LC state and the decrease of k_r value is due to an increase of ΔE_{ST}.

3-3-4 Electrochemical property

Determining Oxidation potential and reduction potential is useful to estimate the hole and electron transfer is occur or not in OLED, and efficient to discuss whether the LUMO and HOMO is affected by substitution or not. To know how the functional group at phenyl moiety of Ir carbene complex affects the LUMO and HOMO, cyclic voltammetry was performed.

The oxidation potentials were determined by cyclic voltammetry in anhydrous THF. The obtained oxidation potentials are summarized in Table 3-4. (The cyclic voltammogram except for *mer*-Ir(pmb)$_3$ are depicted in the chapter of the date).

Table 3-4. Oxidation potentials of the **1a** – **4b** determined by cyclic voltammetry

Complex	$E_{1/2}^{OX}$ [a]	
	a (*fac*)	**b** (*mer*)
1	0.45	0.42
2	0.74	0.59[b]
3	0.84[b]	0.84[b]
4	0.37[b]	0.29[c]

[a] Measured in anhydrous THF purged by argon, values are reported relative to Cp_2Fe/Cp_2Fe+. [b] Voltammograms were not completely reversible. [c] Irreversible.

The oxidation potentials of **1a** and **1b** were found to be 0.45 V and 0.42 V, respectively. The

oxidation potentials of **2a**, **3a** and **3b** were found to be 0.74 V, 0.84 V and 0.84 V, respectively. The oxidation potentials of **4a** and **4b** are 0.37 V and 0.29 V, respectively. These results indicate that electron-withdrawing group stabilized HOMO energy and electron-donating group destabilized HOMO and HOMO is spread largely over phenyl moiety. I could not obtain the reduction potentials, because cyclic voltammograms were irreversible or did not appear in a scan area. From UV-Vis absorption, it is obvious that ^{1}MLCT absorption bands appeared almost the same area for all complexes while oxidation potentials differ among complexes. This indicates that in Ir carbene complexes, not only HOMO but also LUMO is largely affected by substitution of ligand.

3-3-5 Photochemical stability

It is known that some *mer*-isomer of cyclometalated Ir complexes show photochemical *mer*→*fac* geometrical isomerization (*mer*-Ir(ppy)$_3$, *mer*-Ir(F$_2$ppy)$_3$, *mer*-Ir(tpy)$_3$, *mer*-Ir(ppz)$_3$)[6,8,10] and their reaction mechanisms have been discussed.[21] When Ir complexes were used as a phosphorescent dopant in OLED, high durability is required and one of the decompositions reason is chemical reaction from excited state (it is may be self-degradation or reaction with host material surrounding complexes). Such a reasons motivated me to determine photochemical stabilities of the complexes. The Ir carbene complexes were dissolved in anhydrous THF then degassed by freeze-pump-thaw cycles, and irradiated 313 nm light by 400 W middle pressure mercury lamp. In previous study, *mer*-Ir(pmb)$_3$ and *mer*-Ir(pmi)$_3$ did not show photochemical geometrical isomerization,[13] and it is assume that substituted carbene complexes also does not show isomerization or very small isomerization quantum yield. To clarify such question, *mer*-Ir(tpy)$_3$ which quantum yield sufficiently small ($\Phi_{iso} = 1.8 \times 10^{-4}$) was used as a reference. The absorbance of samples at irradiation wavelength (Abs_{313}) was set between 1 and 3 (The concentration was between 3.6×10^{-5} M and 1.5×10^{-4} M, and a volume of solution is 3.5 ml). Figure 3-7 shows the change of UV-Vis and PL spectra. When *mer* Ir(tpy)$_3$ was irradiated for 3 h, only 3.0×10^{-8} mol of complex isomerized. In **1a**, although slight decrease of the absorption spectra was observed, 30% PL intensity was quenched after 45 h irradiation. At this point, no *mer* isomer was observed by HPLC. TLC analysis indicates that undevelopable spot was appeared by developing hexane: ethyl acetate (7: 3) mixture. However, identification resulted in

failure. Other complexes (**2a**, **2b**, **3a**, and **3b**) showed photo-irradiation robustness upon 20-45 h irradiation. From the results of *mer*- or even *fac*-isomers, I conclude that not only **1a** and **1b** but also **2a**, **2b**, **3a** and **3b** do not undergo geometrical isomerization. Photochemical isomerization of cyclometalated Ir complexes such as *mer*-Ir(ppz)$_3$ and *mer*-Ir(tpy)$_3$, the bond rapture from d_π-$d_{\sigma*}$ state is the first step,[12] then hybridization to trigonal bipyramidal structure takes place; and final rehybridization to octahedral structure leads to the isomerization. In the cases of carbene type iridium complexes, it is thought that thermal activation to d_π-$d_{\sigma*}$ state in the excited state is also occurred because k_{nr} value of **1b** is large. There are two possibilities that **1b** does not show photochemical isomerization. The bond rapture may not occur from d_π-$d_{\sigma*}$ or the activation energy barrier to isomerization is too large to form other geometrical isomer. In other carbene complexes, **2b**-**4b**, also show no photochemical isomerization. In **2b** and **3b**, the k_{nr} values are small, therefore, thermal activation to d_π-$d_{\sigma*}$ state in excited state may not occur. Recently, deactivation of blue phosphorescent *fac*-complexes have been reported.[22] Temperature dependence of phosphorescence indicates thermal activation to the nonradiative decay state. Similar state of the *mer*-isomer is also proposed as a key state of the *mer*→*fac* geometrical isomerization,[8,10,21] however, *mer*-isomers of carbene complexes did not isomerize to the corresponding *fac*-isomer. This may indicate that requirement of high activation energy to access the key state for *mer*-isomer of carbene complexes. In total, the photochemical stability of **1b**, **2a**, **2b**, **3a**, **3b**, **4a** and **4b** were very high in degassed solution.

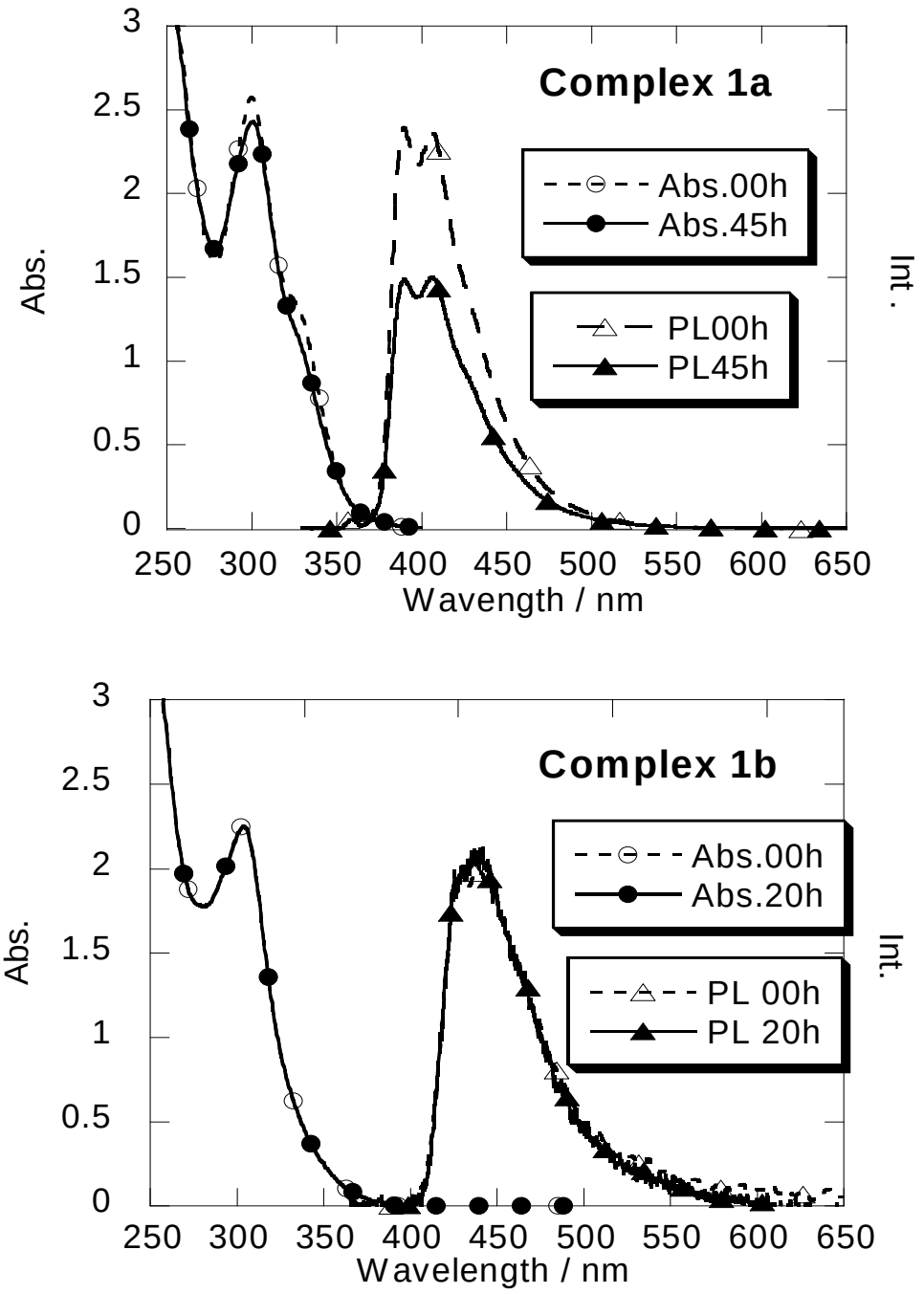

Figure 3-7-1. Absorption and phosphorescence spectra obtained by photochemical stability tests of **1a** and **1b**, before and after irradiation of 313 nm light for 20 – 45 h in degassed anhydrous THF solution.

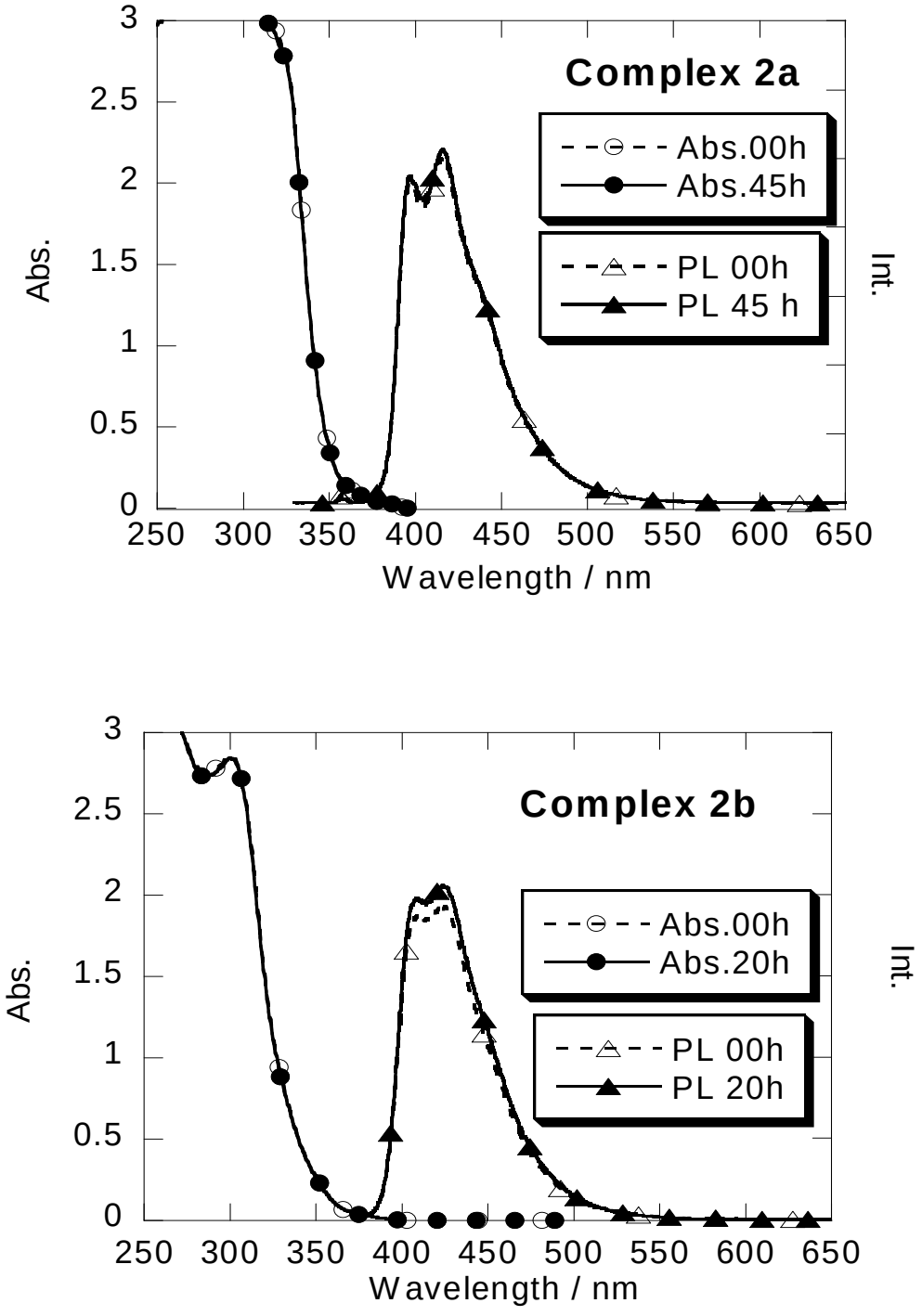

Figure 3-7-2. Absorption and phosphorescence spectra obtained by photochemical stability tests of **2a** and **2b**, before and after irradiation of 313 nm light for 20 – 45 h in degassed anhydrous THF solution.

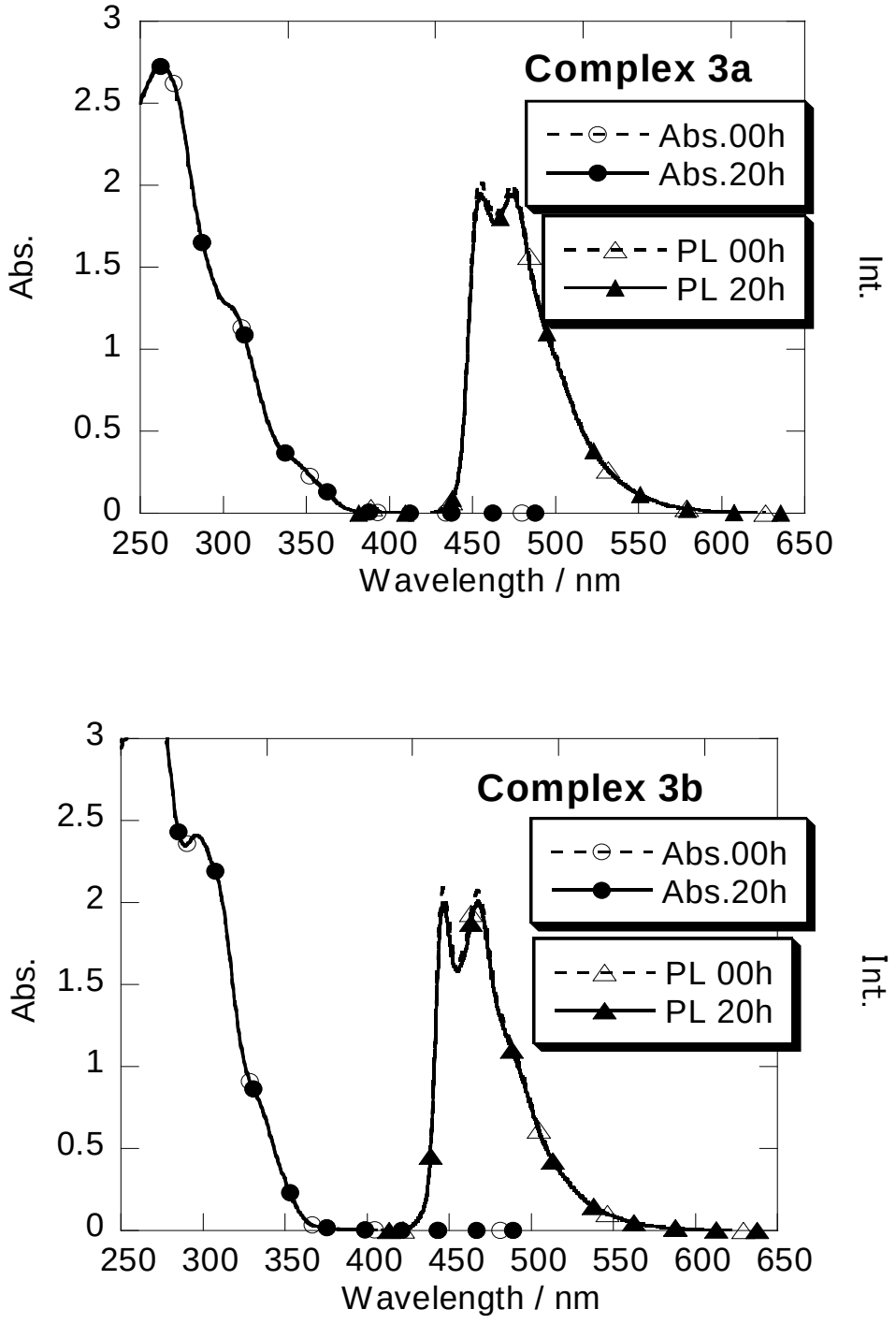

Figure 3-7-3. Absorption and phosphorescence spectra obtained by photochemical stability tests of **3a** and **3b**, before and after irradiation of 313 nm light for 20 h in degassed anhydrous THF solution.

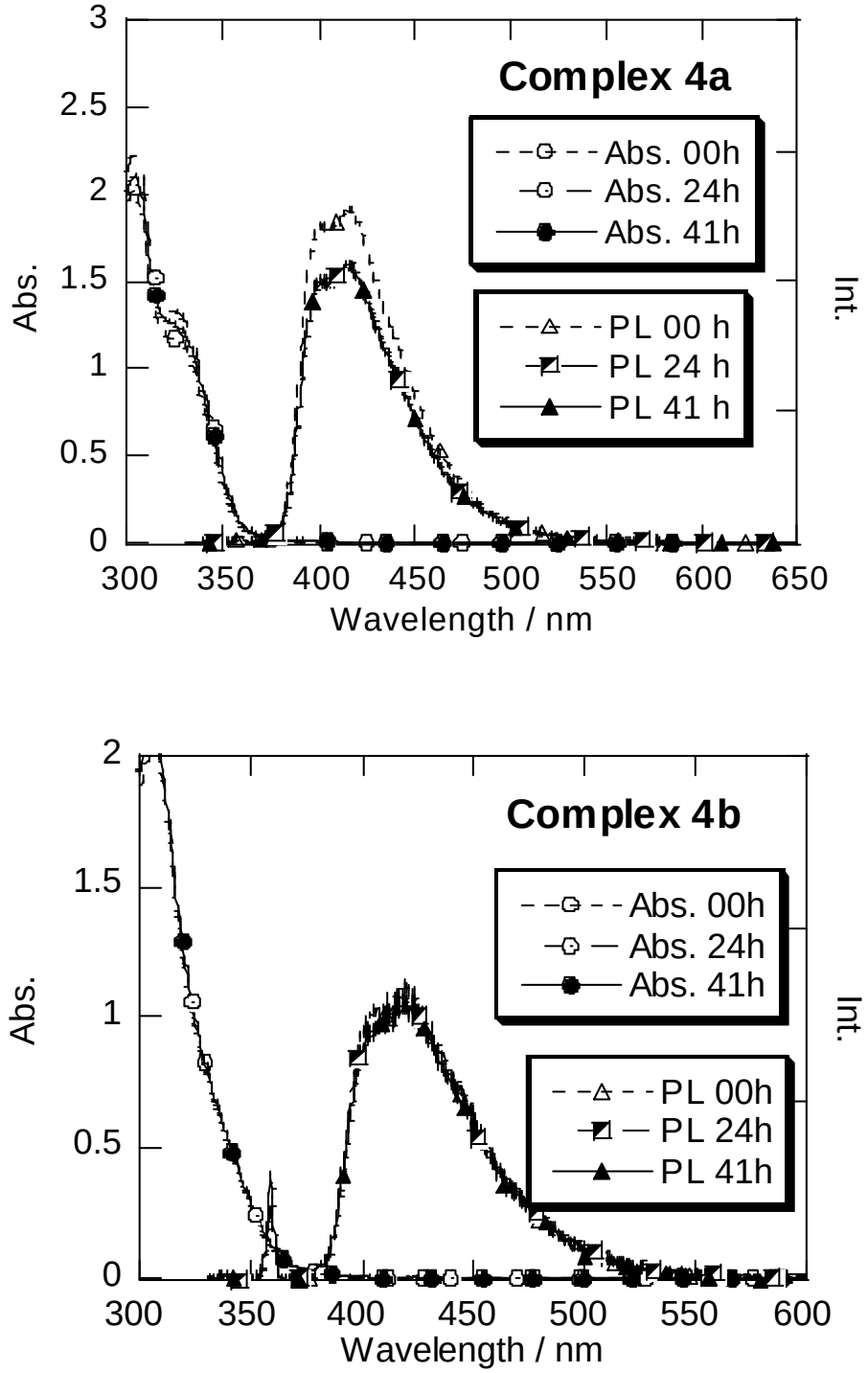

Figure 3-7-4. Absorption and phosphorescence spectra obtained by photochemical stability tests of **4a** and **4b**, before and after irradiation of 313 nm light for 20 – 41 h in degassed anhydrous THF solution.

3-3-6 DFT and TD-DFT calculation

The location of molecular orbital was calculated using optimized geometry of the ground state. It is revealed that in both **4a** and **4b**, the LUMO to LUMO+2 are delocalized over benzimidazole moiety (Figure 3-8) and the HOMO-2 to HOMO (Figure 3-9) are delocalized over Ir-Phenyl moiety. These results are similar to those of $Ir(ppz)_3$. It is reasonable that by substitution on the phenyl moiety, the HOMO level determined by cyclic voltammetry was affected, unless LUMO level could not be discussed because of hard to observe reduction potentials. However, HOMO level is stabilized by electron withdrawing group, the excitation energy is also decreased. This indicates that the LUMO level is also decreased. By MO consideration, although the LUMO is mainly spread over benzimidazol moiety, substituents on phenyl moiety affect both HOMO and LUMO energies. Next, we examined TD-DFT calculation. TD-DFT calculations were useful tool for understanding Ir complexes recently.[7e,16,23] The calculated lowest excitation wavelength of 4a and 4b are 393.1 and 388.9 nm for $S_0 - T_1$ absorption, respectively, and 361.0 nm and 371.9 nm for S_0 - S_1 absorption respectively (Table 3-5). These results of $S_0 - T_1$ absorption wavelength agree with the experimental results of emission spectra. In 4a, the main transition in $S_0 - T_1$ absorption is HOMO → LUMO+2 (51 %) which correspond to the Ir-phenyl to benzimidazol transition. In **4b,** the main transition in $S_0 - T_1$ absorption is HOMO → LUMO (58.9 %) which is also Ir-phenyl to equatorial benzimidazol transition. The $S_0 - T_2$, $S_0 - T_3$, and $S_0 - S_2$ absorptions of **4a** and **4b** are also listed in Table 3-6. The main transitions between these stats are also the Ir-Phenyl to benzimidazol transition. From such a reason, it seems that substitutions do not affect the energy level of LUMO, but it is also thought that increase of ΔE_{ST} is taking place. This question is under investigating.

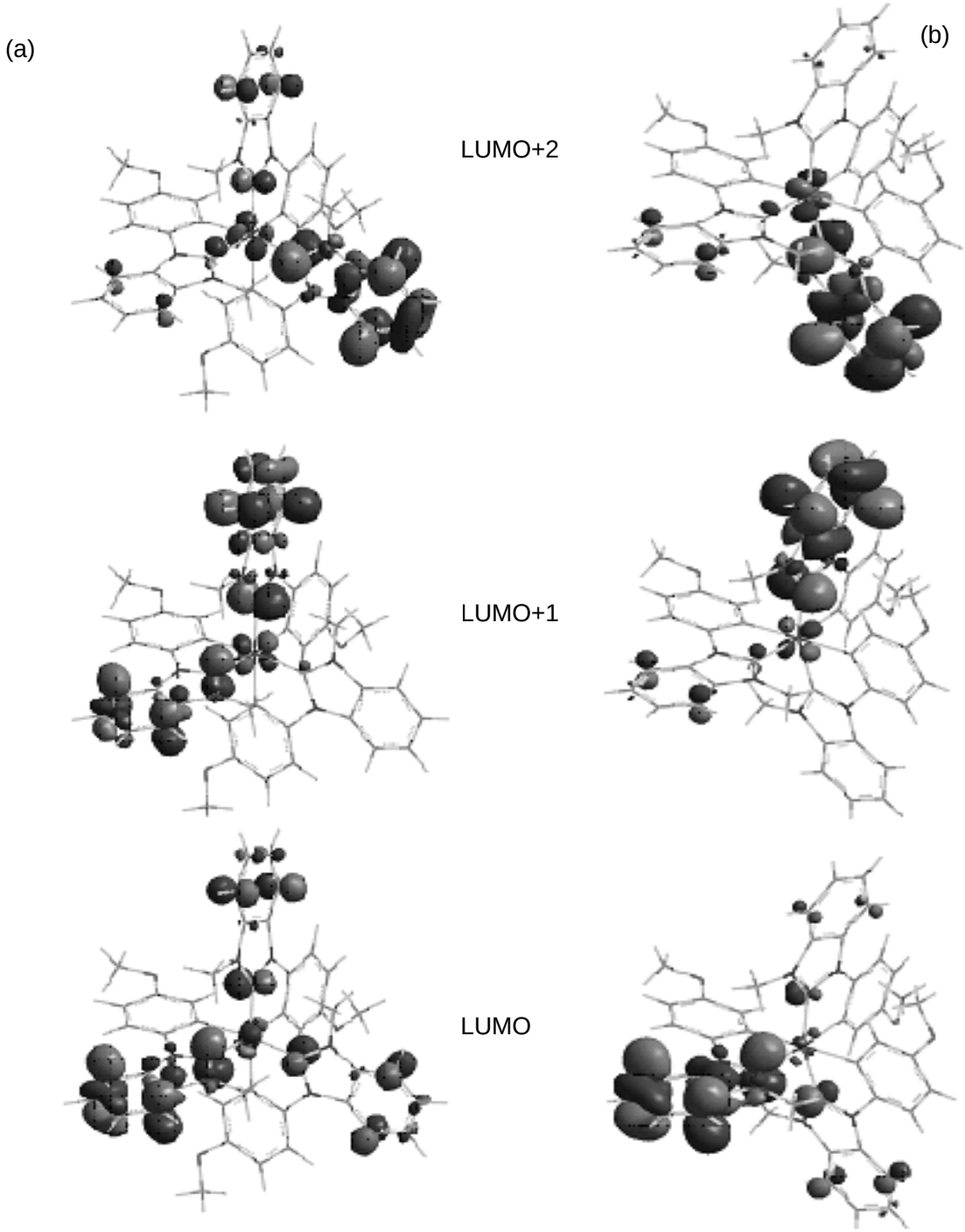

Figure 3-8. LUMO, LUMO + 1, and LUMO + 2 plots of *fac*-(a, leftside column) and *mer*-Ir(Opmb)$_3$ (b, right column) (**4a** and **4b**) obtained for the optimized structure of ground state.

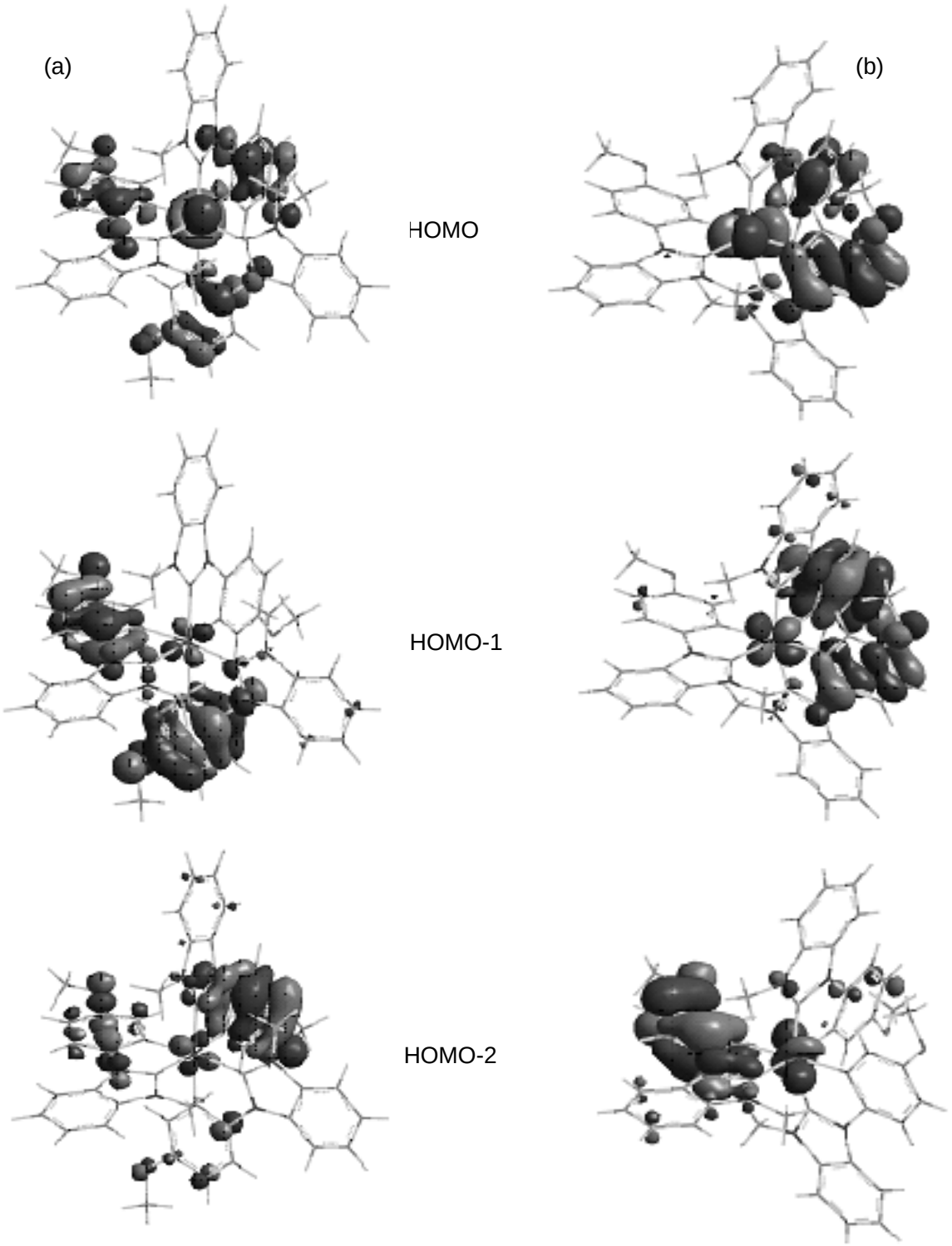

Figure 3-9. HOMO - 2, HOMO -1, and HOMO plots of *fac*-(a, leftside column) and *mer*-Ir(Opmb)$_3$ (b, right column) (**4a** and **4b**) obtained for the optimized structure of ground state.

Table 3-5. Calculated transition wavelength, oscillator strength (*f*), and MOs.

Complex	State	λ_{max} / nm	*f*	Assignments
4a	T_1	393.1	0	HOMO → LUMO+2 (51%)
				HOMO-2 → LUMO+1 (11.9%)
				HOMO → LUMO+1 (10.6%)
	S_1	361.0	0.0509	HOMO → LUMO+1(69.0%)
				HOMO → LUMO+2(31.1%)
4b	T_1	388.9	0	HOMO → LUMO (58.8%)
				HOMO → LUMO+1(16.8%)
				HOMO → LUMO+2(11.5%)
	S_1	371.91	0.0062	HOMO → LUMO (95.6%)

Table 3-6. Calculated transition wavelength, oscillator strength (*f*), and MOs concerned in transition of **4a** and **4b**.

Complex	State	λ_{max} / nm	*f*	Assignments
4a	T_1	393.1	0	HOMO → LUMO+2 (51%)
	T_2	391.5	0	HOMO → LUMO+1 (30.1%)
	T_3	390.4	0	HOMO → LUMO (50.7%)
	S_1	361.0	0.0509	HOMO → LUMO+1(69.0%)
	S_2	357.2		HOMO → LUMO+2(68.4%)
4b	T_1	388.9	0	HOMO-2 → LUMO (53.9%)
	T_2	381.85	0	HOMO → LUMO+1(31.4%)
	T_3	374.2	0	HOMO → LUMO+2(11.5%)
	S_1	371.91	0.0062	HOMO → LUMO (95.6%)
	S_2	359.6	0.0112	HOMO → LUMO+1 (95.3%)

3-4 Conclusion

New substituted tris(phenylbenzimidazolinato) Ir (III) carbene complexes were prepared by one pod syntheses and, their structures, photophysical properties, electrochemical properties, and photochemical stabilities were investigated. The location of HOMO and LUMO and lowest excitation energy were calculated by TD-DFT. The structures were not affected by both electro-withdrawing and electro-donating groups. From cyclic voltammetry, the oxidative potential energy was stabilized by electro-withdrawing group and slightly destabilized by electro-donating group. Luminescent properties were largely affected by functional group on phenyl moiety. The difference of k_r values between *fac* and *mer* isomer having same functional group was small but the difference of k_{nr} value was large in the $Ir(pmb)_3$ and Ir $(Opmb)_3$, relatively small in $Ir(CF_3pmb)_3$ and very small in $Ir(CNpmb)_3$. From DFT calculation, the HOMO delocalized over Ir-phenyl moiety and LUMO, LUMO+1, LUMO+2 delocalized over benzimizazole moiety. The calculated lowest triplet excited energies show good agreement with experimental data. Now we are evaluating the electroluminescent performance of OLED fabricated by above complexes.

3-5 Experimental Section

3-5-1 General Information and Material

All Chemicals used for synthesis were purchased from Aldrich, Kanto chemical, TCI, Wako Pure Chemical Industries, Kishida Chemical, N. E. Chemcat, and Fluya metal and used without further purification. Ir carbene complexes were prepared by one-pot synthesis method which is little modified from literature method.[13] Silver carbonate was used instead of silver oxide when $IrCl_3$ and ligand iodide were reacted (Scheme 3-3). Both *fac* and *mer* isomers were formed by refluxing in 2-ethoxyethanol. The yield is varied depending on kinds of ligand. All complexes were prepared as same procedure. ^1H NMR and ^{13}C NMR spectra were recorded on JEOL JNM-LA 400 and Bruker AVANCE 300. Mass spectra (FAB) were recorded on a JEOL JMS-AX500 double focusing mass spectrometer and Mass spectra (EM-SI) were recorded on Thermo Fisher Scientific Thermo Scientific Exactive spectrometer. Elemental analysis was

performed on Parkin-Elmer 2400.

3-5-2 Synthesis

Synthesis of *fac*-Ir(CF_3pmb)$_3$ and *mer*-Ir(CF_3pmb)

1-methyl-3-(4-trifluoromethylphenyl)benzimidazolium iodide (2.1g, 5.2 mmol), $IrCl_3$ nH_2O (580 mg, 1.65 mmol), silver carbonate (710 mg, 2.6 mmol), sodium carbonate (280 mg, 2.6 mmol) and ethoxyethanol(50 ml) were refluxed for 20 h. Both *mer* and *fac* isomers were formed. After the mixture was cooled to room temperature, diluted with water and the resultant precipitate was filter off, washed with water and methanol, crude product was purified by silica gel column chromatography and *mer* and *fac* isomer were successfully separated. Reprecipitation from CH_2Cl_2 and CH_3OH mixture and desirable compound was obtained as a white solid. 1.1 g of *fac*-Ir(CF_3pmb)$_3$ (68 %) and 0.38 g of *mer*-Ir(CF_3pmb)$_3$ (23%) were obtained. (yield with respect to $IrCl_3$-$3H_2O$)

***fac*-Iridium(III) Tris[1-(4-trifluoromethylphenyl)-3-methylbenzimida-zolin-2-ylidene] (2a)** yield: 1.1 g (62 % with respect to $IrCl_3$-$3H_2O$). ^{1}H NMR (400 MHz, $CDCl_3$): δ (ppm), 8.14 (d, J = 7.9 Hz, 3H, *Bzim*^{7}), 7.90 (d, J = 8.3 Hz, 3H, *Bzim*^{4}), 7.36 (ddd, J = 7.9, 7.5, 1.2 Hz, 3H, *Bzim*^{6}), 7.33 (dd, J = 8.3, 2.0 Hz, 3H, *Ph*^{5}), 7.29 (ddd, J = 8.3, 7.5, 0.8 Hz, 3H, *Bzim*^{5}), 7.22 (dd, J = 8.3, 0.79 Hz, 3H, *Ph*^{6}), 6.74 (d, J = 2.0 Hz, 3H, *Ph*^{3}), 3.27 (s, *J*, 9H, *N*-CH_3), ^{13}C NMR (100 MHz, DMSO): δ (ppm), 187.07 (3C, *Bzim*^{2}), 151.35 (3C, *Ph*^{1}), 148.60 (3C, *Ph*^{2}), 135.75, 131.53, 131.27, 126.04, 124.43, 124.13, 123.57, 123.31, 122.87, 119.01, 111.96, 111.38, 111.18 (33C, *Ph*^{3,4,5,6}, *bzim*^{3a,4,5,6,7,7a}, CF_3) 33.22 (3C, *N*-CH_3). HRMS(EM-SI): calcd. for $C_{45}H_{31}F_9IrN_6$ 1019.2090 [M + H]; found 1019.2094. $C_{45}H_{30}F_9IrN_6$, (1017.96): calcd. C 53.09, H 2.97, N 8.26; found C 52.68, H 2.40, N 8.08.

***mer*-Iridium(III) Tris[1-(4-trifluoromethylphenyl)-3-methylbenzimida-zolin-2-ylidene] (2b):** yield: 0.38 g (23 % with respect to $IrCl_3$-$3H_2O$). ^{1}H NMR (400 MHz, $CDCl_3$): δ (ppm), 8.16 (d, J = 8.3 Hz, 1H, Bzim^7), 8.15 (d, J = 7.9 Hz, 1H, *Bzim*^{7}), 8.11 (d, J = 7.9 Hz, 1H, *Bzim*^{7}), 7.90 (d, J = 8.2 Hz, 1H, *Bzim*^{4}), 7.89 (d, J = 8.0 Hz, 1H, *Bzim*^{4}), 7.88 (d, J = 8.9 Hz, 1H, *Bzim*^{4}), 7.43 – 7.23 (m, 12H, *Bzim*^{5,6}, *Ph*^{5,6}), 7.06

(d, J = 2.0 Hz, 1H, Ph^3), 6.95 (d, J = 2.0 Hz, 1H, Ph^3), 6.76 (d, J = 2.0 Hz, 1H, Ph^3), 3.27 (s, 3H, N-CH_3), 3.24 (s, 3H, N-CH_3), 3.17 (s, 3H, N-CH_3), ^{13}C NMR (100 MHz, $CDCl_3$): δ (ppm), 186.76, 185.07, 183.85 (3C, $Bzim^2$), 152.08, .151.52, 150.46 (3C, Ph^1), 149.58, 148.80, 147.62 (3C, Ph^2), 136.60, 136.55, 136.11, 134.72, 132.60, 132.31, .126.38, 126.26, 126.08, 125.95, 123.55, 123.51, 123.43, 123.35, 122.85, 122.58, 118.95, 118.85, 118.62, 112.18, 111.96, 111.85, 111.49, 111.33, 110.17, 110.07, 109.94 (33C, $Ph^{3,4,5,6}$, $bzim^{3a,4,5,6,7,7a}$, CF_3), 33.63, 33.50, 32.78 (N-CH_3). HRMS (EM-SI): Calcd for $C_{45}H_{31}F_9IrN_6$ 1019.2094 [M + H]; found 1019.2094. $C_{45}H_{30}F_9IrN_6$ (1017.96): calcd. C 53.09, H 2.97, N 8.26; found C 52.82, H 2.63, N 7.85.

***fac*-Iridium(III) Tris(4-cyanophenyl-3-methylbenzimidazolin-2-ylidene) (3a):** yield: 0.048 g (5.8 % with respect to $IrCl_3$-$3H_2O$). ^{1}H NMR (400 MHz, CD_2Cl_2): δ (ppm), 8.14 (d, J = 8.2 Hz, 3H, ($Bzim^7$), 7.94 (d, J = 8.2 Hz, 3H, $Bzim^4$), 7.40 (dd, J = 8.2, 1.9Hz, 3H, Ph^5), 7.39 (ddd, J = 8.2, 7.6, 1.8 Hz, 3H, $Bzim^6$), 7.32(ddd, J = 8.2, 7.5, 1.0 Hz, 3H, $Bzim^5$), 7.28 (dd, J = 8.2, 1.0 Hz, 3H, Ph^6), 6.73(d, J = 1.8 Hz, 3H, Ph^3), 3.25 (s, 9H, N-CH_3). MS (FAB): *m/z* calcd 889.23 ; found 889. $C_{45}H_{30}IrN_9$ (889.00): calcd. C 60.80, H 3.40, N 14.18; found C 60.41, H 3.03, N 14.07.

***mer*-Iridium(III) Tris(4-cyanophenyl-3-methylbenzimidazolin-2-ylidene) (3b):** yield: 0.17 g (21 % with respect to $IrCl_3$-$3H_2O$). ^{1}H NMR (400 MHz, $CDCl_3$): δ (ppm), 8.14 (d, J = 8.3 Hz, 3H, $Bzim^7$), 7.91(d, J = 8.2 Hz, 2H, $Bzim^4$), 7.89 (d, J = 8.1 Hz, 1H, $Bzim^4$), 7.48-7.24 (m, 12H, $Ph^{5,6}$, $Bzim^{5,6}$), 7.06 (d, J = 1.8 Hz, 1H, Ph^3), 7.04 (d, J = 1.9 Hz, 1H, Ph^3), 6.76 (d, J = 1.8 Hz, 1H, Ph^3), 3.28 (s, 3H, N-CH_3), 3.20 (s, 3H, N-CH_3), 3.17 (s, 3H, N-CH_3). ^{13}C NMR (100 MHz, $CDCl_3$): δ (ppm), 186.27, 184.84, 183.15 (3C, $Bzim^2$), 152.74, 152.07, 151.18 (3C, Ph^1), 149.45, 149.01, 147.04 (3C, Ph^2), 141.51, 141.48, 139.41, 136.49, 136.46, 136.05, 132.07, 126.95, 126.68, 126.40, 124.03, 123.95, 123.92, 123.47, 123.39, 123.21, 120.59, 120.35, 112.65, 112.35, 111.88, 111.62, 111.44, 110.63, 110.41, 110.36, 108.10, 107.88, 107.74 (33C, $Ph^{3,4,5,6}$, $bzim^{3a,4,5,6,7,7a}$, CN), 33.86, 33.82, 32.95 (3C, N-CH_3). HRMS (EM-SI): Calcd for $C_{45}H_{30}IrN_9$ 890.23 [M + H]; found 890.23. $C_{45}H_{30}IrN_9$ 0.5 H_2O (898.01): calcd. C 60.17, H 3.48, N 14.04; found C 60.02, H 3.23, N 13.73.

***fac*-Iridium(III) Tris[1-(4-methoxyphenyl)-3-methylbenzimidazolin-2-ylidene] (4a):** yield: 0.19 g (37 % with respect to $IrCl_3$-$3H_2O$). ^1H NMR (400 MHz, $CDCl_3$): δ (ppm), 8.07 (d, J = 8.2 Hz, 3H, *Bzim*^{7}), 7.74 (d, J = 8.6 Hz, 3H, *Bzim*^{4}), 7.28 (ddd, J = 8.2, 6.4, 1.5 Hz, 3H, *Bzim*^{6}), 7.20 (ddd, J = 8.6, 6.4, 0.89 Hz, 3H, *Bzim*^{5}), 7.16 (dd, J = 8.1, 1.3, Hz, 3H, *Ph*^{6}), 6.56 (dd, J = 8.6, 2.9 Hz, 3H, *Ph*^{5}), 6.26 (d, J = 3.0 Hz, 3H, *Ph*^{3}), 3.50 (s, *J*, 9H, OCH_3), 3.24 (s, 9H, *N*-CH_3), MS (FAB): *m/z* calcd 904.27 ; found 905. $C_{45}H_{39}IrN_6O_3$ (904.05): C 59.78, H 4.35, N 9.30; found C 59.51, H 4.06, N 9.24.

***mer*-Iridium(III) Tris[1-(4-methoxyphenyl)-3-methylbenzimidazolin-2-ylidene](4b):** yield: 0.043 g (8.3 % with respect to $IrCl_3$-$3H_2O$). ^1H NMR (400 MHz, $CDCl_3$): δ (ppm), 8.11 (d, J = 8.2 Hz, 1H, *Bzim*^{7}), 8.09 (d, J = 8.1 Hz, 1H, *Bzim*^{7}), 8.03 (d, J = 8.1 Hz, 1H, *Bzim*^{7}), 7.75 (d, J = 8.5 Hz, 1H, *Bzim*^{4}), 7.74 (d, J = 8.5 Hz, 1H, *Bzim*^{4}), 7.71 (d, J = 8.5 Hz, 1H, *Bzim*^{4}), 7.35 – 7.16 (m, 9H, Bzim^{6,7}, *Ph*^{6}), 6.56 (m, 5H, *Ph*^{3,5}), 6.20 (d, J = 2.9 Hz, 1H, *Ph*^{3}), 3.55 (s, 3H, OCH_3), 3.54 (s, 3H, OCH_3), 3.52 (s, 3H, OCH_3), 3.30 (s, 3H, *N*-CH_3), 3.22 (s, 3H, *N*-CH_3), 3.21 (s, 3H, *N*-CH_3), MS (FAB): *m/z* calcd 904.27 ; found 905. $C_{45}H_{39}IrN_6O_3$ (904.05): C 59.78, H 4.35, N 9.30; found C 59.45, H 4.05, N 9.13.

***fac*-Iridium(III) Tris(1-phenyl-3-methylbenzimidazolin-2-ylidene) (1a)** yield: 0.12 g (26 % with respect to $IrCl_3$-$3H_2O$): ^1H NMR (400 MHz, $CDCl_3$): δ (ppm), 8.14 (d, J = 8.2 Hz, 3H, *Bzim*^{7}), 7.86 (d, J = 7.4 Hz, 3H, *Bzim*^{4}), 7.29 (td, J = 7.7, 1.4 Hz, 3H, *Bzim*^{6}), 7.22 (t, J = 6.5 Hz, 3H, *Bzim*^{5}), 7.17 (dd, J = 7.9, 0.95 Hz, 3H, *Ph*^{6}), 7.06 (td, J = 7.6, 1.5 Hz, 3H, *Ph*^{5}), 6.73 (td, J = 7.3, 0.73 Hz, 3H, *Ph*^{4}), 6.68 (dd, J = 7.2, 1.4 Hz, 3H, *Ph*^{3}), 3.27 (s, 9H, *N*-CH_3). ^{13}C NMR (100 MHz, $CDCl_3$) δ (ppm), 189.64 (3C, *Bzim*^{2}), 148.76, 148.65, (6C, *Ph*^{1,2}) 137.03, 136.35, 132.68, 124.67, 122.63, 121.69, 120.88, 112.01, 111.18, 109.52 (30C, *Ph*^{3,4,5,6}, *bzim*^{3a,4,5,6,7,7a}), 33.45 (3C, *N*-CH_3). MS (FAB): *m/z* calcd 814.24 ; found 814.

***mer*-Iridium(III) Tris(1-phenyl-3-methylbenzimidazolin-2-ylidene) (1b):** yield: 0.061 g (13 % with respect to $IrCl_3$-$3H_2O$). ^1H NMR (400 MHz, $CDCl_3$): δ (ppm), 8.18 (d, J = 8.2 Hz, 1H, *Bzim*^{7}), 8.16 (d, J = 8.2 Hz, 1H, *Bzim*^{7}), 8.10 (d, J = 8.2 Hz, 1H, *Bzim*^{7}), 7.85 (d, J = 7.2 Hz, 1H, *Bzim*^{4}), 7.83 (d, J = 7.5 Hz, 1H, *Bzim*^{4}), 7.81 (d, J = 6.7 Hz, 1H, *Bzim*^{4}), 7.38-7.18 (m, 9H, Ph^6, *Bzim*^{5,6}), 7.05-6.97 (m, 2H, *Ph*^{5}), 6.94 (td, J = 7.6, 1.5 Hz, 1H, *Ph*^{5}), 6.90 (dd, J = 7.24, 1.6 Hz, 1H, *Ph*^{4}), 6.85 (dd, J = 7.2, 1.4 Hz, 1H, *Ph*^{4}), 6.71 (td, J

= 7.3, 0.94, 1H, *Ph*[4]), 6.67 (td, *J* = 7.2, 0.94, 1H, *Ph*[3]), 6.64-6.58 (m, 2H, *Ph*[3]), 3.28 (s, 3H), 3.25 (s, 3H), 3.19 (s, 3H). ^{13}C NMR (100 MHz, $CDCl_3$): δ (ppm), 188.40, 186.15, 185.03 (3C, *Bzim*[2]), 150.87, 149.72, 149.35, 148.90, 147.96, 147.92 (6C, *Ph*[1,2]), 144.13, 139.20, 139.03, 136.76, 136.71, 136.35, 132.67, 132.61, 132.59, 124.85, 124.62, 124.43, 122.68, 122.51, 121.91, 121.82, 121.52, 120.65, 120.32, 120.28, 112.45, 111.83, 111.24, 111.15, 109.70, 109.60, 109.46 (30C, *Ph*[3,4,5,6], *bzim*[3a,4,5,6,7,7a]), 33.42, 33.35, 32.81 (3C, *N*-CH_3). MS (FAB): *m/z* calcd 814.24; found 814.

3-5-3 X-ray crystallography

Single crystal of *fac*-Ir(CF_3pmb)$_3$ was grown from $C_2H_2Cl_2$-CH_3OH. Single crystal of *mer*-Ir(Opmb)$_3$ was grown from CH_2Cl_2-CH_3OH. Diffraction data were collected on Bruker SMART APEX CCD diffractmeter with graphite monochromated Mo Ka radiation. The cell parameters for the iridium complexes were obtained from a least-squares refinement of the spots using the SMART program. All calculations were carried out using the SHELXTL package. Initial atomic positions were located by direct methods or Patterson methods and the structures of the compound were refined by the least-squares using XShell program. The crystallographic date for **2a** and **4b** are summarized in Appendix.

3-5-4. Electrochemistry

Cyclic voltammetry were performed in standard compartment cell equipped with BAS Pt working electrode, a platinum wire counter electrode, and Ag/Ag^+ ($Ag/AgNO_3$) reference electrode with HOKUTO DENKO HABF1510 analyzer (Figure 3-10). Anhydrous THF was used as a solvent and tetrabutylammonium tetrafluoroborate was used as a supporting electrolyte. All potentials were reported as a relative to Cp_2Fe/Cp_2Fe^+.

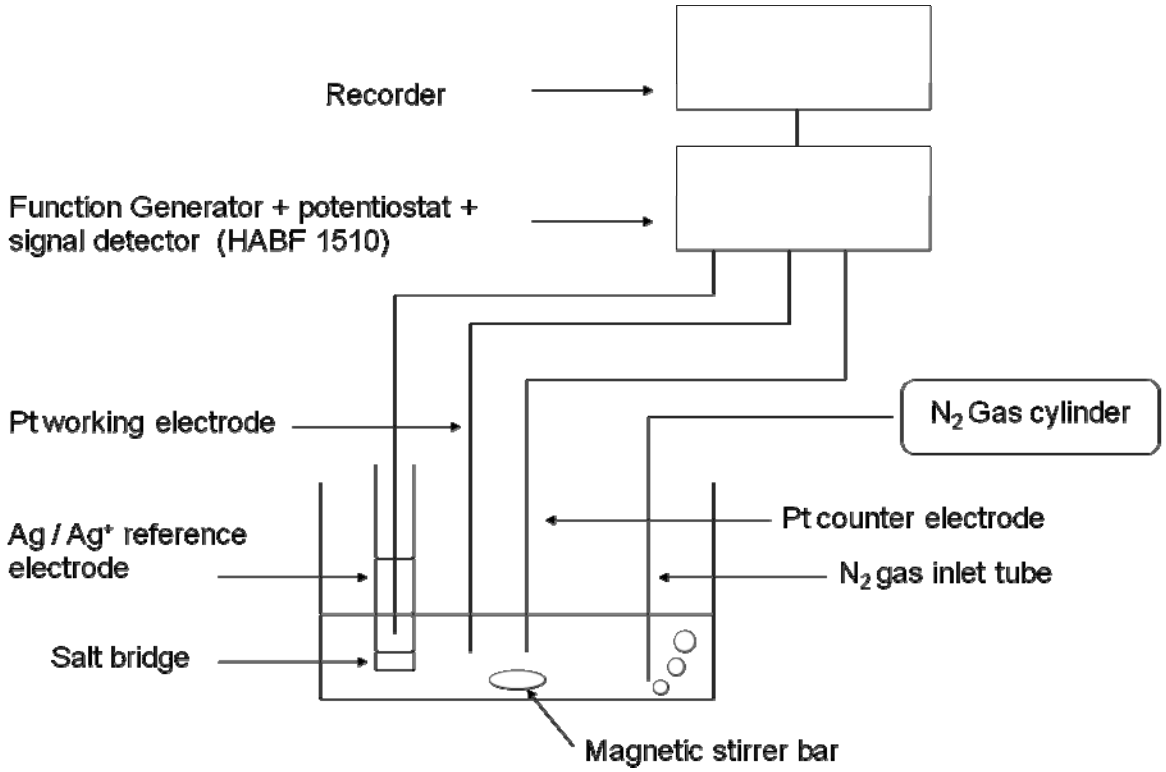

Figure 3-10. Scheme of cyclic voltammetry.

3-5-5. DFT and TD-DFT calculation

DFT and TD-DFT calculations were performed using Gawssian 03 package[24] at the B3LYP/ LANL2DZ level. 6-31G basis sets were employed. The structures obtained from X-ray crystallography were optimized and the location of molecular orbitals such as HOMO and LUMO were calculated with the ground state. TD-DFT calculations were performed with the ground-state geometry to obtain the vertical excitation energies of the low-lying singlet and triplet excited state of the complexes.

3-5-6. Photophysical property

UV-Vis absorption spectra were measured on JASCO-U570 spectrophotometer. PL spectra were measured on JASCO F6010 fluorimeter. Response of the instrument was corrected using rhodamine standard solution. Sample THF solution was degassed by three times freeze─pump thaw cycles, and

introduced into 1cm path length cuvette. Phosphorescence quantum yields were determined by using 9,10-diphenylanthracene in cyclohexane ($\Phi = 0.90$) as reference, and formula $\Phi_X = \Phi_S \times (n_X / n_S)^2 \times (A_X / A_S) \times (Abs_S / Abs_X)$ was used. Here, subscripts X and S indicate sample and reference, respectively, and n is reflective index of solvent, A is the area of emission spectra, and Abs is absorbance at the excitation wavelength (Abs is set around 0.20). PL lifetimes were measured by a single photon counting instrument (Horiba NAES 550) or by PL lifetimes were measuring on SPEX 270 M spectrometer equipped with photomultiplier tube and Hewlett Packard 54510B digital oscilloscope using Hoya Continuum Surelite-I Nd^{3+}:YAG laser 355 nm pulse as excitation source. Stabilizer free anhydrous THF was used as a solvent for measuring PL quantum yield and PL lifetime (purchased from Wako Chemicals).

Photochemical stability: Photochemical stability was measured in anhydrous THF degassed by three times freeze─pump thaw cycles. Irradiation was performed using 313 nm line of 400 W middle pressure mercury lumps (RIKO). *fac*-$Ir(tpy)_3$ was used as a reference for determining photochemical isomerization quantum yield. The reaction was checked by UV-Vis spectra and PL spectra and after irradiation for 20 - 40 h, then sample tube was opened then condensed by evaporation of solvent, and analyzed by TLC.

3-6 References

[1] a) M. A. Baldo, D. F. O'Brien, Y. You, A. Shoustikov, S. Sibley, M. E. Thompson, S. R. Forrest, *Nature* **1998**, *395*, 151–154, b) M. A. Baldo, S. Lamansky, P. E. Burrows, M. E. Thompson, S. R. Forrest, *Appl. Phys. Lett.* **1999**, *75*, 4–6.

[2] H. Yersin (Ed.), *Highly Efficient OLEDs with Phosphorescent Materials,* Wiley-VCH, Weinheim, **2008** references cited therein.

[3] Y.-L. Tung, S-W. Lee, Y. Chi, Y.-T. Tao, C.-H. Chien, Y-M. Cheng, P.-T. Chou, S.-M. Peng, C.-S. Liu, *J. Mater. Chem.* **2005**, *15*, 460–464.

[4] a) A. Tsuboyama, H. Iwawaki, M. Furugori, T. Mukaide, J. Kamatani, S. Igawa, T. Moriyama, S. Miura, T. Takiguchi, S. Okada, M. Hoshino, K. Ueno, *J. Am. Chem. Soc.* **2003**, *125*, 12971–12979, b) M. Tavasli, S. Bettington, I. F. Perepichka, A. S. Batsanov, M. R. Bryce, C. Rothe, A. P. Monkman, *Eur. J. Inorg. Chem.* **2007**, 4808–4814.

[5] S. Tokito, T. Iijima, T. Tsuzuki, F. Sato, *Appl, Phys. Lett.* **2003**, 83, 2459–2461.

[6] A. Tamayo, B. D. Alleyne, P. I.Djurovich, S. Lamansky, I. Tsyba, N. N. Ho, R. Bau, M. E. Thompson, *J. Am. Chem. Soc*. **2003**, *125*, 7377–7387.

[7] a) S. Lamansky, P. Djurovich, D. Murphy, F. A.-Razzaq, H.- E. Lee, C. Adachi, P. E. Burrows, S. R. Foorest, M. E. Thompson, *J. Am. Chem. Soc.* **2001**, *123*, 4304–4312, b) Y. You, S. Y. Park, *J. Am. Chem. Soc.* **2005**, *127*, 12438–12439, c) S. Kappaun, S. Eder, S. Sax, K. Mereiter, E. J. W. List, C. Slugove, *Eur. J. Inorg. Chem.* **2007**, 4207–4215, d) C. Yi, C.-J. Yang, J. Liu, M. Xu, J.-H. Wang, Q.-Y. Cao, X.-C. Gao, *Inorg. Chimi. Acta.* **2007**, *360*, 3493–3498, e) X. Gu, T. Fei, H. Zhang, H. Xu, B. Yang, Y. Ma, X. Liu, *Eur. J. Inorg. Chem*. **2009**, 2407-2414,

[8] T. Karatsu, T. Nakamura, S. Yagai, A. Kitamura, K. Yamaguchi, Y. Matsushima, T. Iwata, Y. Hori, T. Hagiwara, *Chem. Lett.* **2003**, *32*, 886–887.

[9] a) M. Xu, R. Zhou, G. Wang, Q. Xiao, W. Du, G. Che, *Inorg. Chim. Acta.* **2008**, *361*, 2407–2412, b) H. Jang, C. H. Shin, N. G. Kim, K. Y. Hwang, Y. Do, *Synthetic Metals*, **2005**, *154*, 157–160.

[10] T. Karatsu, E. Ito, S. Yagai, A. Kitamura, *Chem. Phys. Lett.* **2006**, *424*, 353–357.

[11] C.-H. Yang, S.-W. Li, Y. Chi, Y.-M. Cheng, Y.-S. Yeh, P.-T. Chou, G.-H. Lee, C.-H. Wang, C.-F. Shu, *Inorg. Chem.* **2005**, *44*, 7770–7780.

[12] a) G. Treboux, J. Mizukami, M. Yabe, S. Nakamura, *Chem. Lett.* **2007**, *36*, 1344-1345, b) L. Yang, F. Okada, K. Kobayashi, K. Nozaki, Y. Tanabe, Y. Ishii, M. Haga, *Inorg. Chem.* **2008**, *47*, 6681–6691.

[13] a) T. Sajoto, P. I. Djurovich, A. B. Tamayo, M. Yousufuddin, R. Bau, M. E. Thompson, R. J. Holmes, S. R. Forrest, *Inorg. Chem.* **2005**, *44*, 7992–8003, b) T. Sajoto, P. I. Djurovich, A. B. Tamayo, J. Oxgaard, A. A. Goddard III, M. E. Thompson, *J. Am. Chem. Soc*, **2009**, *131*, 9813–9822.

[14] R. J. Holmes, S. R. Forrest, T. Sajoto, A. Tamayo, P. I. Djurovich, M. E. Thompson, J. Brooks, Y.-J. Tung, B. W. D'Andrade, M. S. Weaver, R. C. Kwong, J. J. Brown, *Appl. Phys. Lett.* **2005**, *87*, 243507-1–243507-3.

[15] S. Haneder, E. D. Como, J. Feldmann, J. M. Lupton, C. Lennartz, P. Erk, E. Fuchs, O. Molt, I. Münster, C. Schildknecht, G. Wagenblast. *Adv. Mater.* **2008**, *20*, 3325–3330.

[16] C.-F. Chang, Y.-M. Cheng, Y. Chi, Y.-C. Chiu, C.-C. Liu, G.-H. Lee, P.-T. Chou, C.-C. Chen, C.-H. Chang, C.-C. Wu, *Angew. Chem. Int. Ed.* **2008**, *47*, 4542–4545.

[17] a) C.-H. Chien, S. Fujita, S. Yamato, T. Hara, T. Yamagata, M. Watanabe, K. Mashima, Dalton Trans. **2008**, 916–923, b) P. B. Hitchcock, M. F. Lappert, P. Terreros, *J. Organomet. Chem.* **1982**, *239*, C26–C30.

[18] L. Zhu, P. Guo, G. Li, J. Lau, R. Xie, J. You, *J. Org. Chem.* **2007**, *72*, 8535–8538.

[19] J Li, P. I. Djurovich, B. D. Alleyne, M. Yousufuddin, N. N. Ho, J. C. Thomas, J. C. Peters, R.Bau, M. E. Thompson. *Inorg. Chem,* **2005,** *44*, 1713–1727.

[20] J. H. Jou, M.-F. Hsu, W.-B. Wang, C.- L. Chin, Y.- C. Chung, C.-T Chen, J.-J. Shyue, S.-M. Shen, M.-H. Wu, W.-C. Chang, C.-P. Liu, S.-Z. Chen, H.-Y. Chen, *Chem. Mater.* **2009**, *21*, 2565–2567.

[21] K. Tsuchiya, E. Ito, S. Yagai, A. Kitamura, T. Karatsu, *Eur. J. Inorg. Chem*. **2009**, 2104-2109.

[22] T. Sajoto, P. I. Djurovich, A. B. Tamayo, J. Oxgaard, W. A. Goddard III, M. E. Thompson, *J. Am. Chem.Soc.,* **2009**, *131*, 9813–9822.

[23] S.-J. Liu, Q. Zhao, Q.-L. Fan, W. Huang, *Eur. J. Inorg. Chem*. **2008,** 2177-2185.

[24] M. J. Frisch, G. W. Trucks, H. B. Schlegel, G. E. Scuseria, M. A. Robb, J. R. Cheeseman, J. A. Montgomery Jr, T. Vreven, K. N. Kudin, J. C. Burant, J. M. Millam, S. S. Iyengar, J. Tomasi,V. Barone, B. Mennucci, M. Cossi, G. Scalmani, N. Rega, G. A. Petersson, H. Nakatsuji, M. Hada, M. Ehara, K. Toyota, R. Fukuda, J. Hasegawa, M. Ishida, T. Nakajima, Y. Honda, O. Kitao, H. Nakai, M. Klene, X. Li, J. E. Knox, H. P. Hratchian, J. B. Cross, C. Adamo, J. Jaramillo, R. Gomperts, R. E.Stratmann, O. Yazyev, A. J. Austin, R. Cammi, C. Pomelli, J. W. Ochterski, P. Y. Ayala, K. Morokuma, G. A. Voth, P. Salvador, J. J. Dannenberg, V. G. Zakrzewski, S. Dapprich, A. D. Daniels, M. C. Strain, O. Farkas, D. K. Malick, A. D. Rabuck, K. Raghavachari, J. B. Foresman, J. V. Ortiz, Q. Cui, A. G. Baboul, S. Clifford, J. Cioslowski, B. B. Stefanov, G. Liu, A. Liashenko, P. Piskorz, I. Komaromi, R. L. Martin, D. J. Fox, T.Keith, M. A. Al-Laham, C. Y. Peng, A. Nanayakkara, M.Challacombe, P. M. W. Gill, B. Johnson, W. Chen, M. W.Wong, C. Gonzalez, J. A. Pople, *Gaussian 03*, Revision B.03,Gaussian, Inc., Pittsburgh, PA, **2003**.

Chapter 4

Conclusion and Future Prospect

Luminosity factor is the photophysical parameter for the sensitivities of human eyes. Blue and red color luminosity factors are very small comparing to that of green. In addition, triplet phosphorescent materials are needed to fabricate OLED devices due to the efficiency of recombination of a hole and an electron. However, triplet excited state (phosphorescent state) has lower triplet energy than that of singlet excited state (fluorescent state), therefore, it is hard to achieve the aim. Development of blue phosphorescence materials has been increasing its importance in these days.

In chapter 2, it has been revealed that the enantiomers of separated *mer*-Ir(ppz)$_3$ retains some part of a chiral information during photochemical isomerization to the corresponding *fac*-isomers. It was suggested that in *mer*-Ir(ppz)$_3$, the axial Ir-N bond is dissociated and rehybridization to the TBP (trigonal bipyramidal) transition state. This has been known as Adamson's empirical rule, however, it has not been evaluated to Ir complexes since then. I have investigated about this matter, and succeeded to obtain rational explanations. This was also supported by TD-DFT quantum chemical calculations. From this study, an avoidance of the ^{3}MLCT and ^{3}LC mixed emissive state from activation to a non emissive bond dissociative LF state is important to obtained highly blue phosphorescent Ir complexes.

In chapter 3, the photophysical property of Ir carbene complexes has been studied to improve their phosphorescent property by simple substitution using several functional groups. In *fac* isomer, the phosphorescent quantum yield was increased by both electro-donation and -withdrawing group in *fac* isomer. In *mer* isomer, the complexes having electro-withdrawing group showed the large enhancement of phosphorescent quantum yields. Electro-withdrawing groups also increased the photohchemical stability in both *fac* and *mer* isomer. In all substituted complexes, although the non radiative deactivation rate constants were decreased, the radiative rate constants were also unfortunately decreased, and therefore the excited state lifetimes were increased (see Table 3-3 in chapter 3). The short lifetime is important in OLED devices because longer lifetime leads to increase of triplet-triplet self annihilation of Ir complexes. Investigations of EL performance must be examined.

I have studied about the excited state properties to obtain high performance blue phosphorescent Ir complexes, and I have obtained several fundamental insights as mentioned above. This study also harvests another benefits as mentioned following.

The use of circular polarized luminescence from enantio-separated Ir complexes and obtain the enantio-pure Ir complexes is beneficial.[1] I and my co-workers continued the study about photochemical enantioselective isomerization of Ir complexes. We obtained two interesting results. *mer*-Ir(ppz)$_2$(tpy) showed completely enantioselective *mer*-to *fac* photochemical isomerization (i.e. Δ-*mer*-isomer is photochemically converted to only Δ-*fac*-isomer). The large solvent dependency of photochemical isomerization enantioselectivity of *mer*-Ir(ppz)$_3$ is also observed. The photochemical isomerizations of Δ-*mer*-Ir(ppz)$_3$ yielded Λ-*fac*-Ir(ppz)$_3$ in toluene, CH_2Cl_2, THF, and CH_3OH, which results are inverted from the result observed in CH_3CN, and the enantioselectivities are also different between these solvents. Now, obtaining enantio-pure *fac* isomer needs pre-enatio-separation of *mer* isomer, however if enantio-pure *fac*-isomer is obtained from racemic *mer*-isomer by only photoirradiation, the field of chiral chemistry of Ir complexes will be drastically progressed. Using chiral solvent and proper ligand or using chiral Ru complex photosensitizer[2] may be enabled to realize this method.

The control of excited state property of Ir carbene complexes will be useful as a technique for improving other photonic application like a sensor, sensitizer, and photovoltaic cell.

References

[1] F. J. Coughlin, M. S. Westrol, K. D. Oyler, N. Byrne, C. Kraml, E. Z-. Colman, M. S. Lowry, S. Bernhard, *Inorg. Chem.* **2008**, *47*, 2039–2048.

[2] T. Hamada, H. Ohtsuka, S. Sakai, *Chem. Lett.* **2000**, 364–365.

Acknowledgements

First of all, I would like to express my profound thanks to my supervisor, Prof. Dr. Takashi Karatsu for guiding me to the present work. He strongly, patiently and kindly supported my research.

I would like to thank also following people:

Prof. Dr. Kyoichi Saito (Chiba University) for his acceptance the chief investigator for this doctoral thesis. Prof. Dr. Akihide Kitamura (Chiba University), Prof. Dr. Shogo Shimazu (Chiba University), Prof. Dr. Masahito Kushida (Chiba University) for their acceptance the investigator for this doctoral thesis.

Ms. Kyoko Endo, Mr. Junji Mizukami, Mr. Seiji Akiyama, and Masayoshi Yabe (Mitsubishi Chemical Group Science and Technology Research Center) for their valuable discussion and experimental assistance in Chapter 3.

Prof. Dr. Akihide Kitamura, Prof. Dr. Shiki Yagai and my colleague for their supporting my study in the laboratory I belong to.

Finally, I profoundly thank my parents and my brother for their patient supporting in many aspects for 9 years since I entered Faculty of material science of Chiba University.

January 2010

Kazuyoshi Tsuchiya

本研究を行なうにあたり、主任指導教官としてご指導下さった唐津孝教授（千葉大学工学部共生応用化学科エネルギー変換材料化学研究室）に深く感謝するとともに心より御礼申し上げます。お忙しい中、本学位論文の主査を引き受けてくださった斎藤恭一教授（千葉大学工学部共生応用化学科バイオマテリアル研究室）に御礼申し上げます。さらに副査を引き受けて下さった北村彰

英教授（千葉大学工学部共生応用化学科エネルギー変換材料化学研究室）、島津省吾教授（千葉大学工学部共生応用化学科触媒化学研究室）、串田正人准教授（千葉大学工学部共生応用化学科バイオプロセス化学研究室）に御礼申し上げます。

また、以下の方々にも御礼申し上げます。

Chapter 3 の研究において、錯体の合成法及び発光特性の考察等で多大なご援助、ご助言をいただきました三菱化学科学技術研究センターの遠藤恭子様、水上潤二様、秋山誠治様、矢部昌義様に御礼申し上げます。

研究室において、研究に対するご助言や実験の指導でお世話になりました北村彰英教授、矢貝史樹助教に御礼申し上げます。また研究室の学生の方々にも御礼申し上げます。

最後に、千葉大学工学部物質工学科に入学してから博士後期課程修了に至るまで、9 年間もの長い間、支え続けて下さった両親と兄に深く感謝申し上げます。

2010 年 1 月

土屋　和芳

List of publications

Main paper

[1] K. Tsuchiya, E. Ito, S. Yagai, A. Kitamura, T. Karatsu : Chirality in the Photochemical *mer*→*fac* Geometrical Isomerization of Tris(1-phenylpyrazolato,*N*,$C^{2'}$) iridium(III), *Eur. J. Inorg. Chem.*, **2009**,, 2104‐2109.

[2] K. Tsuchiya, S. Yagai, A. Kitamura, T. Karatsu, K. Endo, J. Mizukami, S. Akiyama, M. Yabe : Synthesis and Photophysical Properties of Substituted Tris(Phenylbenzimida- zolinato) Ir(III) Carbene Complexes as a Blue Phosphorescent Material, *Eur. J. Inorg. Chem*., **2010**, 926‐933.

Relevant papers

土屋　和芳, 唐津　孝　：　青色りん光を発するイリジウム錯体, 光化学, ３８巻, １号, ４０‐４２頁, ２００７年.

学会発表

国際学会

（口頭発表）

［1］ ○K. Tsuchiya, S. Yagai, A. Kitamura, T. Karatsu, k. Endo, M. Yabe : Photophysical Properties of Blue Phosphorescent tris (4-Substituted Phenylbenzimidazolinato Ir(III) carbene complexes. The 2008 Korea-Japan Symposium on Frontier Photoscience, YL07, Jeju, Korea, September 2008.

[2] ○T. Karatsu, K. Tsuchiya, T. Sugizaki, S. Yagai, A. Kitamura : PHOTOCHEMICAL MER-FAC ISOMERIZATION OF BLUE TO RED PHOSPHORESCENT TRISCYCLO- METALATED Ir(III) COMPLEXES, *18 th ISPPCC*, IL-5, Sapporo, Japan, July 2009.

[3] ○T. Karatsu, K. Tsuchiya, H. Iwaki, S. Yagai, A. Kitamura : Chirality in the photo- chemical *mer* → *fac* geometrical isomerization of Iridium(III) triscyclometalated complexes., The 2008

Korea-Japan Symposium on Frontier Photoscience, IL25, Jeju, Korea, September 2008.

（ポスター発表）

[1] ○K. Tsuchiya, S. Yagai, A. Kitamura, T. Karatsu, K. Endo, J. Mizukami, S. Akiyama, M. Yabe：SYNTHESIS AND PHOTOPHYSICAL PROPERTY OF SUBSTITUTED TRIS(PHENYLBENZIMIDAZOLINATO) Ir(III) CARBENE COMPLEXES AS A BLUE PHOSPHRESCENT MATERIAL., 18th ISPPCC, P131, Sapporo, Japan, July 2009.

国内学会

（口頭発表）

[1] ○土屋和芳，岩城宏樹，矢貝史樹，北村彰英，唐津　孝　：　シクロメタレート型 Ir(III) 錯体の光異性化と反応機構の考察、第２１回配位化合物の光化学討論会，O-09，北里大学相模原キャンパス，２００８年８月.

[2] ○土屋和芳，唐津　孝，岩城宏樹，矢貝史樹，北村彰英　：　トリスシクロメタレート型 Ir(Ⅲ)錯体の光による幾何及び光学異性化，日本化学会第８８回春季年会，2E6-45，立教大学池袋キャンパス，２００８年３月.

（ポスター発表）

[1] ○土屋和芳，唐津　孝，矢貝史樹，北村彰英　：　有機 Ir 金属錯体の光異性化挙動の研究，光化学討論会，3P58，信州大学松本キャンパス，２００７年９月.

[2] 唐津　孝，○岩城宏樹，土屋和芳，矢貝史樹，北村彰英　：　トリスシクロメタレート Ir(III)錯体の光による幾何及び光学異性化反応に対する配位子の効果，日本化学会第８９春季年会，2PA-071，日本大学理工学部船橋キャンパス，２００９年３月.

[3] 唐津　孝，○今井奈津子，岩城宏樹，土屋和芳，矢貝史樹，北村彰英　：　Ir トリスシクロメタレート錯体における mer→fac 幾何異性化で誘起される光学異性化とその機構，２００９年光化学討論会，2P095，群馬県桐生市，２００９年９月.

Appendix

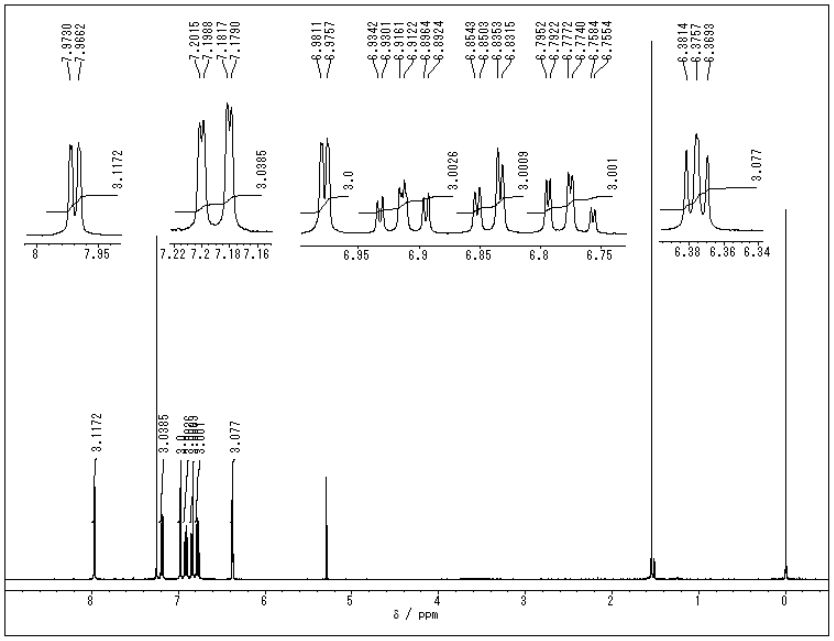

Figure A1. ^{1}H NMR spectrum of *fac*-Ir(ppz)$_3$ (400 MHz, $CDCl_3$, at the ambient temperature).

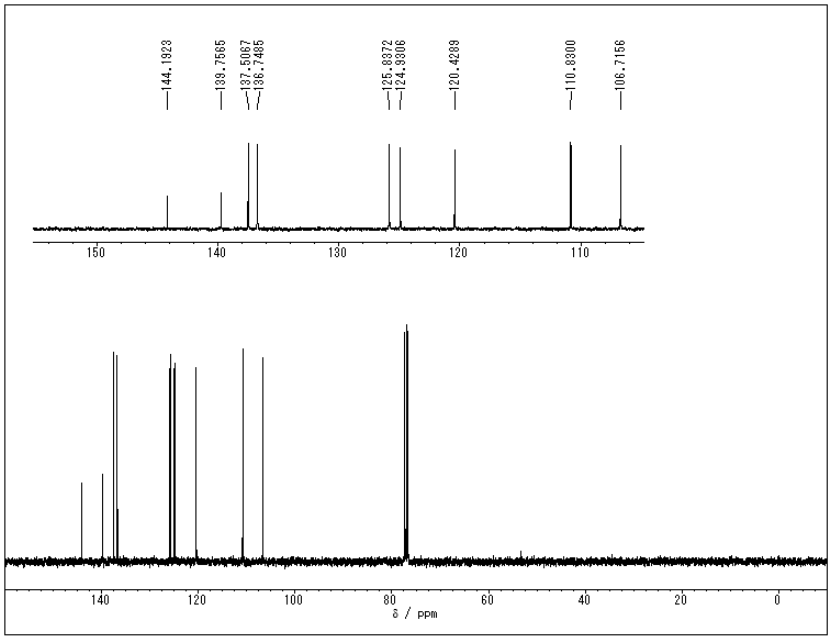

Figure A2. ^{13}C NMR spectrum of *fac*-Ir(ppz)$_3$ (100 MHz, $CDCl_3$, at the ambient temperature).

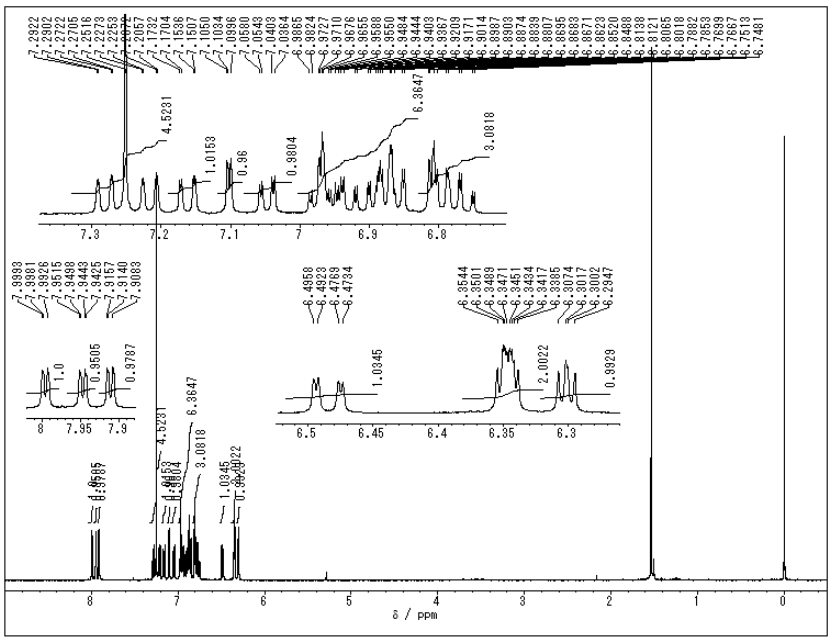

Figure A3. ^{1}H NMR spectrum of *mer*-Ir(ppz)$_3$ (400 MHz, $CDCl_3$, at the ambient temperature).

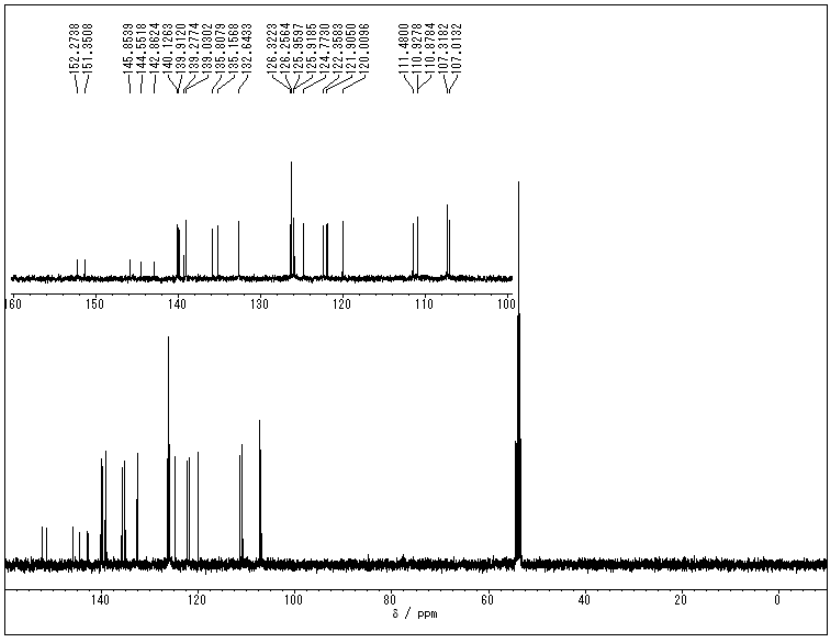

Figure A4. ^{13}C NMR spectrum of *mer*-Ir(ppz)$_3$ (100 MHz, CD_2Cl_2, at the ambient temperature).

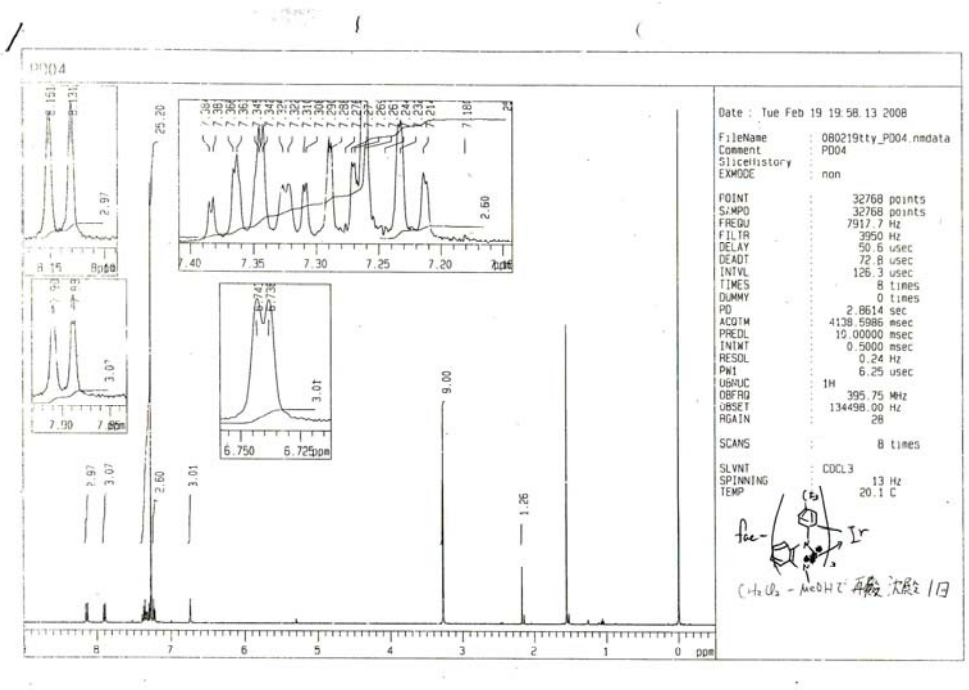

Figure A5. ^{1}H NMR spectrum of *fac*-Ir(CF_3pmb)$_3$ (400 MHz, $CDCl_3$, at the ambient temperature).

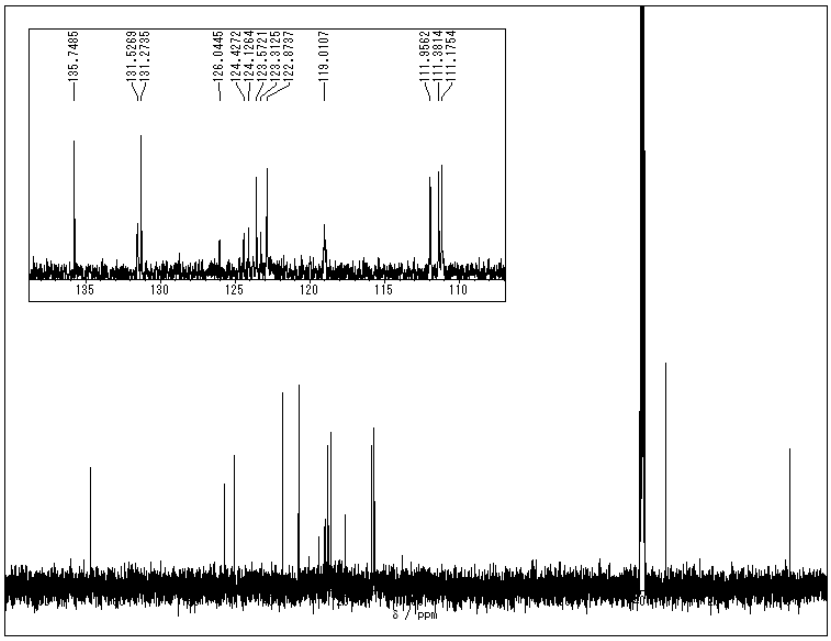

Figure A6. ^{13}C NMR spectrum of *fac*-Ir(CF_3pmb)$_3$ (100 MHz, DMSO, at the ambient temperature).

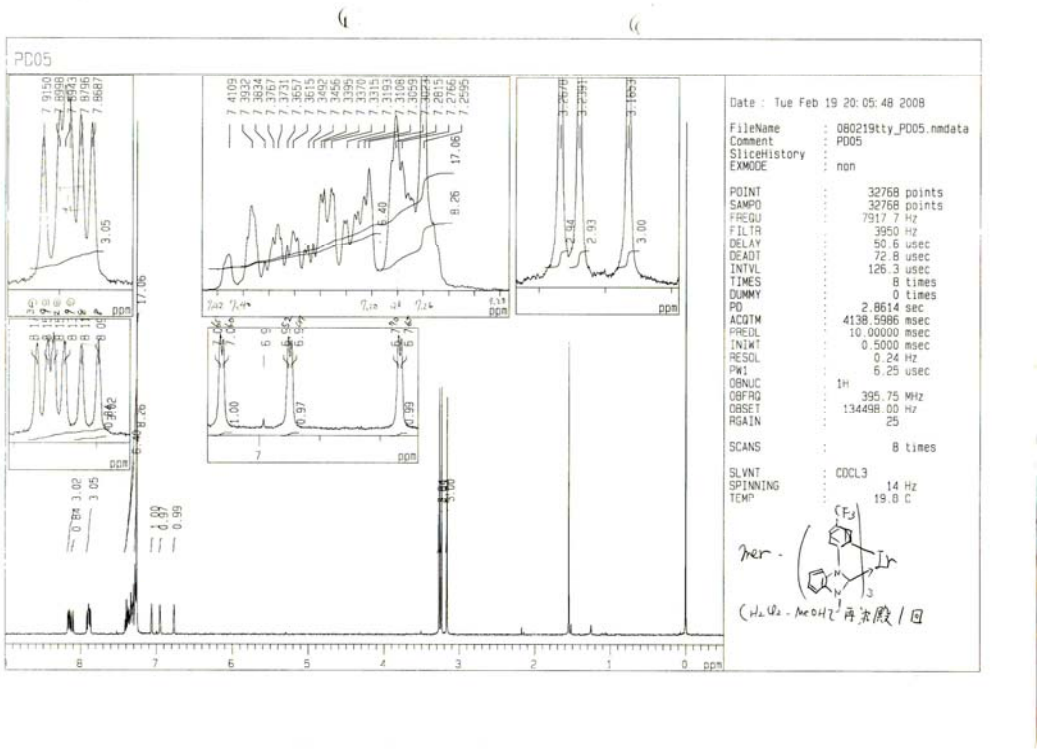

Figure A7. ^{1}H NMR spectrum of *mer*-Ir(CF_3pmb)$_3$ (400 MHz, $CDCl_3$, at the ambient temperature).

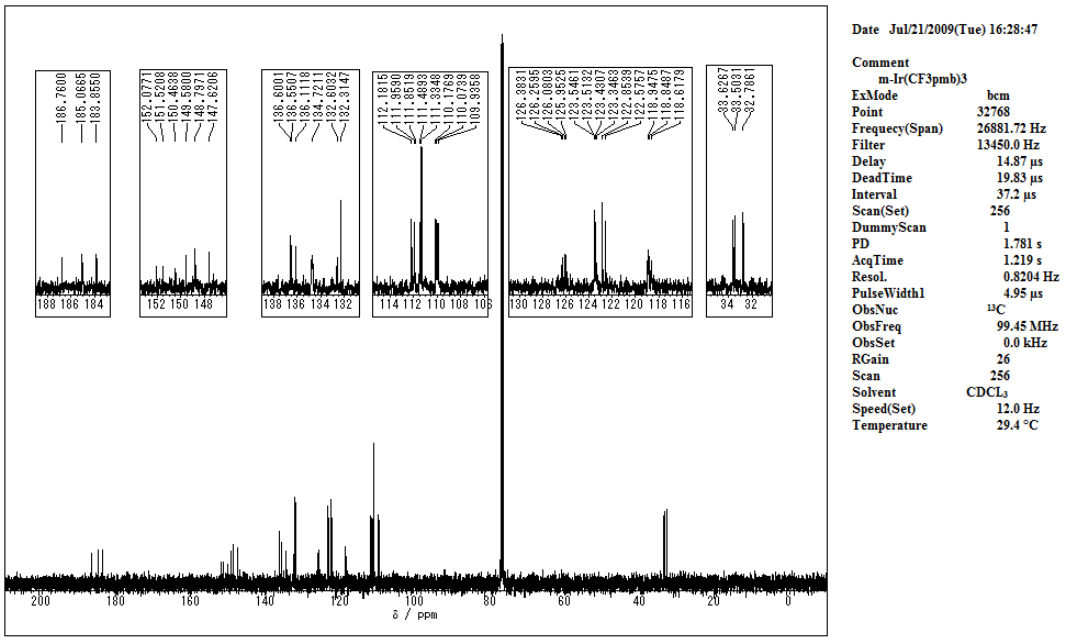

Figure A8. ^{13}C NMR spectrum of *mer*-Ir(CF_3pmb)$_3$ (100 MHz, $CDCl_3$, at the ambient temperature).

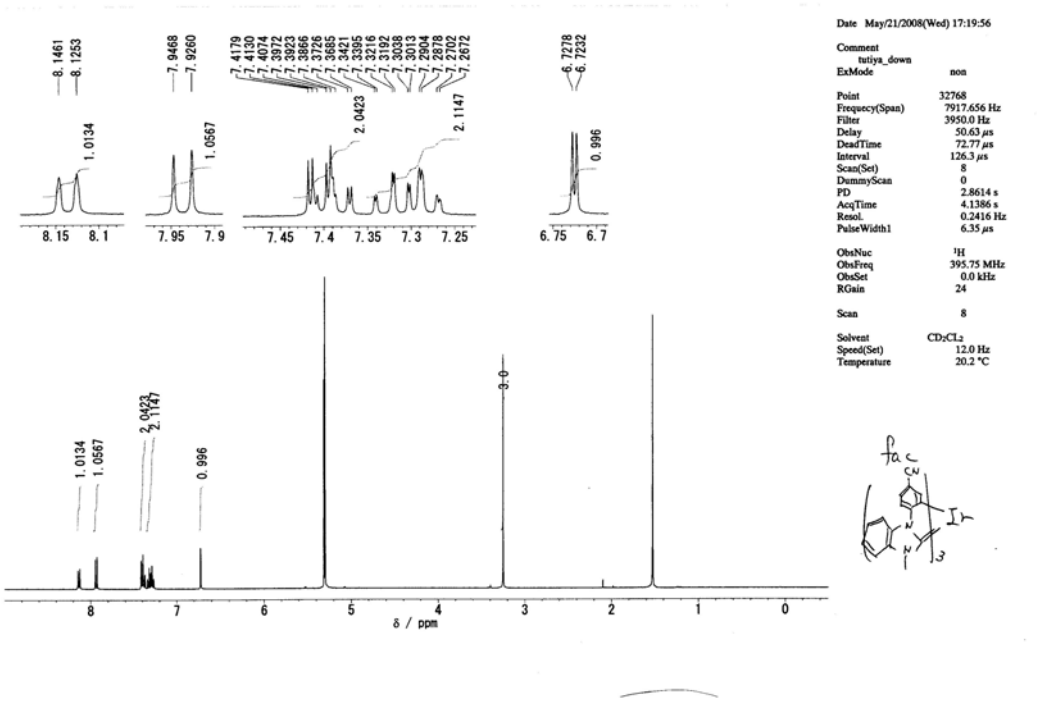

Figure A9. ^{1}H NMR spectrum of *fac*-Ir(CNpmb)$_3$ (400 MHz, CD_2Cl_2, at the ambient temperature).

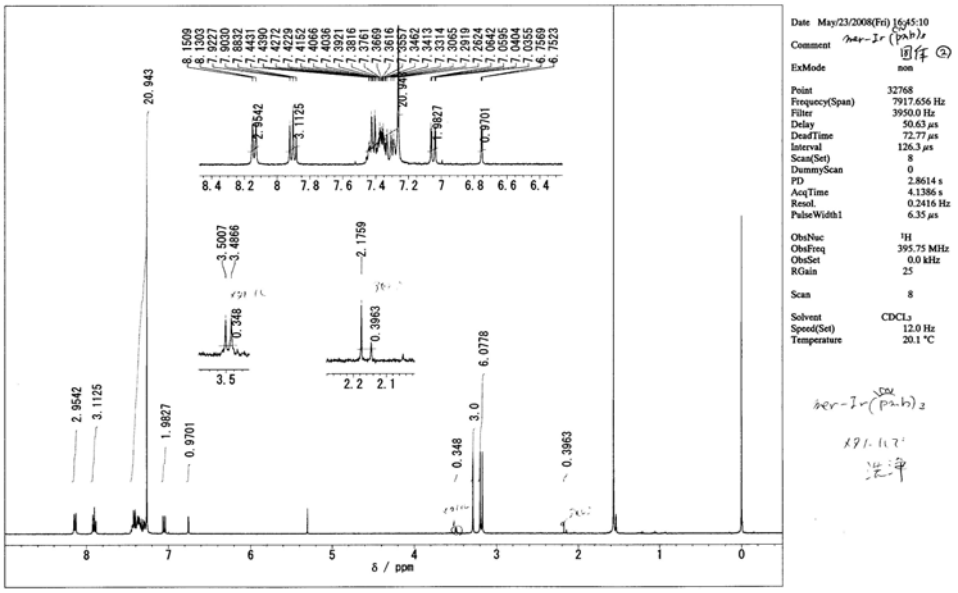

Figure A10. ^{1}H NMR spectrum of *mer*-Ir(CNpmb)$_3$ (400 MHz, $CDCl_3$, at the ambient temperature).

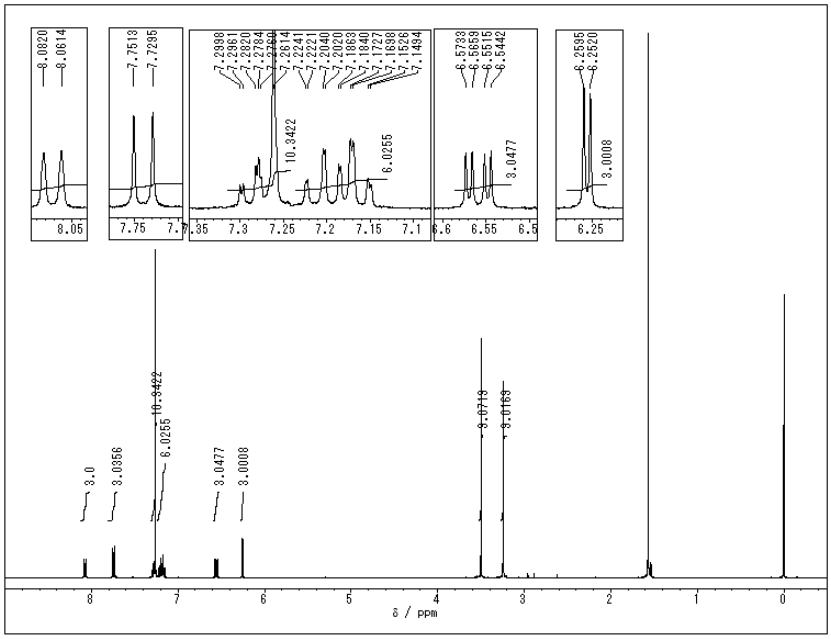

Figure A11. ^{1}H NMR spectrum of *fac*-Ir(Opmb)$_3$ (400 MHz, $CDCl_3$, at the ambient temperature).

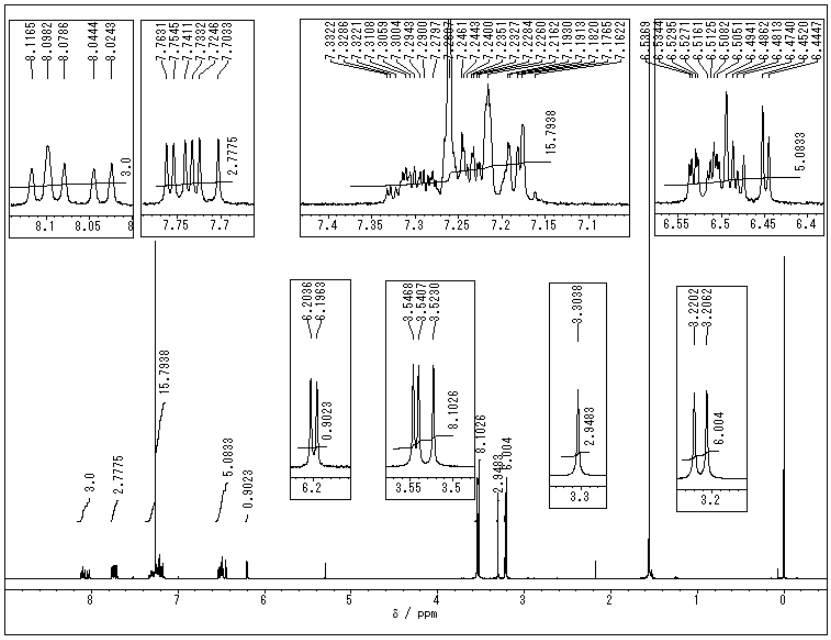

Figure A12. ^{1}H NMR spectrum of *mer*-Ir(Opmb)$_3$ (400 MHz, $CDCl_3$, at the ambient temperature).

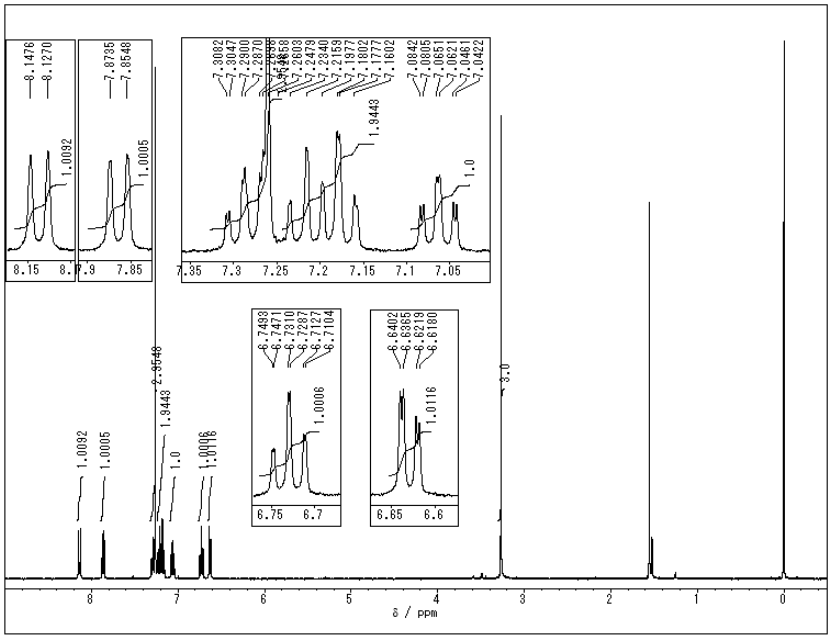

Figure A13. ^{1}H NMR spectrum of *fac*-Ir(pmb)$_3$ (400 MHz, $CDCl_3$, at the ambient temperature).

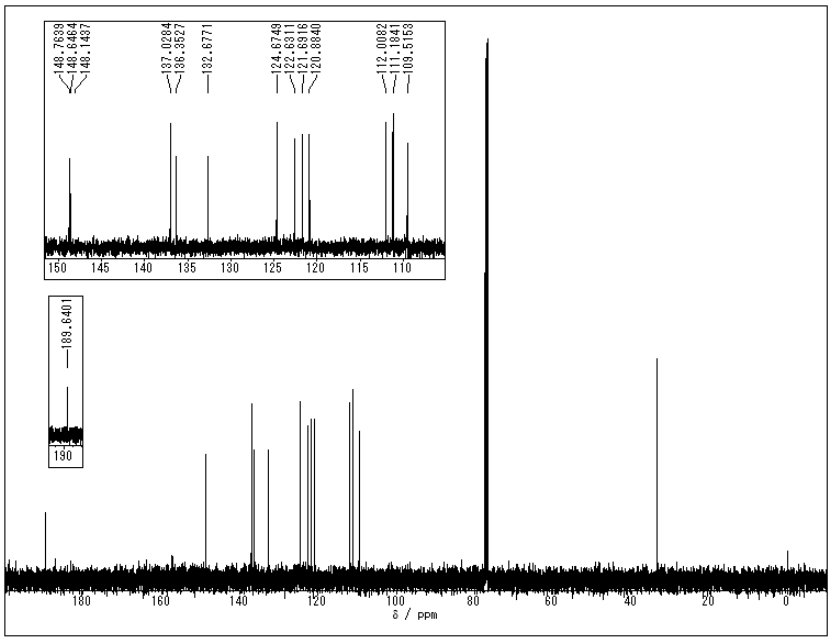

Figure A14. ^{13}C NMR spectrum of *fac*-Ir(pmb)$_3$ (100 MHz, $CDCl_3$, at the ambient temperature).

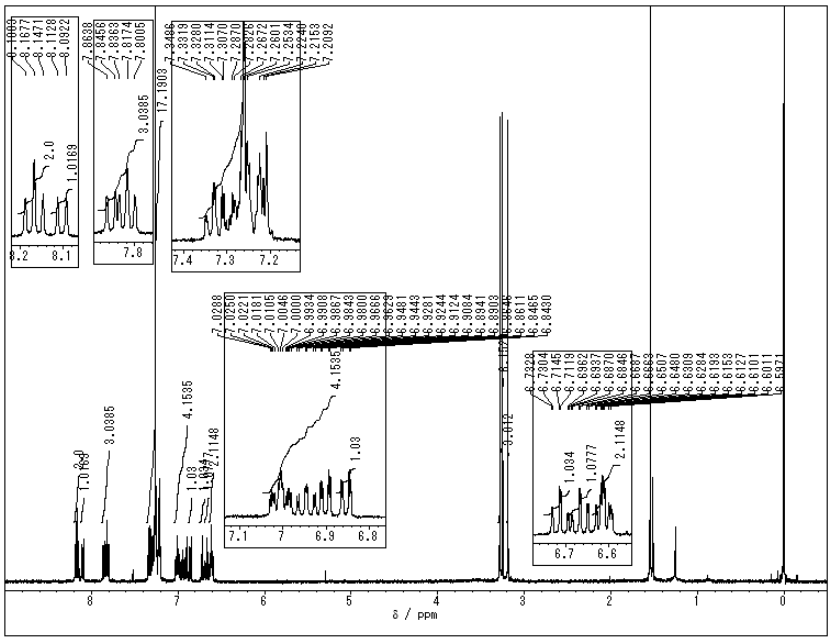

Date May/19/2008(Mon) 14:52:28

Comment

ExMode	non
Point	32768
Frequecy(Span)	7917.656 Hz
Filter	3950.0 Hz
Delay	50.63 µs
DeadTime	72.77 µs
Interval	126.3 µs
Scan(Set)	8
DummyScan	0
PD	2.8614 s
AcqTime	4.1386 s
Resol.	0.2416 Hz
PulseWidth1	6.35 µs
ObsNuc	^{1}H
ObsFreq	395.75 MHz
ObsSet	0.0 kHz
RGain	25
Scan	8
Solvent	$CDCl_3$
Speed(Set)	12.0 Hz
Temperature	20.4 °C

Figure A15. ^{1}H NMR spectrum of *mer*-Ir(pmb)$_3$ (400 MHz, $CDCl_3$, at the ambient temperature).

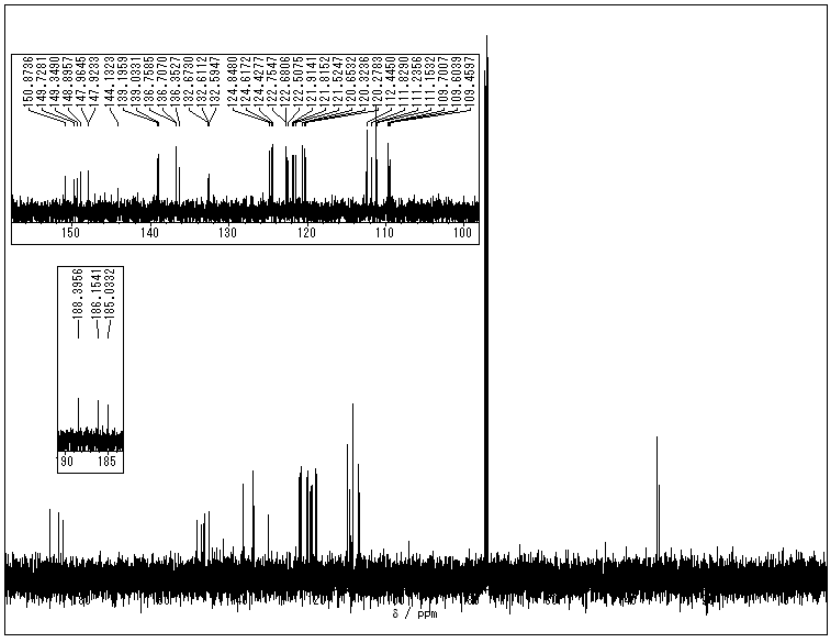

Date Apr/27/2009(Mon) 16:01:23

Comment
mer-Ir(pmb)3 20 mg

ExMode	bcm
Point	32768
Frequecy(Span)	26881.72 Hz
Filter	13450.0 Hz
Delay	14.87 µs
DeadTime	19.83 µs
Interval	37.2 µs
Scan(Set)	64
DummyScan	1
PD	1.781 s
AcqTime	1.219 s
Resol.	0.8204 Hz
PulseWidth1	4.95 µs
ObsNuc	^{13}C
ObsFreq	99.45 MHz
ObsSet	0.0 kHz
RGain	26
Scan	64
Solvent	$CDCl_3$
Speed(Set)	12.0 Hz
Temperature	27.4 °C

Figure A16. ^{13}C NMR spectrum of *mer*-Ir(pmb)$_3$ (100 MHz, $CDCl_3$, at the ambient temperature).

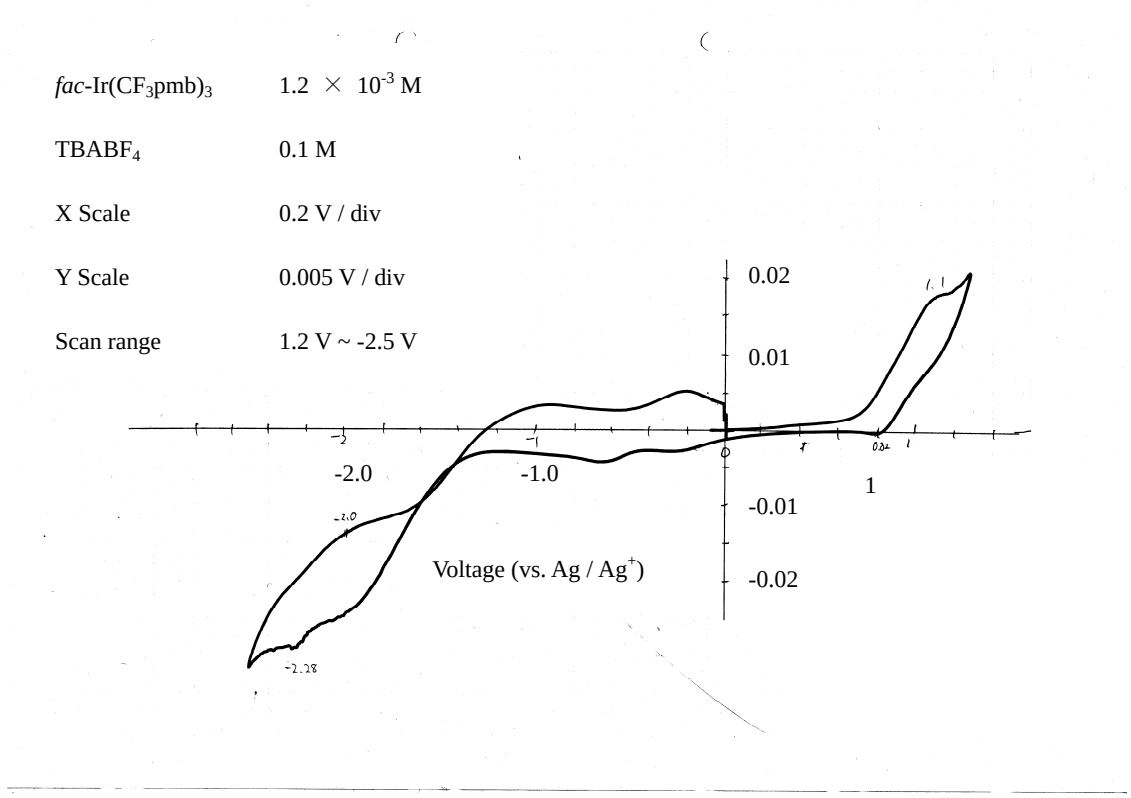

Figure A17. Cyclic voltamgram of *fac*-Ir(CF_3pmb)$_3$ in anhydrous THF.

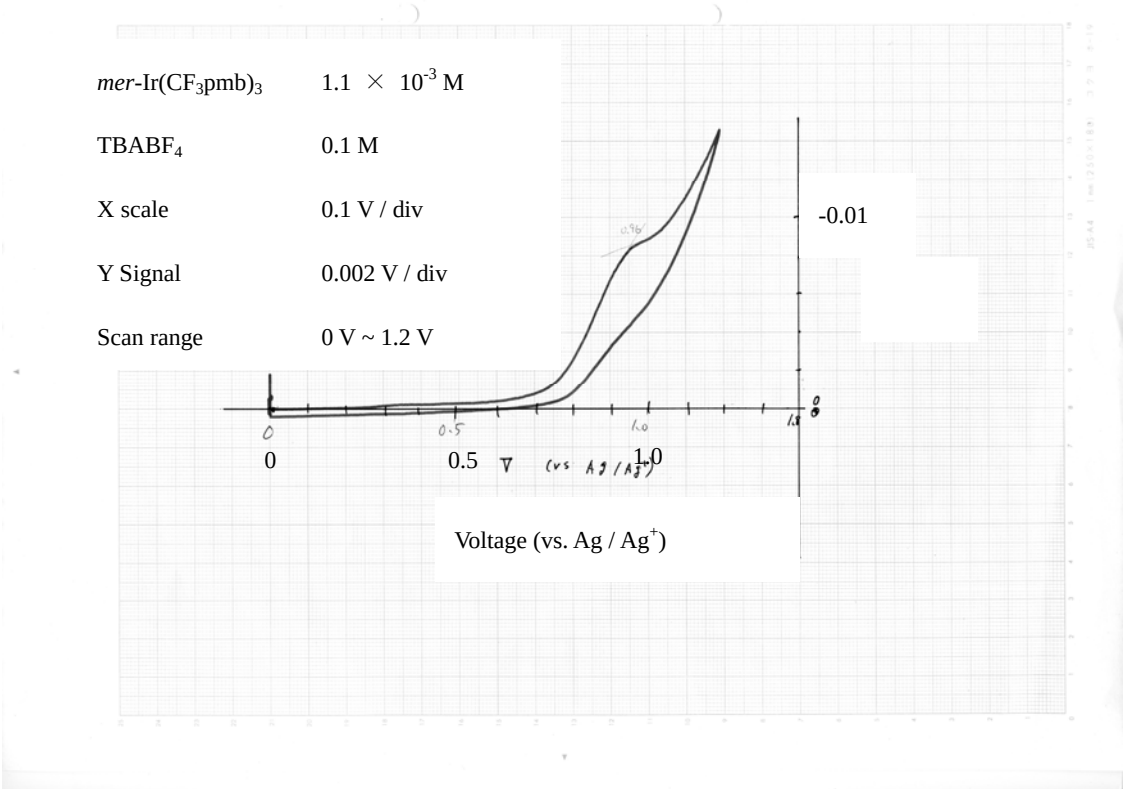

Figure A18. Cyclic voltamgram of *mer*-Ir(CF_3pmb)$_3$ in anhydrous THF.

fac-Ir(CNpmb)$_3$	1.2 × 10^{-3} M
$TBABF_4$	0.1 M
X scale	0.1 V / div
Y Signal	0.005 V / div
Scan rate	0.2 v / s
Scan range	0 V ~ 1.5 V

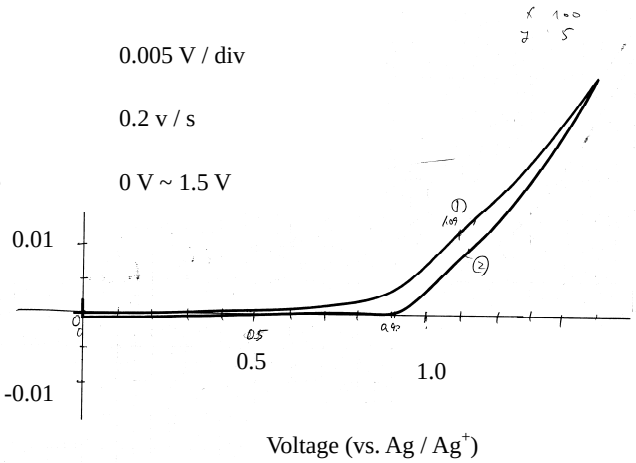

Figure A19. Cyclic voltamgram of *fac*-Ir(CNpmb)$_3$ in anhydrous THF.

mer-Ir(CNpmb)$_3$	1.5 × 10^{-3} M
$TBABF_4$	0.1 M
X scale	0.1 V / div
Y Signal	0.005 V / div
Scan rate	0.2 V / s

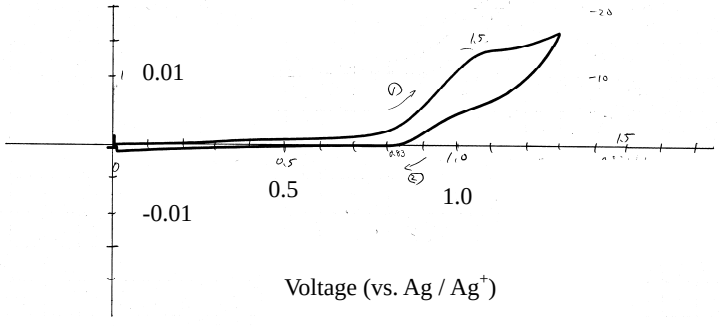

Figure A20. Cyclic voltamgram of *mer*-Ir(CNpmb)$_3$ in anhydrous THF.

fac-Ir(Opmb)$_3$	1.2 × 10^{-3} M
$TBABF_4$	0.1 M
X scale	0.2 V / div
Y Signal	0.005 V / div
Scan rate	0.1 V / S
Scan range	-2.5 V ~ 1.2V

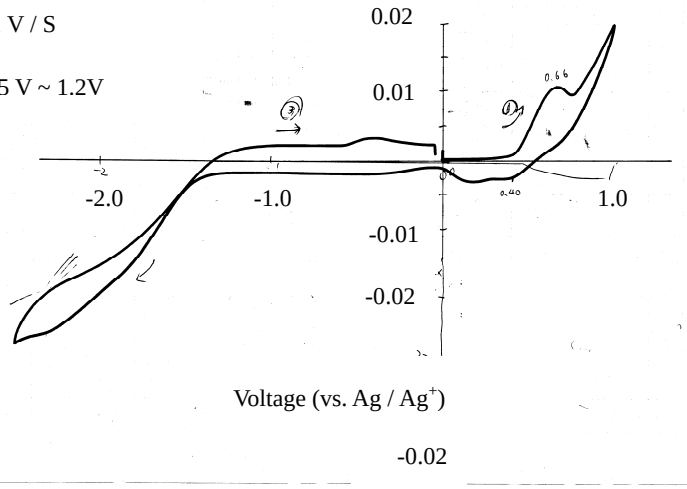

Figure A21. Cyclic voltamgram of *fac*-Ir(Opmb)$_3$ in anhydrous THF.

mer-Ir(Opmb)$_3$	1.3 × 10^{-3} M
$TBABF_4$	0.1 M
X scale	0.2 V / div
Y Signal	0.005 V / div
Scan rate	0.1 V / S
Scan range	-2.5 V ~ 0.8V

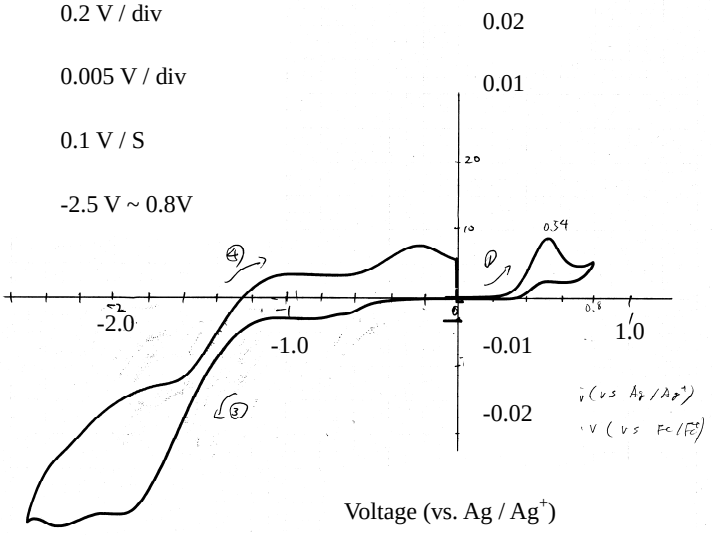

Figure A22. Cyclic voltamgram of *mer*-Ir(Opmb)$_3$ in anhydrous THF.

fac-Ir(pmb)$_3$	1.2 × 10^{-3} M
$TBABF_4$	0.1 M
X scale	0.1 V / div
Y Signal	0.005 V / div
Scan rate	0.2 V / S
Scan range	0 V~ 1.2 V

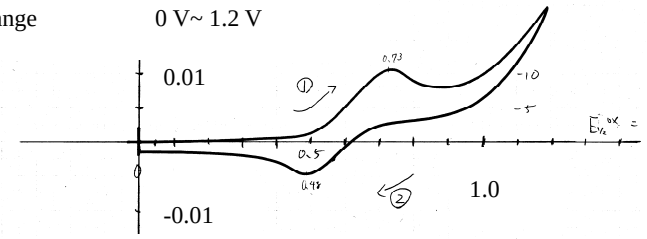

Figure A23. Cyclic voltamgram of *fac*-Ir(pmb)$_3$ in anhydrous THF.

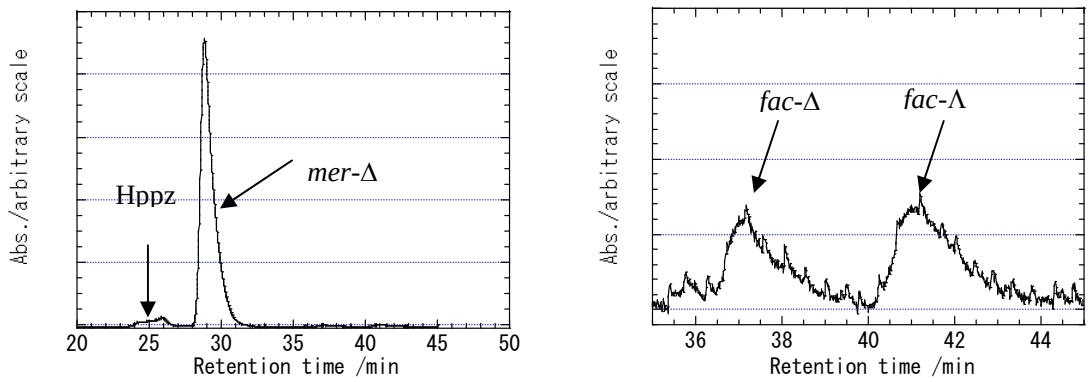

Before heated

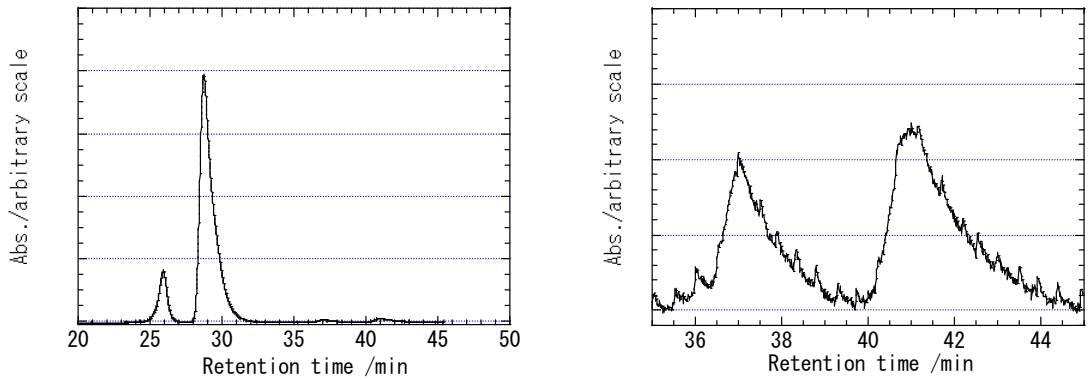

Heated for 8 h at 140 °C

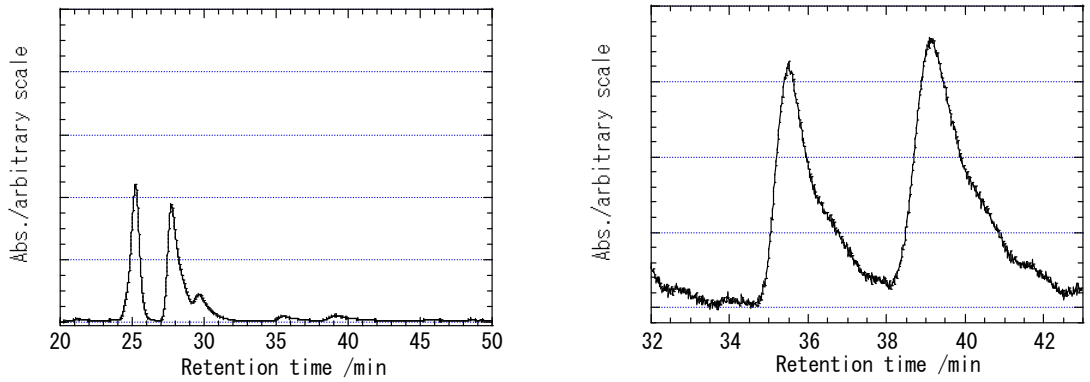

Heated for 8 h at 180 °C

Figure A24. HPLC charts obtained from heating Δ-*mer*-Ir(ppz)$_3$. Overall view (left column) and expanded view (right column).

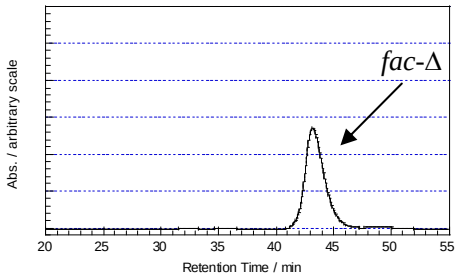

Before heated

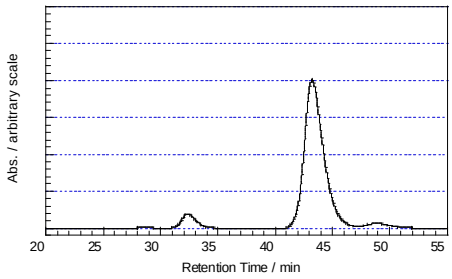

Heated for 24h at 140 °C

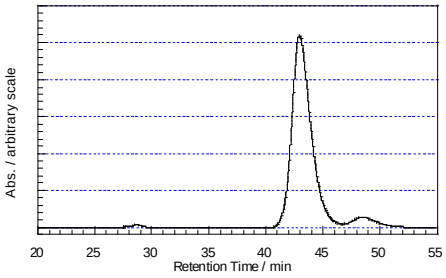

Heated for 24h at 160 °C

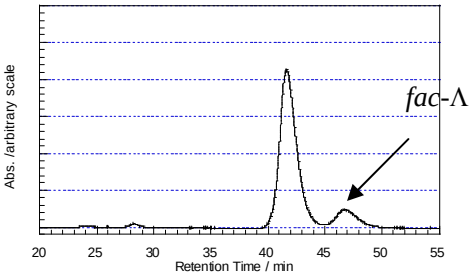

Heated for 19 h at 180 °C

Figure A25. HPLC charts obtained from heating Δ-*fac*-Ir(ppz)$_3$